NON-EQUILIBRIUM PROCESSES AND ERGODICITY-BREAKING IN ISOLATED QUANTUM SYSTEMS

Scott Richard Taylor

A Thesis Submitted for the Degree of PhD
at the
University of St Andrews

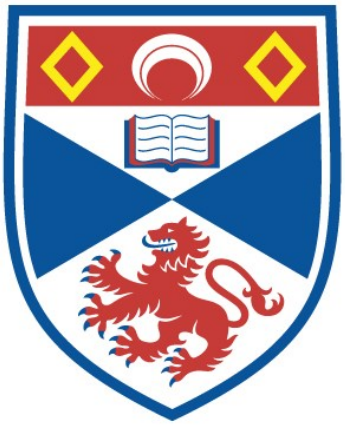

2019

Non-equilibrium processes and ergodicity-breaking in isolated quantum systems

Scott Richard Taylor

University of
St Andrews

This thesis is submitted in partial fulfilment for the degree of

Doctor of Philosophy (PhD)

at the University of St Andrews

February 2019

Candidate's declaration

I, Scott Richard Taylor, do hereby certify that this thesis, submitted for the degree of PhD, which is approximately 20,700 words in length, has been written by me, and that it is the record of work carried out by me, or principally by myself in collaboration with others as acknowledged, and that it has not been submitted in any previous application for any degree.

I was admitted as a research student at the University of St Andrews in August 2014.

I received funding from an organisation or institution and have acknowledged the funder(s) in the full text of my thesis.

Date Signature of candidate

Supervisor's declaration

I hereby certify that the candidate has fulfilled the conditions of the Resolution and Regulations appropriate for the degree of PhD in the University of St Andrews and that the candidate is qualified to submit this thesis in application for that degree.

Date Signature of supervisor

Permission for publication

In submitting this thesis to the University of St Andrews we understand that we are giving permission for it to be made available for use in accordance with the regulations of the University Library for the time being in force, subject to any copyright vested in the work not being affected thereby. We also understand, unless exempt by an award of an embargo as requested below, that the title and the abstract will be published, and that a copy of the work may be made and supplied to any bona fide library or research worker, that this thesis will be electronically accessible for personal or research use and that the library has the right to migrate this thesis into new electronic forms as required to ensure continued access to the thesis.

I, Scott Richard Taylor, confirm that my thesis does not contain any third-party material that requires copyright clearance.

The following is an agreed request by candidate and supervisor regarding the publication of this thesis:

Printed copy

No embargo on print copy.

Electronic copy

No embargo on electronic copy.

Date Signature of candidate

Date Signature of supervisor

Underpinning Research Data or Digital Outputs

Candidate's declaration

I, Scott Richard Taylor, understand that by declaring that I have original research data or digital outputs, I should make every effort in meeting the University's and research funders' requirements on the deposit and sharing of research data or research digital outputs.

Date Signature of candidate

Permission for publication of underpinning research data or digital outputs

We understand that for any original research data or digital outputs which are deposited, we are giving permission for them to be made available for use in accordance with the requirements of the University and research funders, for the time being in force.

We also understand that the title and the description will be published, and that the underpinning research data or digital outputs will be electronically accessible for use in accordance with the license specified at the point of deposit, unless exempt by award of an embargo as requested below.

The following is an agreed request by candidate and supervisor regarding the publication of underpinning research data or digital outputs:

No embargo on underpinning research data or digital outputs.

Date Signature of candidate

Date Signature of supervisor

Non-equilibrium processes and ergodicity-breaking in isolated quantum systems

Author:
Scott R. Taylor

Supervisor:
Dr Chris A. Hooley

University of
St Andrews

This thesis is submitted in partial fulfilment of the requirements for the degree of Doctor of Philosophy in Theoretical Physics

at the

University of St Andrews

February 2019

"We were always loyal to lost causes, the professor said. Success for us is the dark of the intellect and of the imagination."

'Ulysses', James Joyce

Abstract

In this thesis we consider isolated quantum systems influenced by disorder and external driving, and explore aspects of localisation and ergodicity-breaking in three different models.

We first consider the XYZ spin chain in a disordered magnetic field; this system breaks the U(1) symmetry of the XXZ model and therefore violates the conservation of the z component of the total magnetisation. We identify a quantum phase transition between an ergodic phase and a many-body localised phase at a finite disorder strength that is strongly dependent on the size of the U(1) symmetry-breaking term. We also investigate the breakdown of thermalisation by studying the matrix elements of local operators in the basis of the system's eigenstates, and we find suggestive evidence of sub-diffusive energy transport at disorder strengths preceding the localisation transition.

We then consider a two-level time-dependent quantum system that is influenced by a fluctuating classical noise term. We show that the noise does not fully randomise the quantum state if the fluctuations of every noise parameter coupled to the system are perfectly correlated; the state of the system instead becomes distributed over a finite subset of the full state space.

Lastly we consider a one-dimensional Anderson-localised system that is affected by randomly fluctuating onsite potentials. We explore how the spatiotemporal correlations between these onsite potentials affect the delocalisation of a particle initially localised on a single site.

Acknowledgements

I would first like to thank my supervisor, Chris Hooley, both for giving me this opportunity and for his support, patience, and guidance throughout my studies. He has a remarkable enthusiasm for all physics, an optimism that no pessimist can extinguish, and a great sense of fun. The experience of a PhD hinges on the relationship a student has with their supervisor, and I am glad to consider mine a good friend.

I would like to thank Antonello Scardicchio for being a great source of guidance and insight, and I look forward to working with him more in the near future. I must also thank Andrey Shytov, who properly introduced me to theoretical physics and inspired me to pursue it beyond my undergraduate degree.

I owe a great deal of gratitude to Maxi Schulz, a fellow student, friend, and collaborator. He has been involved in many of the most enjoyable moments of my PhD, both scientific and social, and I am so glad that we will continue working together over the next year.

There are many other people who I must thank for making my time in St Andrews so enjoyable: Aidan, Artem, Chris C., Connor, Conor, Dave, Deep, Elliott, Federico, Francisco, Ian, Igor, Jack, Jon, J-P, Justyna, Kyle, Laura, Lewis, Maja, Maria Laura, Matt N., Matt T., Nat, Oliver, Pippa, Rebecca, Rhea, Sam, Steph, Veronika, and Vish. The pies, pints, cups of tea and coffee, games of badminton, aimless walks around town, and everything else we did together made for a fantastic four years.

Life extends far beyond the town of St Andrews, and I owe a lot to friends that I made before my PhD. From my time in Exeter I must thank Alex, Jack, and Sam, who taught me that physics is best done with friends. I am also grateful for the support of my friends from home who remain close despite

us living so far apart. Thank you Ben, George, Jack, Jim, Josh, and Toby, who have no connection to physics, but always ask about what I'm working on.

I will forever be grateful to Fiona for her support and companionship over the past years, and for her ability to make me smile even on the worst days. She is my best friend, and there is truly nobody I would rather spend my time with.

Finally, I could not neglect to thank my family, whose literally unwavering support and constant encouragement has gotten me to where I am today. Thank you so much for everything; I could never have done this without you.

This work was supported by the CM-CDT under the EPSRC (UK) grant EP/L015110/1.

Contents

Abstract

Acknowledgements **i**

Introduction **1**

1 Many-body localisation **3**

1.1 Disorder-induced localisation 3

1.1.1 Anderson localisation 3

1.1.2 Localisation in interacting models 7

1.1.3 Experimental observations of localisation 8

1.2 Thermalisation in quantum systems 10

1.2.1 Thermalisation 10

1.2.2 Emergent integrability in many-body localised systems 11

1.2.3 The eigenstate thermalisation hypothesis 12

1.3 Many-body localisation in spin chains 14

1.4 Signatures of many-body localisation 17

1.4.1 Spectral statistics 17

1.4.2 Entanglement 20

1.4.3 Eigenvector measures 22

1.4.4 Breakdown of the eigenstate thermalisation hypothesis 23

2 Systems with time-dependent parameters **26**

2.1 Time-evolution in quantum systems 26

2.1.1 Systems with time-independent Hamiltonians 27

2.1.2 Systems with time-dependent Hamiltonians 28

2.1.3 The adiabatic theorem 30

2.1.4 The Landau-Zener problem 31

2.2 Systems with time-dependent noise 33
2.2.1 'White' noise 34
2.2.2 'Real' noise 36

3 The disordered XYZ spin chain 39
3.1 The XYZ spin chain 39
3.2 The disorder-free XYZ spin chain 41
3.3 Many-body localisation in the XYZ spin chain 42
3.3.1 Signatures in the eigenenergy spectrum 43
3.3.2 Signatures in the entanglement 48
3.3.3 Signatures in the Shannon entropy 49
3.3.4 The many-body mobility edge 51
3.3.5 The effect of breaking the U(1) symmetry 53
3.4 Thermalisation in the XYZ spin chain 55
3.4.1 Diagonal elements 55
3.4.2 Off-diagonal elements 59
3.5 Summary and outlook 60

4 Correlated noise in few-level quantum systems 61
4.1 The model 61
4.2 The fidelity plateau 63
4.3 Requirements for the fidelity plateau 66
4.3.1 Negligible transitions due to $[\mathcal{H}_0, \mathcal{H}_n] \neq 0$ 67
4.3.2 Negligible non-adiabatic transitions 68
4.3.3 Completely dephased components of the wavefunction 69
4.4 Numerical demonstration 70
4.5 Imperfectly correlated noise 77
4.6 Summary and outlook 79

5 Time-dependent disorder in Anderson-localised systems 80
5.1 The model 80
5.2 Some simple limits 82
5.3 Gaussian noise 84

5.4 Power-law noise 88
5.5 Diffusive noise 89
5.6 Summary and outlook 91

Summary **92**

Bibliography **95**

List of Figures

1.1 Phase diagram of the disordered XXZ model 16
1.2 Histograms of the off-diagonal matrix elements of s_n^z in the eigenbasis of the disordered XXZ model 25

2.1 Transition probabilities in the Landau-Zener problem 33

3.1 Spectral statistics in the disorder-free XYZ model 41
3.2 Location of the MBL transition in the disordered XYZ model . 44
3.3 Spectral statistics in the disordered XYZ model 45
3.4 Finite-size scaling analysis of spectral statistics in the disordered XYZ model 46
3.5 Values of the finite-size scaling exponent ν from the analysis of the disordered XYZ model 47
3.6 Fluctuations of entanglement entropy in the disordered XYZ model 48
3.7 Finite-size scaling analysis of fluctuations of entanglement entropy in the disordered XYZ model 49
3.8 Fluctuations of Shannon entropy in the disordered XYZ model 50
3.9 Finite-size scaling analysis of fluctuations of Shannon entropy in the disordered XYZ model 50
3.10 Energy-resolved phase diagrams of the disordered XYZ model 52
3.11 Schematic of double-hopping processes in the XYZ model . . 53
3.12 Violation of the eigenstate thermalisation hypothesis in the diagonal elements of the bond energy operator in the disordered XYZ model 56
3.13 Scaling of the diagonal elements of the bond energy operator with state space dimension in the disordered XYZ model . . . 57

3.14 Scaling exponent of the diagonal elements of the bond energy operator in the disordered XYZ model 58
3.15 Distributions of the off-diagonal elements of the bond energy operator in the disordered XYZ model 59

4.1 Distribution of the final state on the Bloch spheres of the noise Hamiltonian $\mathcal{H}_n(T)$ and the clean Hamiltonian $\mathcal{H}_0(T)$ in the strong-noise limit 66
4.2 Schematic of the plateau in a plot of the disorder-averaged fidelity as a function of exposure time T 70
4.3 Disorder-averaged fidelity as a function of exposure time T . . 72
4.4 Disorder-averaged fidelity as a function of noise strength ϵ . . 73
4.5 Absolute deviation of the disorder-averaged fidelity from the plateau value as a function of noise strength ϵ and exposure time T 74
4.6 Histogram of the fidelity as a function of time showing the plateau behaviour 75
4.7 Histograms of the fidelity as a function of time not showing the plateau behaviour 76
4.8 Decay of the population imbalance in a system with imperfectly correlated noise 79

5.1 Expansion of a particle in a disorder-free tight-binding model 82
5.2 Expansion of a particle in a time-independent Anderson insulator 83
5.3 Expansion of a particle due to noise with Gaussian temporal correlations 85
5.4 Expansion of a particle due to noise with Gaussian spatiotemporal correlations 86
5.5 Comparison of Gaussian and power-law correlation functions 87
5.6 Expansion of a particle due to noise with power-law temporal correlations 89

Introduction

When writing a mathematical model to describe a physical system, the first step is often an idealised simplification, such as a perfectly harmonic oscillator or a completely translationally invariant tight-binding model. However, reality is rarely so perfect, and will always feature some amount of disorder and randomness, which we must necessarily understand to fully describe nature. However, the study of disordered systems is not merely a pragmatic attempt to more accurately describe the physical realisations of a particular model. Since the latter half of the 20^{th} century, the study of localisation in disordered quantum systems has revealed physics that cannot be found in their non-disordered counterparts, and violations of the laws of thermodynamics. This has once again highlighted fundamental questions about the emergence of thermodynamics and thermalisation in isolated quantum systems.

All of the work included in this thesis concerns quantum systems that are disordered in some sense, and some of the systems considered are also described by a time-dependent Hamiltonian. Therefore, Chapter 1 will be an introductory chapter exploring the effects of time-independent disorder on quantum systems, specifically localisation in both single-particle and interacting models. Chapter 2 will be an introductory chapter that addresses time evolution in quantum systems, and also with variables that fluctuate in time in a non-deterministic manner, i.e. noise.

Chapter 3, the first chapter of original research, will explore the effects of disorder on the XYZ spin chain. The XXZ spin chain has become a popular model for the study of many-body localisation, and the XYZ spin chain is a generalisation of this model that does not conserve the total number of

particles when rewritten in the fermionic language. We demonstrate that there is a many-body localisation transition in this model, which occurs at a disorder strength that is strongly dependent on the strength of the non-number-conserving term.

Chapter 4 considers a few-level quantum system with a Hamiltonian that has both a smoothly time-dependent component and a noisy component that fluctuates rapidly and randomly in time. We show that, when the noise in every parameter of the Hamiltonian is perfectly correlated, the fluctuations are unable to cause the complete randomisation of the quantum state of the system. We make analytical predictions of the strength of the noise required to observe this behaviour, and test them numerically.

In Chapter 5 we consider the effects of smoothly fluctuating disorder on an Anderson-localised system. We expose the Anderson insulator to additional time-dependent onsite potentials that fluctuate randomly with certain correlations in both space and time. We explore the effects of these spatiotemporal correlations, showing that temporal correlations can lead to an intermediate period of subdiffusive transport, and that long-ranged spatial correlations can inhibit transport at later times. We then discuss the idea of using this as a toy model for the ergodic phase of a many-body localisable model.

Chapter 1

Many-body localisation

Many-body localisation (MBL) is currently the subject of intense research, for both practical reasons (such as possible applications in quantum computing), and also in the context of fundamental questions in physics (such as the thermalisation of quantum systems). In this chapter we will discuss localisation due to disorder, and its relevance to thermalisation. We will then briefly outline the results of recent research into MBL in the context of spin chains, before discussing aspects of the phenomenology of MBL systems.

1.1 Disorder-induced localisation

1.1.1 Anderson localisation

The study of disordered quantum systems began sixty years ago, with P. W. Anderson's work on the localisation of a single particle on a disordered lattice [1]. This phenomenon is now known as 'Anderson localisation', and has been the subject of significant scientific interest in the decades since its discovery [2, 3]. The Hamiltonian for a particle hopping on a d-dimensional lattice with random on-site potential energies is

$$\mathcal{H} = -J \sum_{\langle \mathbf{i},\mathbf{j} \rangle} \left(|\mathbf{i}\rangle\langle\mathbf{j}| + |\mathbf{j}\rangle\langle\mathbf{i}| \right) + \sum_{\mathbf{i}} \epsilon_{\mathbf{i}} |\mathbf{i}\rangle\langle\mathbf{i}|, \tag{1.1}$$

where $\langle \mathbf{i}, \mathbf{j} \rangle$ denotes pairs of nearest-neighbour sites, $|\mathbf{i}\rangle$ is the quantum state corresponding to the particle existing on site $\mathbf{i} = (i_1, i_2, ..., i_d)$, J is the hopping amplitude, and $\epsilon_{\mathbf{i}} \in [-W, W]$ are the energies of the particle on site $\mathbf{i}$,

which are uncorrelated numbers drawn from a uniform distribution.

One might ask, what is the probability of finding a particle, initially located at the origin, still there at a time t, i.e. what is $p(t) = |\langle \mathbf{0}|\psi(t)\rangle|^2$ if $|\psi(0)\rangle = |\mathbf{0}\rangle$? This is a simple problem in two extreme limits:

The disorder-free model ($W = 0$)

In the absence of disorder, (1.1) is the standard translationally invariant tight-binding model, which has Bloch-wave eigenstates. On a hypercubic lattice with periodic boundary conditions in d dimensions, these eigenstates $|\phi_{\mathbf{k}}\rangle$ and their associated eigenenergies $E_{\mathbf{k}}$ have the form

$$|\phi_{\mathbf{k}}\rangle = L^{-d/2} \sum_{\mathbf{j}} e^{-i\mathbf{k}\cdot\mathbf{j}} |\mathbf{j}\rangle, \qquad E_{\mathbf{k}} = -2J \sum_{n=1}^{d} \cos k_n \tag{1.2}$$

for a lattice with L sites in every direction, where the quasimomentum components obey the condition $k_n L = 2\pi m_n$ with $m_n \in \{0, 1, ..., L-1\}$. The initial state $|\mathbf{0}\rangle$ must be constructed using a phase-coherent superposition of every eigenstate, which are plane waves that propagate ballistically with a velocity $\mathbf{v}_k = \nabla_k E_k$ (setting $\hbar = 1$, which we will assume throughout this thesis). The time-dependent wavefunction is given by

$$\big\langle \mathbf{j}\big|\psi(t)\big\rangle = \frac{1}{L^d} \sum_{\mathbf{k}} e^{i\mathbf{k}\cdot\mathbf{j} + i2Jt\sum_{n=1}^{d}\cos(k_n)}, \tag{1.3}$$

and taking the thermodynamic limit $L \to \infty$, this becomes [4]

$$\big\langle \mathbf{j}\big|\psi(t)\big\rangle = \int_0^{2\pi} \frac{\mathrm{d}^d k}{(2\pi)^d} e^{i\mathbf{k}\cdot\mathbf{j} + i2Jt\sum_{n=1}^{d}\cos(k_n)} = i^d \prod_{n=1}^{d} \mathcal{J}_{j_n}(2Jt), \tag{1.4}$$

where $\mathcal{J}_\alpha(x)$ is the α^{th} order Bessel function of the first kind [5]. Bessel functions asymptotically decay as $x^{-1/2}$, and so we find $p(t) = |\langle \mathbf{0}|\psi(t)\rangle|^2 \sim t^{-d}$. As one would expect for ballistic expansion, the width of the density grows linearly in time [4]:

$$\sigma(t) = \sqrt{\langle\psi(t)|\mathbf{x}^2|\psi(t)\rangle - \langle\psi(t)|\mathbf{x}|\psi(t)\rangle^2} = \sqrt{2d}Jt. \tag{1.5}$$

We can intuitively understand the forms of $p(t)$ and $\sigma(t)$: the width of the density grows linearly in time in each direction, so the height of the density must decay with a power of t for each direction in order to remain normalised.

The infinite-disorder limit ($J/W \to 0$)
In this limit the position basis is the eigenbasis of the system

$$|\phi_{\mathbf{n}}\rangle = |\mathbf{n}\rangle, \qquad E_{\mathbf{n}} = \epsilon_{\mathbf{n}}, \tag{1.6}$$

and the Hamiltonian generates no dynamics: $|\psi(t)\rangle = e^{-i\epsilon_{\mathbf{0}}t}|\mathbf{0}\rangle$. As a result, the wavepacket does not spread, $\sigma(t) = \sigma(0) = 0$, and the return probability is constant in time $p(t) = p(0) = 1$.

This then leaves the question of what happens at intermediate disorder strengths, which is of course the interesting case. In a picture where a particle propagates ballistically between scattering events at 'impurities' (which are the disorder), the outcome is diffusive motion:

$$\overline{\langle x^2\rangle(t)} = 2Dt, \tag{1.7}$$

where D is the diffusion constant, the bar denotes an average over disorder realisations, and t must be much larger than the scattering time τ. A perturbative calculation using the golden rule can estimate the scattering rate, $\Gamma = \tau^{-1}$, from the disorder potential. By considering the plane-wave solutions of the clean problem, $|\mathbf{k}\rangle$, and treating the disorder potential, $V = \sum_{\mathbf{n}} \epsilon_{\mathbf{n}}|\mathbf{n}\rangle\langle\mathbf{n}|$, as the perturbation, the scattering rate depends on the disorder strength as $\Gamma \sim W^2$ (with k-dependent prefactors). This gives the scaling of the diffusion constant [4]:

$$D = v_g^2\tau \sim \frac{1}{\Gamma} \sim \frac{1}{W^2}, \tag{1.8}$$

where v_g is the k-dependent group velocity. Anderson predicted that, contrary to the expression above (which is always finite for $W > 0$), all transport may cease for large enough W and the system becomes an insulator (i.e. $p(t)$

does not decay to zero). This lack of transport is a defining characteristic of a localised phase. It is also the case that the eigenstates, $|\phi_m\rangle$, become localised in space, decaying exponentially at large distances from their centre, $\mathbf{j}_m^0$, with a localisation length ξ [2]:

$$\langle \mathbf{j} | \phi_m \rangle \sim e^{-|\mathbf{j}_m^0 - \mathbf{j}|/\xi}. \tag{1.9}$$

This exponential localisation of a quantum particle is a result of destructive interference between the multiple reflected components of the wavefunction from the potential barriers due to the disorder on each site [2, 6].

The dimensionality of the system is a significant factor in localisation. In $d = 1$ it has been proven that every eigenstate of the Anderson model is localised, even in the presence of vanishingly small disorder [7], where the localisation length diverges as $\xi \sim W^{-2}$ [2]. Similarly, in $d = 2$, scaling arguments indicate that there is also no localisation transition as a function disorder strength, and all states are localised [8]. In $d \geq 3$ it is known that the system will undergo a transition to a localised phase above a critical disorder strength W_c [4]. In this case the entire spectrum does not localise simultaneously: for weak disorder, only the energy states in the highest and lowest regions of the spectrum are localised, and the states in the middle of the spectrum are extended. The energy separating the localised and extended states is known as the mobility edge. As we increase the disorder strength, the delocalised part of the spectrum shrinks, and at $W = W_c$ all states become localised [2].

Localisation is a purely wave-mechanical effect with no counterpart for classical particles, which can be seen by considering the classical equivalent of a particle moving in a disordered landscape. If the potential energy of the particle $V(x)$ has a maximum value of $V_{\max}$, and the total energy of the particle $E < V_{\max}$, then the particle will be 'localised' between two of the classical turning points where $V(x) = E$. However, for $E > V_{\max}$ the particle

can travel throughout the system, with a velocity v that changes with position as $v(x) = \sqrt{2(E - V(x))/m}$, where m is its mass. This is in clear contrast to the quantum system which is localised at all energies for any disorder strength in $d \leq 2$. For disorder with a long-tailed distribution, such as a Gaussian distribution which has no finite $V_{\max}$, the results are qualitatively the same, although the critical disorder strength W_c decreases [9].

1.1.2 Localisation in interacting models

The existence of localisation in the presence of interactions between the particles was debated for several decades, with some studies suggesting that localisation may persist in the presence of short-ranged interactions and others suggesting that interactions would destroy the Anderson insulator [10–13]. More recently, D. M. Basko, I. L. Aleiner, and B. L. Altshuler studied a disordered model of interacting fermions with localised single-particle eigenstates; they showed that for small but finite temperatures, a many-body mobility edge exists even in the presence of weak interactions, and the system can undergo a transition to a localised phase with exactly zero conductivity [14]. This interacting version of Anderson localisation is known as many-body localisation (MBL).

Localisation in an interacting system is not characterised by such a simple quantity as the localisation length in the single-particle problem, and instead we must consider whether excitations can propagate through the system, or whether the system relaxes to a state with memory of its initial conditions. However, we can think about this problem in an analogous way to the single-particle system, by considering it as localisation in state space rather than in real space. In this picture the Hamiltonian describes the state of the system 'hopping' on a complicated graph where the nodes represent states in the system's many-body Fock space [14–16]. The MBL transition then corresponds to a change in the structure of the eigenstates from being extended to localised in Fock space [17]. It is worth noting that this is not as trivial as considering an Anderson model with uncorrelated disorder on a

lattice with an interesting geometry; the different many-body states can be connected by several paths, and these paths are not statistically independent [14, 17].

The transition between the delocalised and localised phases is unusual in that it has no signatures in thermodynamic variables, but is evident in the individual many-body eigenstates of the Hamiltonian [18], as we will discuss later in this chapter. A great deal of interest has been generated by the fact that the transition cannot be described in the framework of equilibrium statistical mechanics [19].

1.1.3 Experimental observations of localisation

The enduring interest in localisation has undoubtedly been stimulated by successful experimental observations. Localisation and the Anderson transition have been observed in transport measurements on solid-state systems, which have been well summarised by B. Kramer and A. MacKinnon [2]. These studies have found evidence for localisation in many observables, including: the dielectric susceptibility, the magnetoresistance, and the fluctuations and dependences on temperature and doping of the conductance in disordered samples. Anderson localisation has also been explored in light in disordered media [20], however, this is a difficult system to study experimentally [21], and light's vector character means that the extrapolation from particles to photons is non-trivial [22].

More recently, advances in the manipulation of cold-atom systems have resulted in access to quantum systems that can be engineered and controlled to an unprecedented degree of precision [23, 24]. In cold-atom setups the cloud of atoms can be imaged directly, offering the opportunity to truly observe the density profile, and more details of the wavefunction itself are available through interference experiments. These measurements can be performed by determining the shape of the atom cloud from the absorption of light shone through it, which can be employed to ascertain the real space and

momentum distributions, or by observing the occupation of individual sites in lattice systems [24]. Lattice models can be constructed by exposing the atoms to laser standing waves, known as 'optical lattices', which mimic the periodic potential of a crystal. These optical lattices naturally contain no impurities or imperfections, they do not contain phonons, and they can be created in a range of geometries and dimensionalities by employing sophisticated setups with several lasers [25, 26]. A quasiperiodic potential of the form $h_n = W\cos(\beta\pi n)$, where β is an irrational number, can be generated by adding an additional weak lattice with a periodicity that is incommensurate with the original lattice. This is known as the Aubry-André model [27], and the predicted localisation transition at finite W has been observed in non-interacting particles in an optical lattice [28]. True disorder can be realised in cold-atom systems by exposing the atoms to a laser speckle pattern, and Anderson localisation has also been observed in these systems [29]. Additionally, the interaction strength is easily tuned in these experiments [23], allowing experimentalists to study the many-body localisation transition.

The localisation transition in cold-atom setups has been observed in a number of ways in both fermionic and bosonic systems. In one-dimensional non-interacting Bose-Einstein condensates, localisation has been observed through direct measurements of the localisation length from the exponential decay of the density profile [28, 29]. This localisation was also tested by confirming that the density did not expand in space when the confining potential was switched off. Many-body localisation has been observed by measuring the relaxation of initially ordered states. An initially staggered density of interacting fermions in a one-dimensional quasiperiodic lattice was found not to relax to a uniform density above a critical disorder strength [30], and similar behaviour was found for a domain wall configuration in a two-dimensional system of bosons [31]. Interacting fermions in a three-dimensional disordered lattice have also been found to localise, even at finite temperature, above a critical disorder strength [32]. A magnetic field was applied to the atoms for a short time, after which the lattice potential was

removed and the momentum distribution measured to determine the velocity of the centre of mass; this velocity dropped to zero when the disorder was increased above a critical value.

1.2 Thermalisation in quantum systems

1.2.1 Thermalisation

The thermalisation of quantum systems is a fundamental question in physics, and it has received a great deal of attention [18, 33–37]. In a classical system, this relaxation to a thermal state is understood to be a result of particle collisions redistributing energy between the different degrees of freedom of the system. This appears in the form of non-linearity in the system's equations of motion, which makes it 'chaotic' (meaning that its dynamics are exponentially sensitive to even infinitesimal changes to the initial conditions), and it is not possible to predict the behaviour of the system over long periods of time [37]. As a result, the time evolution causes the system to 'forget' its initial conditions, and it tends to a state which is well described by a few average thermodynamic quantities. This relies on the system obeying Boltzmann's ergodic hypothesis, that given an infinite amount of time, the system will explore its entire state space in an unbiased way (i.e. that a long-time average is equivalent to an ensemble average). However, the Schrödinger equation describes unitary time evolution,

$$|\psi(0)\rangle = \sum_\alpha c_\alpha |\alpha\rangle \quad \rightarrow \quad |\psi(t)\rangle = \sum_\alpha c_\alpha e^{-iE_\alpha t}|\alpha\rangle, \tag{1.10}$$

where $|\alpha\rangle$ are eigenstates of the system with eigenenergies E_α, which clearly retains knowledge of the initial state in the amplitudes c_α, and can never sample its entire state space in this way.

An isolated quantum system has no contact with a thermal reservoir by definition, but we may consider a small subsystem, and ask whether the rest of the system acts as a reservoir. If this is the case, then the long-time steady

state of the subsystem can be described by the laws of statistical mechanics, and the subsystem thermalises, even though the system as a whole remembers its initial conditions. For a localised system this is not the case; the system retains a local memory of its initial state, and so a generic subsystem will fail to reach thermal equilibrium [18].

1.2.2 Emergent integrability in many-body localised systems

Localised systems are not the only examples of systems that fail to thermalise: this is a well-known feature of integrable systems. Integrable systems possess an extensive number of non-trivial conserved quantities, and they are often exactly solvable by Bethe Ansatz methods [38]. The large number of conserved quantities restricts the dynamics, making it impossible for the system to reach a thermal state, and the long-time steady state will instead be described by an appropriately constructed 'generalised Gibbs ensemble' [39]. However, these systems are fragile and even weak perturbations are known to break the integrability. In MBL systems, on the other hand, the non-thermalising behaviour is robust to arbitrary small local perturbations to the Hamiltonian [18].

The related phenomenology of MBL and integrable systems is not a coincidence: a certain type of integrability emerges deep in the MBL phase. This integrability appears in the form of an extensive set of independent mutually-commuting quasilocal operators $\{I_\alpha\}$ that commute with the Hamiltonian, which are known as local integrals of motion (LIOMs) [40–44]. These operators are quasilocal in the sense that they have a finite spatial extent, which suppresses transport and thermalisation as the system retains a local memory of its initial conditions. If we construct a LIOM centred at R_α from a superposition of local operators, then the contribution of each local operator decays exponentially with its distance from R_α [42, 43]. The LIOMs can be constructed by a quasilocal unitary operation Ω on the Pauli basis: $I_\alpha = \Omega^\dagger s^z_\alpha \Omega$ [41, 45]. In a weakly interacting system the LIOMs can be viewed as dressed

Pauli operators: I_α will have a significant overlap with the original Pauli operator, and the overlap with the other Pauli operators will decay exponentially in real space [18]. An MBL Hamiltonian can be written in diagonal form as a non-linear combination of the LIOMs:

$$\mathcal{H} = E_0 + \sum_\alpha h_\alpha \, I_\alpha + \sum_{\alpha,\beta} J_{\alpha\beta} \, I_\alpha I_\beta + \sum_{n=1}^{\infty} \sum_{\alpha,\beta,\{\gamma\}} K^n_{\alpha\{\gamma\}\beta} \, I_\alpha I_{\gamma_1} ... I_{\gamma_n} I_\beta, \quad (1.11)$$

and the eigenstates of $\mathcal{H}$ are the simultaneous eigenstates of $\{I_\alpha\}$, which can be uniquely labelled by their eigenvalues. The quasilocal structure of the LIOMs implies that the interaction strengths $J_{\alpha\beta}$ and $K^n_{\alpha\{\gamma\}\beta}$ decay exponentially with distance [18, 40]. The phenomenology of many-body localised systems, which we will discuss later in this chapter, can be successfully described in terms of LIOMs [18, 40].

1.2.3 The eigenstate thermalisation hypothesis

The eigenstate thermalisation hypothesis (ETH) provides a mathematical route through which the expectation values of certain operators can become thermal, and is usually applied to operators that act only on a few particles [37, 46–49]. The underlying idea is that the eigenstates of the system are already thermal, and that this property is revealed by the dephasing of the phase-coherent initial state due to unitary time evolution [46]. The long-time average of the expectation value of an operator A in the state $|\psi(t)\rangle$ from (1.10) is given by:

$$\begin{aligned} \langle\langle A \rangle\rangle_T &= \lim_{T\to\infty} \frac{1}{T} \int_0^T \mathrm{d}t \langle \psi(t)|A|\psi(t)\rangle \\ &= \lim_{T\to\infty} \frac{1}{T} \int_0^T \mathrm{d}t \sum_{\alpha,\beta} c^\star_\alpha c_\beta e^{-i(E_\beta - E_\alpha)t} \langle\alpha|A|\beta\rangle \\ &= \sum_\alpha |c_\alpha|^2 \langle\alpha|A|\alpha\rangle \end{aligned} \quad (1.12)$$

where we have assumed that the energies E_α are non-degenerate, so the off-diagonal terms cancel in the average over time. This expression contains knowledge of the initial conditions through the populations $|c_\alpha|^2$, so for

arbitrary states and operators there is no reason why this should correspond to a thermal value.

Additionally, the fluctuations of $\langle A \rangle$ are controlled by the size of its off-diagonal elements:

$$\begin{aligned} \left\langle \left(\langle A \rangle - \langle \langle A \rangle \rangle_T \right)^2 \right\rangle_T &= \left\langle \Big(\sum_{\alpha \neq \beta} c_\alpha^\star c_\beta e^{-i(E_\beta - E_\alpha)t} \langle \alpha | A | \beta \rangle \Big)^2 \right\rangle_T \\ &= \sum_{\alpha \neq \beta} |c_\alpha|^2 \, |c_\beta|^2 \, \left| \langle \alpha | A | \beta \rangle \right|^2 , \end{aligned} \tag{1.13}$$

where the restriction of $\alpha \neq \beta$ results from subtracting the $\alpha = \beta$ terms in (1.12), and the simplification in the last line is a result of the phases averaging to zero in all other terms. In order for the time average (1.12) to be meaningful (i.e. that the value stays close to its average), we require that these fluctuations must be small in the thermodynamic limit.

The ETH ansatz is that the matrix elements of A have the same statistical properties as:

$$\langle \alpha | A | \beta \rangle = \overline{A}(E) \delta_{\alpha,\beta} + e^{-s(E)V/2} f(E, \omega) R_{\alpha,\beta}, \tag{1.14}$$

where $E = (E_\alpha + E_\beta)/2$, $\omega = E_\beta - E_\alpha$, $s(E)$ is the microcanonical entropy density, V is the system volume, $\overline{A}(E)$ and $f(E, \omega)$ are smooth functions, and $R_{\alpha,\beta}$ is a random variable with zero mean and unit variance [33]. The distribution of $R_{\alpha,\beta}$ is often taken to be Gaussian, based on the conjecture by Berry that the components of the eigenstates in a thermalising system follow a Gaussian distribution [34]. Importantly, $\overline{A}(E)$ is equal to the microcanonical expectation value of the observable A at energy E.

We can see the consequences of this ansatz by constructing a quantum state $|\psi_{E_0}\rangle$ from an arbitrary superposition of eigenstates within a small energy

window δE around E_0. We then find that the average value (1.12) becomes:

$$\begin{aligned}\langle\langle\psi_{E_0}|A|\psi_{E_0}\rangle\rangle_T &= \sum_\alpha |c_\alpha|^2\, \overline{A}(E_\alpha) \approx \overline{A}(E_0) \sum_\alpha |c_\alpha|^2 \\ &= \overline{A}(E_0),\end{aligned} \tag{1.15}$$

so the quantum and the thermodynamic expectation values are equivalent. Furthermore, the average size of the off-diagonal elements in (1.14) decays exponentially with the system size, which is consistent with the fluctuations of the average (1.13) vanishing in the thermodynamic limit [37].

1.3 Many-body localisation in spin chains

Recently, MBL has been studied mostly in spin chain systems, which exhibit the relevant physics in a simple setting. The one-dimensional spin-1/2 XXZ chain is an extensively studied model, which has the Hamiltonian:

$$\mathcal{H}_{\mathrm{XXZ}} = \sum_{n=1}^{L} \left[s_n^x s_{n+1}^x + s_n^y s_{n+1}^y + \Delta s_n^z s_{n+1}^z + h_n s_n^z \right], \tag{1.16}$$

where $s_n^\mu = \sigma_n^\mu/2$ is the operator for the μ component of the spin on site n, Δ is the Ising anisotropy, h_n is a random on-site field drawn from a uniform distribution $h_n \in [-W, W]$, and L is the length of the chain. This expression corresponds to periodic boundary conditions, with site $L+1$ being equivalent to site 1. (Note that this is by no means the only spin system in which MBL has been studied [41, 45, 49–53].) This model can be mapped to a system of spinless fermions on a one-dimensional lattice using the Jordan-Wigner transformation [54]:

$$\begin{aligned} s_n^z &\longleftrightarrow c_n^\dagger c_n - \frac{1}{2}; \\ s_n^+ &\longleftrightarrow c_n^\dagger\, e^{i\pi \sum_{j=1}^{n-1} c_j^\dagger c_j}; \\ s_n^- &\longleftrightarrow e^{-i\pi \sum_{j=1}^{n-1} c_j^\dagger c_j}\, c_n, \end{aligned} \tag{1.17}$$

where $c_n^\dagger$ and c_n are the creation and annihilation operators for a fermion on site n respectively. This gives an alternative representation of the Hamiltonian

(up to irrelevant constants):

$$\mathcal{H}_{\mathrm{XXZ}} = \sum_{n=1}^{L} \left[\frac{1}{2} \left(c_n^\dagger c_{n+1} + c_{n+1}^\dagger c_n \right) + \Delta c_n^\dagger c_n c_{n+1}^\dagger c_{n+1} + h_n c_n^\dagger c_n \right]. \quad (1.18)$$

In this language it is clear that Δ corresponds to the strength of a nearest-neighbour interaction. We will only discuss the physics of one-dimensional models, as these are the most thoroughly investigated and well understood systems, and they are the focus of the work in the following chapters.

Numerical studies of this system indicate that in the isotropic 'Heisenberg' limit ($\Delta = 1$) the MBL transition occurs at $W_c \simeq 3.7$, and suggest the existence of a mobility edge at weaker disorder [55–57]. Fig. 1.1 [55] shows the phase diagram of this model, as determined by a finite-size scaling analysis of the energy spectrum and eigenstate properties on system sizes up to $L = 22$. In this study, the transition was determined by analysing the structure of the energy spectrum, the half-chain entanglement entropy and the size of its fluctuations, the Shannon entropy, and fluctuations in the half-chain magnetisation. We will discuss some of these measures in the next section. These types of study, despite pushing the boundaries of what is achievable by exact numerical methods, are still far from the thermodynamic limit. The extracted critical exponents violate bounds derived under quite general assumptions (i.e. that the MBL transition separates a localised phase from a phase that satisfies the ETH) [58], suggesting that the scaling regime has not yet been reached, and the possibility of the existence of a many-body mobility edge has been questioned [59].

Recently, attention has turned to the delocalised region with $W < W_c$, where a variety of interesting physics may be studied [17]. Several numerical studies have observed anomalous subdiffusive spin transport in the XXZ model [60–62], most effectively by studying the scaling of the spin current with system length $j \sim L^{-\gamma}$ ($\gamma = 1$ corresponds to diffusive transport, $\gamma > 1$ corresponds to subdiffusive transport, and γ diverges at the MBL

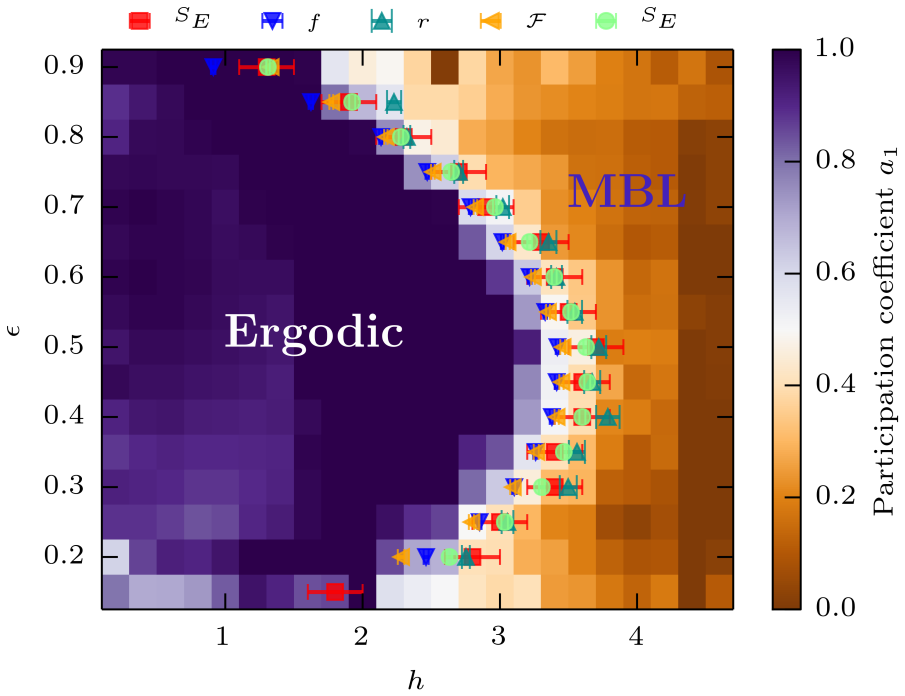

FIGURE 1.1: The phase diagram of the XXZ model (1.16) as a function of disorder strength h and energy density ϵ, showing the two phases and the mobility edge. The critical disorder strength was determined from an exact diagonalisation study of system sizes up to $L = 22$. The location of the MBL transition is determined from the spectral statistics (turquoise upwards-pointing triangles), entanglement entropy (red squares), fluctuations of the entanglement entropy (green circles), the decay of a long-wavelength spin density (blue downwards-pointing triangles), and the fluctuations of the half-chain magnetisation (yellow left-pointing triangles). The colour scheme indicates the scaling of the Shannon entropy with system size (D_1 in the notation used in Section 1.4.3). Figure reproduced from [55].

transition). The transport is subdiffusive for all disorder strengths in the strongly interacting regime ($\Delta > 1$), while a transition between diffusive and subdiffusive transport exists at finite W in weakly interacting systems ($\Delta < 1$) [62]. This anomalous transport has been linked to long-tailed (i.e. non-Gaussian) distributions for the off-diagonal matrix elements of local spin operators in the ergodic phase [63]. It was found that these systems satisfy a modified version of the ETH in the subdiffusive regime, in which the scaling of the variance of the off-diagonal matrix elements with system size requires power-law corrections to the exponential in (1.14) [63]. Furthermore, it has been shown that energy transport is diffusive when the disorder is weak, and the system undergoes a transition to subdiffusive transport at a finite disorder strength (which depends on the strength of the interactions) before the MBL transition [64–66]. Subdiffusive spin transport has also been observed in a periodically driven Floquet version of the model, with associated long-tailed distributions of the matrix elements of local spin operators in the eigenstates of the Floquet unitary [67]. It is interesting to note that in this system, which does not conserve energy, the MBL phase is still present [68–72].

1.4 Signatures of many-body localisation

1.4.1 Spectral statistics

The statistical properties of a model's eigenenergy spectrum have become one of the key diagnostics of the MBL transition [49–52, 55, 60, 61, 66, 73–75]. This approach to studying the properties of a system has its roots in nuclear physics [37], and more recently has become associated with integrable quantum systems, where it can be used as a diagnostic of integrability [38]. The quantities of interest are the gaps between adjacent energy levels $\delta_n = E_n - E_{n-1}$, where E_n are the ordered eigenenergies of the Hamiltonian, and in particular their statistical distribution [75, 76].

More recently, the gap-ratio parameter

$$r_n = \min\left(\frac{\delta_n}{\delta_{n+1}}, \frac{\delta_{n+1}}{\delta_n}\right) \tag{1.19}$$

was introduced [73], which is an attractive quantity as it does not depend on the density of states (the 'unfolding' procedure to remove this dependence from δ_n is non-trivial [75–77]). These quantities are clearly a measure of the level-repulsion between eigenstates. In an integrable model the extensive number of conserved quantities suppresses the level repulsion, as they split the state space into a extensive number of independent sectors. The eigenstates in each sector are not influenced by those in other sectors, so their eigenenergies will not be correlated, and the distribution of level spacings can have significant weight near zero. On the other hand, in non-integrable and non-localised models there are fewer conserved quantities to suppress matrix elements, and the resulting level repulsion causes the distribution of level spacings to vanish at zero.

In the context of MBL we would therefore expect to find level-repulsion in the ergodic phase and no level-repulsion in the localised phase; the transition is often located by determining the disorder strength at which this behaviour changes. We may gain a cartoon understanding of this difference by considering a single particle on a disordered lattice. In a localised state, the wavefunction decays exponentially in space, and therefore it has negligible overlap with another localised state at a distance $\Delta x \gg \xi$. The hybridisation between these states is then exponentially small, and a significant level repulsion (i.e. repulsion on the scale of the typical level spacing) requires consecutive eigenstates to be located nearby in space, which is vanishingly unlikely in the thermodynamic limit. We will therefore not observe the power-law suppression of the level-gap distribution that we would see in ergodic systems. In contrast, two extended states will necessarily have significant weight on the same parts of the lattice, and the Hamiltonian may couple them, resulting in a finite gap between their eigenenergies. In the interacting

MBL phase, this argument becomes that two consecutive eigenstates will generically differ by an extensive number of eigenvalues of the LIOMs, so the Hamiltonian cannot hybridise them to produce level repulsion on the scale of the typical level spacing [40].

To put this on a more quantitative footing, in the localised phase the eigenenergies are effectively independent random numbers, and are thus described by a Poisson distribution:

$$P_P(\delta) = \frac{1}{\alpha} \exp\left(-\frac{\delta}{\alpha}\right) \quad \rightarrow \quad P_P(r) = \frac{2}{(1+r)^2} \tag{1.20}$$

where α is the average level spacing. The form of $P_P(r)$ can be derived by showing that the ratio of two uncorrelated Poisson-distributed variables, $\tilde{r}$, has the distribution $P_P(\tilde{r}) = (1+\tilde{r})^{-2}$, and the factor of two is a result of the contribution from $\tilde{r} > 1$, as $P_P(\tilde{r}^{-1}) = \tilde{r}^2 P_P(\tilde{r})$.

In the thermalising phase, the level statistics have been found to follow the statistics of a random-matrix ensemble; for models with real Hamiltonians (such as the XXZ model in (1.16)) this is the Gaussian orthogonal ensemble (GOE). The distribution of δ in this case is well described by 'Wigner's surmise' [78, 79]:

$$P_{\mathrm{GOE}}(\delta) = \beta\delta \exp(-\gamma\delta^2), \tag{1.21}$$

where β and γ are appropriately chosen constants. An appropriate 'Wigner-like surmise' has been derived for r [79]:

$$P_{\mathrm{GOE}}(r) = \frac{27}{4} \frac{r + r^2}{(1 + r + r^2)^{5/2}}, \tag{1.22}$$

and the residual discrepancy is well captured by the correction term:

$$\delta P(r) = \frac{C}{(1+r)^2} \left(\frac{r}{1+r^2} - \frac{c_1 r^2}{(1+r^2)^2} \right), \tag{1.23}$$

where the value of $C \approx 0.466756$ is found by a fit to numerical data, and

$c_1 = \frac{2\pi-4}{4-\pi}$ to satisfy normalisation conditions. The averages and second moments of these distributions are shown in Table 1.1, which can be compared to the numerical data to determine whether or not the system is localised. In Fig. 1.1 turquoise upwards triangles show the position of the MBL transition as determined by $\langle r \rangle$.

Distribution	$\langle r \rangle$	$\langle r^2 \rangle$
$P_P(r)$	$\ln 4 - 1$ ≈ 0.386294	$3 - \ln 16$ ≈ 0.227411
$P_{\mathrm{GOE}}(r)$	$2(2-\sqrt{3})$ ≈ 0.535898	≈ 0.351522
$P_{\mathrm{GOE}}(r) + \delta P(r)$	≈ 0.530745	≈ 0.346437

TABLE 1.1: Moments of the gap-ratio parameter r calculated from the distributions corresponding to localised and ergodic systems.

1.4.2 Entanglement

A key observation is that the entanglement across a cut in the system behaves differently in the ergodic and localised phases. The entanglement between two parts of a system, A and its complement B, can be quantified by the von Neumann entanglement entropy

$$S_{\mathrm{vN}}(\rho_A) = -\mathrm{Tr}\rho_A \ln \rho_A, \tag{1.24}$$

where ρ_A is the reduced density matrix of subsystem A, found by tracing over the degrees of freedom in subsystem B in the full-system density matrix. The ergodic phase is characterised by long-range entanglement, so the von Neumann entanglement entropy across a cut grows with the volume of the subsystem (i.e. $\sim l^d$ for a subsystem of linear size l), whereas in the localised phase the entanglement is short-ranged, so the entanglement entropy follows an area law (i.e. $\sim l^{d-1}$) [18]. It is straightforward to show that the von Neumann entropy is equal to the thermodynamic entropy S_{th} for a thermal

density matrix, $\rho \sim \exp(-\beta H)$:

$$\begin{aligned} S_{\mathrm{vN}}(\rho_{\mathrm{th}}) &= -\mathrm{Tr}\rho_{\mathrm{th}} \ln \rho_{\mathrm{th}} \\ &= -\mathrm{Tr} \sum_{\alpha} \frac{1}{Z} e^{-\beta E_\alpha} \ln \left(\frac{1}{Z} e^{-\beta E_\alpha} \right) |\alpha\rangle\langle\alpha| \\ &= \beta \sum_{\alpha} \frac{1}{Z} e^{-\beta E_\alpha} E_\alpha + \ln Z \sum_{\alpha} \frac{1}{Z} e^{-\beta E_\alpha} \\ &= \beta E + \ln Z = \beta E - \beta F = \beta T S_{\mathrm{th}} \\ &= S_{\mathrm{th}}, \end{aligned} \tag{1.25}$$

where Z is the partition function and we have set $k_B = 1$. As S_{th} is extensive in system size by definition, the area-law scaling in the localised phase clearly signifies a failure to thermalise.

It was observed that the fluctuations in the entanglement entropy of the eigenstates have a maximum at the MBL transition, and this has become a common diagnostic of the critical disorder strength [50, 55]. This peak can be understood in a simple way: in the vicinity of the MBL transition, a small difference in disorder strength (or energy density, in the presence of a mobility edge) can cause the entanglement properties to change, so the variance of entanglement entropy will diverge with system size over a window that contains the MBL transition as it includes both extended and localised states [50]. The red squares and green circles in Fig. 1.1 show the position of the MBL transition as determined by the scaling properties and fluctuations of the entanglement entropy respectively.

The time-dependence of the entanglement entropy also has distinctive features in the MBL phase. If we initialise a system in a non-entangled state (which is not an eigenstate), and observe how the entanglement entropy across a cut depends on time, we find an unbounded logarithmic growth with time, $S \sim \ln(Vt)$, where V is the interaction strength [80–82]. Contrastingly, in a thermalising phase the entanglement growth shows a power-law

behaviour [18]. This is also distinct from the non-interacting Anderson insulator, which shows no spreading of entanglement after an initial fast relaxation [18, 81].

1.4.3 Eigenvector measures

The behaviour of the wavefunction is perhaps the most obvious indicator of localisation, as it directly indicates the populations of individual basis states within the eigenstates of the model. A common method in non-interacting systems is to measure the moments of eigenstates $|\psi_\alpha\rangle$ in the position basis $\{|x\rangle\}$ [17]:

$$I_q^\alpha = \sum_x |\langle x|\psi_\alpha\rangle|^{2q} . \tag{1.26}$$

A fully extended state will scale with the system size V as $\langle x|\psi_\alpha\rangle \sim V^{-1/2}$, and $I_q^\alpha \sim V^{1-q}$, while a localised state decays exponentially with distance, so $I_q^\alpha \sim$ constant as long as the system extends beyond the localisation length. The inverse participation ratio (IPR), defined as I_2^α, quantifies the inverse number of sites occupied by $|\psi_\alpha\rangle$ in real space. In an ergodic state the IPR will decay as V^{-1}, but if $I_2^\alpha \sim V^{-D_2}$ where $0 < D_2 < 1$, the state is sub-extensive in real space, and is described as delocalised but non-ergodic. We may generalise this to other moments of $|\psi_\alpha\rangle$ as $I_q^\alpha \sim V^{D_q(1-q)}$; if these generalised dimensions D_q depend on q, as is the case at the Anderson transition [3], the eigenstate is called multifractal.

An analogous approach is taken in many-body systems, applying the idea of localisation in state space. For an eigenstate $|\alpha\rangle$ the moments are defined as [17, 83]:

$$I_q^\alpha = \sum_n |\langle n|\alpha\rangle|^{2q} \sim \mathcal{N}^{D_q(1-q)} \tag{1.27}$$

where $|n\rangle$ is a basis with dimension $\mathcal{N}$ (in a chain of d-level systems with length L, for example, $\mathcal{N} = d^L$). For a thermalising state, we expect to see a result similar to that for a fully random matrix in the GOE: $I_2^\alpha \approx 3/\mathcal{N}$ [83]. These quantities clearly depend on the basis chosen for $|n\rangle$, and while the position basis is the obvious one for single-particle localisation, the choice

is less obvious in an interacting system. To study localisation in real space one might study the IPR of an eigenstate in the Pauli basis [83], while the IPR of an arbitrary state with respect to the energy eigenstates is related to its survival probability [84].

Another quantity related to D_q is the Renyi entropy:

$$S_q^{(R),\alpha} = \frac{1}{1-q} \ln \left(I_q^\alpha \right) \sim D_q \ln \mathcal{N}, \tag{1.28}$$

and the Shannon entropy corresponds to the $q \to 1$ limit:

$$S_{\mathrm{Sh}}^\alpha = \lim_{q \to 1} S_q^{(R),\alpha} = -\sum_n |\langle n|\alpha\rangle|^2 \ln |\langle n|\alpha\rangle|^2 , \tag{1.29}$$

which allows us to calculate D_1 (as $I_1^\alpha \equiv 1$). The colour scheme in Fig. 1.1 corresponds to D_1, showing the difference in the scaling of S_{Sh} with system size between the ergodic and localised phases. It has been noted that S_{Sh} and S_{vN} exhibit very similar behaviour, but the Shannon entropy is less expensive to calculate numerically [83].

1.4.4 Breakdown of the eigenstate thermalisation hypothesis

In a phase that fails to thermalise we can expect that operators will not be well described by the ETH ansatz, which we can thus use to test for the MBL phase. A key assumption of the ETH is that the expectation values of local observables taken with respect to the eigenstates of the Hamiltonian, known as eigenstate expectation values (EEVs), are smooth functions of their eigenenergies. Therefore examining the statistical distribution of the difference between the EEVs of consecutive eigenstates, $\delta\langle O_n\rangle = \langle O\rangle(E_{n+1}) - \langle O\rangle(E_n)$, offers a simple method for determining whether or not a system is localised [48, 49, 85]. In the thermalising phase this should be peaked at zero with a width that decreases with increasing system size [48, 86], whereas this will not be the case in the localised phase. Considering the operator s_n^z as an example, deep in the localised phase one would expect the eigenstates to tend to the Pauli basis states with the eigenenergies dependent on the

specific disorder realisation. In this limit, the expectation values of s_n^z will be those of a spin either aligned or anti-aligned with the field (i.e. $\pm 1/2$), with no correlation between the values in neighbouring eigenstates. As a result, the distribution of $\delta\langle s_n^z\rangle$ will be sharply peaked around the values 0 and ± 1, which correspond to neighbouring eigenstates with the same or different expectation values respectively.

The off-diagonal elements can also be used as a diagnostic of interesting behaviour. While the diagonal elements of an operator describe the average values of quantities, the off-diagonal elements are associated with the relaxation to these averages. As such, the behaviour of off-diagonal elements in the ergodic phase preceding the MBL transition has received recent interest. It has been found in numerical studies that the onset of anomalous subdiffusive transport is accompanied by a change in the distributions of off-diagonal matrix elements, which develop long tails, violating Berry's conjecture that the fluctuations should be Gaussian [63, 67]. This behaviour is demonstrated in Fig. 1.2 [63], where the distributions are consistently Gaussian for all system sizes with weak disorder, but develop long tails when the disorder is stronger. The matrix elements of spin operators in the one-dimensional disordered XXZ model were also shown to satisfy a modified version of the ETH, which includes a power-law correction to the exponential decay of the off-diagonal elements with system size,

$$\langle\alpha|A|\beta\rangle \propto e^{-s(E)L/2}L^{\gamma/2}R_{\alpha,\beta}, \qquad |E_\alpha - E_\beta| < L^{-\gamma-1}, \tag{1.30}$$

where the additional power-law comes from the behaviour of $f(E,\omega)$ in (1.14) [37, 63]. This power-law is related to the subdiffusive transport through the current scaling exponent γ [63].

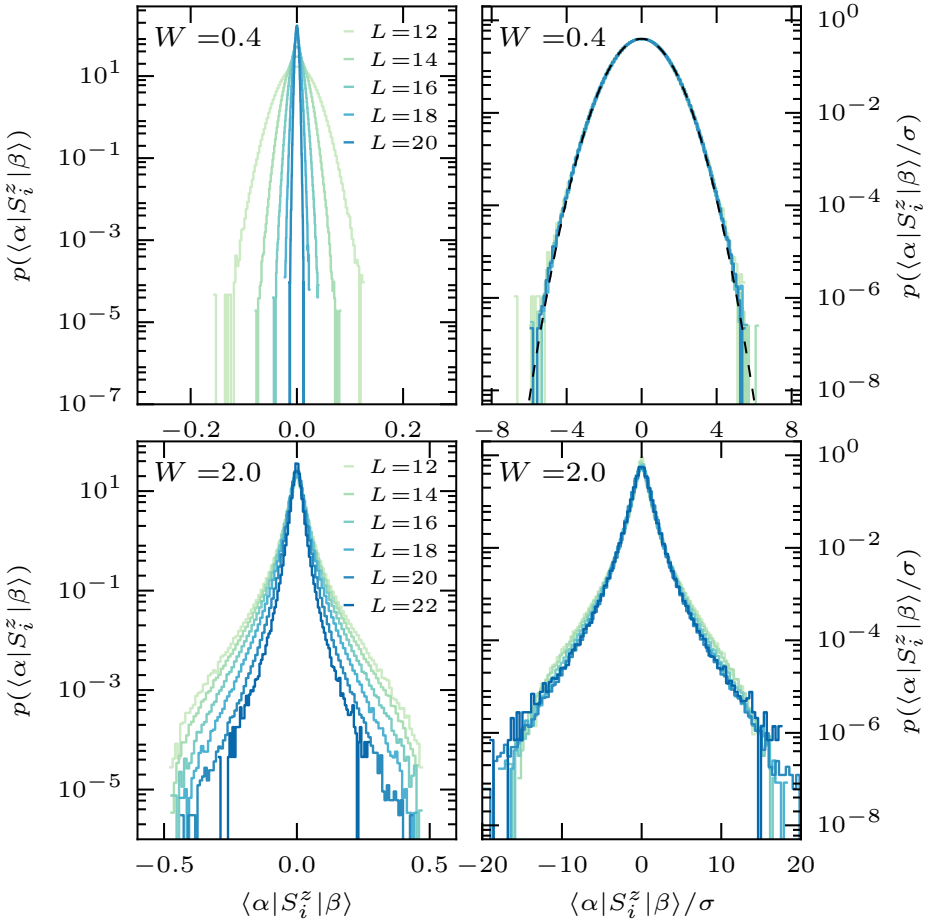

FIGURE 1.2: The distributions of off-diagonal elements of s_n^z in the eigenbasis of the disordered XXZ model for weak disorder (upper panels) and stronger disorder (lower panels). The panels on the right have been rescaled horizontally by the standard deviation of the data, and the successful collapse of all system sizes onto the same curve shows that the results are indicative of the true behaviour in the thermodynamic limit. Figure reproduced from [63].

Chapter 2

Systems with time-dependent parameters

When a system is affected by time-dependent parameters (i.e. when it exists in a time-dependent environment) it adds another layer of complexity to its equations of motion. In this chapter we will discuss the effects of this time-dependence on quantum systems, namely non-adiabatic effects caused by a time-dependent Hamiltonian. These effects have become increasingly prominent with the development of sophisticated cold-atom experiments in which the timescales of the dynamics can be on the order of milliseconds; this is slow enough that it is experimentally viable to change the Hamiltonian much faster than the system can react, and to properly probe non-equilibrium quantum effects. We will then move on to consider systems which are affected by classical noise, both 'white' noise and noise with more structure in its temporal correlations, and we will discuss the practicalities of determining the time-evolution of such systems.

2.1 Time-evolution in quantum systems

The dynamics of a quantum system are governed by the Schrödinger equation, which describes the time-dependence of a quantum state $|\psi(t)\rangle$ due to a Hamiltonian $\mathcal{H}(t)$:

$$i\partial_t|\psi(t)\rangle = \mathcal{H}(t)|\psi(t)\rangle. \tag{2.1}$$

If we define the unitary operator which evolves a state from an initial time t_0 to a final time t, $|\psi(t)\rangle = U(t,t_0)|\psi(t_0)\rangle$, it follows that the unitary obeys the same equation:

$$i\partial_t U(t) = \mathcal{H}(t)U(t), \tag{2.2}$$

where $U(t) := U(t,0)$.

A generic expression for $U(t)$ (known as a Dyson series) can be derived by integrating (2.2) and repeatedly inserting the resulting equation into itself:

$$\begin{aligned}
U(t) &= 1 - i\int_0^t \mathrm{d}t'\mathcal{H}(t')U(t') \\
&= 1 - i\int_0^t \mathrm{d}t'\mathcal{H}(t')\left[1 - i\int_0^{t'} \mathrm{d}t''\mathcal{H}(t'')U(t'')\right] \\
&= 1 - i\int_0^t \mathrm{d}t'\mathcal{H}(t') - \int_0^t \mathrm{d}t'\int_0^{t'} \mathrm{d}t''\mathcal{H}(t')\mathcal{H}(t'') \\
&\quad + i\int_0^t \mathrm{d}t'\int_0^{t'} \mathrm{d}t''\int_0^{t''} \mathrm{d}t'''\mathcal{H}(t')\mathcal{H}(t'')\mathcal{H}(t''') + ... \\
&= \mathcal{T}\sum_{n=0}^{\infty}\frac{(-i)^n}{n!}\left(\int_0^t \mathrm{d}t'\mathcal{H}(t')\right)^n \\
&= \mathcal{T}\exp\left(-i\int_0^t \mathrm{d}t'\mathcal{H}(t')\right)
\end{aligned} \tag{2.3}$$

where $\mathcal{T}$ is the time-ordering operator which dictates that the following operators must act in order of increasing time, as enforced by the limits of the integrals in the third line. The factor of $1/n!$ in the penultimate line appears as a result of extending the upper limits of each integration to t, which includes the $n!$ possible orderings of the n operators in the integrand.

2.1.1 Systems with time-independent Hamiltonians

The form of U in (2.3) immediately suggests that for systems in which $\mathcal{H}(t) = \mathcal{H}$, the logical choice of basis is the eigenbasis of the Hamiltonian $\{|n\rangle\}$. Clearly $U(t)$ is also diagonal in this basis, so there can be no transitions, and

the unitary and quantum state at all times can be written simply as:

$$\begin{aligned} U(t) &= \sum_n e^{-iE_n t} \big|n\big\rangle\big\langle n\big| \\ \big|\psi(t)\big\rangle &= \sum_n \big\langle n\big|\psi(0)\big\rangle \; e^{-iE_n t} \; \big|n\big\rangle \end{aligned} \tag{2.4}$$

where E_n is the energy eigenvalue of the eigenstate $|n\rangle$.

2.1.2 Systems with time-dependent Hamiltonians

The problem is more complicated if we consider a system in which the Hamiltonian $\mathcal{H}(t)$ changes in time, as the eigenbasis of the Hamiltonian becomes time-dependent and transitions between these instantaneous eigenstates are possible. If $\mathcal{H}(t)$ changes smoothly from $\mathcal{H}(0) = \mathcal{H}^{(i)}$ to $\mathcal{H}(T) = \mathcal{H}^{(f)}$, we can gain some insight by writing the state in the instantaneous eigenbasis of $\mathcal{H}(t)$, $\{|n(t)\rangle\}$:

$$\big|\psi(t)\big\rangle = \sum_n c_n(t) \big|n(t)\big\rangle. \tag{2.5}$$

The Schrödinger equation then gives the equations of motion for the amplitudes $c_n(t)$:

$$i\partial_t c_n(t) = E_n(t) c_n(t) - i \sum_m \big\langle n(t)\big|\partial_t\big|m(t)\big\rangle c_m(t), \tag{2.6}$$

where $E_n(t)$ is the instantaneous eigenenergy of $|n(t)\rangle$. Importantly this has off-diagonal terms of the form $\langle n(t)|\partial_t|m(t)\rangle$, which generate transitions between the instantaneous eigenstates of $\mathcal{H}(t)$. A more intuitive form of (2.6) in terms of the time-derivative of the Hamiltonian is:

$$\begin{aligned} i\partial_t c_n(t) = \Big(E_n(t) - i\big\langle n(t)\big|\partial_t\big|n(t)\big\rangle\Big) c_n(t) \\ - i \sum_{m\neq n} \frac{\big\langle n(t)\big|\partial_t \mathcal{H}(t)\big|m(t)\big\rangle}{E_m(t) - E_n(t)} c_m(t). \end{aligned} \tag{2.7}$$

This can be shown by taking the inner product of the time-derivative of $\mathcal{H}(t)|m(t)\rangle$ and $|n(t)\rangle$ with $m \neq n$:

$$\begin{aligned}
\langle n(t)|\partial_t\Big[\mathcal{H}(t)|m(t)\rangle\Big] &= \langle n(t)|\partial_t\Big[E_m(t)|m(t)\rangle\Big] \\
\langle n(t)|\Big[\partial_t\mathcal{H}(t)|m(t)\rangle + \mathcal{H}(t)\partial_t|m(t)\rangle\Big] &= E_m(t)\langle n(t)|\partial_t|m(t)\rangle \\
\langle n(t)|\Big[\partial_t\mathcal{H}(t)|m(t)\rangle + E_n(t)\partial_t|m(t)\rangle\Big] &= E_m(t)\langle n(t)|\partial_t|m(t)\rangle \\
\langle n(t)|\partial_t\mathcal{H}(t)|m(t)\rangle &= (E_m(t) - E_n(t))\,\langle n(t)|\partial_t|m(t)\rangle
\end{aligned} \tag{2.8}$$

where the $\partial_t E_m(t)\langle n(t)|m(t)\rangle$ term that would appear on the second line vanishes due to orthogonality.

There are two simple limits where the evolution can generically be described exactly.

The sudden limit ($T \to 0$)

If a system is prepared in a state $|\psi(0)\rangle$, and at $t = 0$ the Hamiltonian is instantaneously changed from $\mathcal{H}^{(i)}$ to $\mathcal{H}^{(f)}$, the system has no time to react. As a result, the evolution of the system can be trivially evaluated in $\{|n_f\rangle\}$, the eigenbasis of $\mathcal{H}^{(f)}$:

$$\begin{aligned}
|\psi(0)\rangle &= \sum_n \langle n_i|\psi(0)\rangle\ |n_i\rangle = \sum_n \langle n_f|\psi(0)\rangle\ |n_f\rangle \\
|\psi(t)\rangle &= \sum_n\ \langle n_f|\psi(0)\rangle\ e^{-iE_n^{(f)}t}\ |n_f\rangle,
\end{aligned} \tag{2.9}$$

where $E_n^{(f)}$ is the eigenenergy of the state $|n_f\rangle$. Despite the apparent simplicity of this limit, the study of sudden changes to the parameters of a many-body Hamiltonian (known as a 'quantum quench') is an active area of theoretical research with a rich phenomenology [87].

The adiabatic limit ($T \to \infty$)

The opposite limit, in which the Hamiltonian changes infinitely slowly with time, can be understood by noting that the off-diagonal terms in (2.6) contain

a time-derivative, so must decrease in magnitude as T^{-1}. Thus, as $T \to \infty$ the transitions between the instantaneous eigenstates of $\mathcal{H}(t)$ vanish, and the system will adiabatically follow this basis. In other words, the populations of the instantaneous eigenstates of $\mathcal{H}(t)$ are constant in time, and they accumulate a relative phase:

$$\big|\psi(t)\big\rangle = \sum_n \big\langle n(0)\big|\psi(0)\big\rangle \; e^{-i\int_0^t \mathrm{d}t' E_n(t')+i\phi_n(t)} \; \big|n(t)\big\rangle. \tag{2.10}$$

The first contribution to the phase, known as dynamical phase, is a simple generalisation of the linear phase accumulation in (2.4). The second contribution is known as geometric phase, which has the form:

$$\phi_n(t) = i\int_0^t \mathrm{d}\tau \langle n(\tau)|\partial_\tau|n(\tau)\rangle \tag{2.11}$$

and results from the changing eigenbasis of the Hamiltonian. Note that $\phi_n(t)$ is a real number, so this is purely a contribution to the phase and has no effect on the populations of levels.

2.1.3 The adiabatic theorem

The adiabatic theorem states that a quantum system in an instantaneous eigenstate will remain in that eigenstate if a perturbation acts on it sufficiently slowly and if there is a gap separating the eigenenergy from the rest of the spectrum [88]. This corresponds to the $T \to \infty$ limit discussed above, and we shall now consider this more quantitatively to understand when the state $|\psi(t)\rangle$ can be accurately approximated by (2.10). A derivation of these results can be found in [89].

To the next order beyond the adiabatic approximation, the probability for a non-adiabatic transition to occur between the states m and n is given by:

$$P_{m\to n} = \left|\int_0^T \mathrm{d}t e^{i\int_0^t \mathrm{d}t'(E_n(t')-E_m(t'))} \frac{\langle n(t)|\partial_t \mathcal{H}(t)|m(t)\rangle}{E_n(t)-E_m(t)}\right|^2. \tag{2.12}$$

A rough approximation of the transition probability can be made by assuming

that $\Delta E_{n,m}(t) = E_n(t) - E_m(t)$ and $D_{n,m}(t) = \langle n(t)|\partial_t \mathcal{H}(t)|m(t)\rangle$ are constant in time:

$$\begin{aligned} P_{m\to n} &\approx \left|\frac{D_{n,m}}{\Delta E_{n,m}^2}\right|^2 2\left[1-\cos(\Delta E_{n,m}\, T)\right] \\ &\sim \left|\frac{D_{n,m}}{\Delta E_{n,m}^2}\right|^2, \end{aligned} \tag{2.13}$$

where we have discarded the details in the second line, noting only that $2(1-\cos x)$ is a number of order 1 for a typical (i.e. non-fine-tuned) time T. Assuming that $\Delta E_{n,m}(t)$ and $D_{n,m}(t)$ are smooth functions of time, the transition probability between these two states will generally be smaller than

$$P_{m\to n} \lesssim \mathrm{Max}\left|\frac{D_{n,m}(t)}{\Delta E_{n,m}(t)^2}\right|^2, \tag{2.14}$$

where the maximum is taken over t. The condition that $P_{m\to n} \ll 1$ gives us a criterion for the validity of the adiabatic approximation. It is worth noting that the criterion of the right-hand side of (2.14) being much smaller than one is overly restrictive in practice, but has been used to good effect in protocols designed to minimise non-adiabatic transitions [90].

2.1.4 The Landau-Zener problem

Non-adiabatic effects are well illustrated in the Landau-Zener problem, a time-dependent quantum system solved simultaneously by L. D. Landau [91], C. Zener [92], E. Majorana [93], and E. C. G. Stueckelberg [94] in 1932. They considered a two-level system in which two states with an energy difference that depends linearly on time with a 'speed' v are coupled by a constant parameter Δ:

$$\mathcal{H}_{\mathrm{LZ}}(t) = \frac{vt}{2}\sigma^z + \frac{\Delta}{2}\sigma^x, \tag{2.15}$$

where σ^μ are Pauli matrices in the $\{|\uparrow\rangle, |\downarrow\rangle\}$ basis. The system is initialised in the state $|\psi(t=-\infty)\rangle = |\downarrow\rangle$, and the quantity of interest is the probability

that it will be in the same state at $t = +\infty$:

$$P_{\mathrm{LZ}} = \left| \langle \downarrow | \psi(t = +\infty) \rangle \right|^2. \tag{2.16}$$

The instantaneous eigenstates of the system are

$$\begin{aligned} \big| + (t) \big\rangle &= \sin\theta(t) \left| \uparrow \right\rangle - \cos\theta(t) \left| \downarrow \right\rangle \\ \big| - (t) \big\rangle &= \cos\theta(t) \left| \uparrow \right\rangle + \sin\theta(t) \left| \downarrow \right\rangle \end{aligned} \tag{2.17}$$

where $\theta(t) = \arctan\left(\Delta/(vt)\right)/2$, with $\theta \in [0, \pi/2]$. The corresponding eigenenergies are

$$E_{\pm} = \pm\frac{1}{2}\sqrt{v^2 t^2 + \Delta^2}, \tag{2.18}$$

so this model has an avoided crossing at $t = 0$, where the energy gap is $E_+ - E_- = \Delta$. Note that at $t = \pm\infty$ the states $|\uparrow\rangle$ and $|\downarrow\rangle$ are the eigenstates of the system, but they exchange their roles as the ground and excited states, so P_{LZ} gives the probability that a non-adiabatic transition does occur.

The solutions to the equations of motion for $c_\uparrow$ and $c_\downarrow$, the coefficients of the basis states in $|\psi(t)\rangle$, are given by parabolic cylinder functions (a particular limit of the standard hypergeometric function) [5]. We may therefore state an exact expression for the transition probability:

$$P_{\mathrm{LZ}} = \exp\left(-\frac{\pi\Delta^2}{2v}\right). \tag{2.19}$$

This expression contains the behaviour we saw when considering the adiabatic theorem: the transition probability increases as the process happens more quickly (increasing v) and when the eigenenergies are closer together (decreasing Δ). Fig. 2.1 shows the transition probability of the Landau-Zener problem as a function of time for four combinations of v and Δ which all correspond to the same P_{LZ}. Although the curves tend to the same value as $t \to \infty$, the curves corresponding to a larger Δ (i.e. a larger energy gap between the adiabatic states) change in magnitude over a shorter window

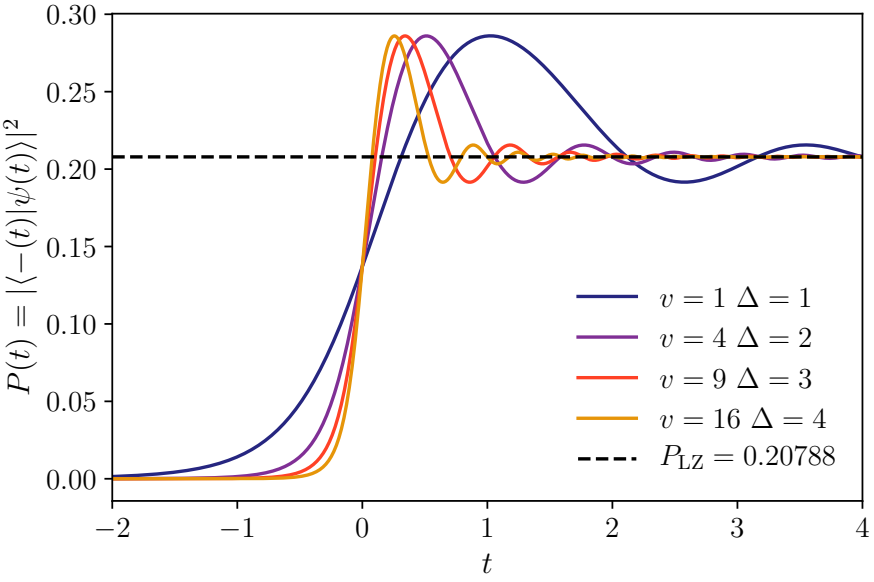

FIGURE 2.1: The probability of a non-adiabatic transition in the Landau-Zener problem, shown as a function of time for four sets of parameters with the same value of P_{LZ}. Note that the rescaling $\Delta \to \gamma\Delta$ and $v \to \gamma^2 v$ allows us to collapse the $P(t)$ curves onto a single line by rescaling time as $t \to \gamma t$.

of time, showing that the non-adiabatic effects are strongest when the eigenstates are closest together in energy (around $t = 0$), as indicated in (2.14).

2.2 Systems with time-dependent noise

While we often consider time-dependent systems that are tightly controlled, we may also be interested in systems where the time-dependence is not deterministic. In this section we will consider systems that are affected by parameters which fluctuate randomly with time; we shall call the fluctuations in these parameters 'noise'. Of course, knowledge of the behaviour of such a system under a single realisation of the noise is somewhat meaningless. It is far more instructive to learn about the statistical properties of the system's behaviour under the influence of many realisations of the noise (i.e. its average behaviour and the size of fluctuations around this average), and how these properties relate to the statistical properties of the noise.

A very simple example of this can be seen in a Gaussian random walk: a particle can hop in a one-dimensional landscape, and the length of each hop x_n is independently drawn from a Gaussian distribution with average μ and standard deviation σ. After N hops, the particle is at a position $X_N = \sum_{n=1}^{N} x_n$, which is itself a Gaussian-distributed variable with an average of $N\mu$ and a standard deviation of $\sigma\sqrt{N}$. This square-root growth of the standard deviation is a common feature of simple random processes and is typical of diffusion.

2.2.1 'White' noise

A key component of noisy processes is the stochastic variable $\eta(t)$, which fluctuates rapidly and randomly according to some statistical distribution. The distribution of $\eta(t)$ is often chosen to be Gaussian, due to its simple properties. The two-time correlator of $\eta(t)$ is given by:

$$g(t, t') = \overline{\eta(t)\eta(t')} = \Lambda^2\, \delta(t - t'), \tag{2.20}$$

where the bar denotes an average over realisations of the noise. The delta function indicates that the value of the noise at a time t is completely uncorrelated with its value at any other time, and this type of noise is often described as 'white' (the Fourier transform of the delta function in time is a constant, so the spectrum of the noise features equally important contributions from all frequencies) [95, 96]. These variables appear in stochastic differential equations, such as the Langevin equation. The original Langevin equation, written down by P. Langevin in his 1908 paper [97], describes the velocity of a particle undergoing Brownian motion in a fluid:

$$m\, \partial_t v(t) = -\lambda v(t) + \eta(t), \tag{2.21}$$

where m is the particle's mass, λ describes the strength of the viscous drag experienced by the particle, and $\eta(t)$ is a stochastic variable representing the fluctuating force that the particle experiences from many collisions with the molecules that make up the fluid. As such, this equation does not take into

account the specific motion of the molecules in the fluid. The exact solution of this equation for a given realisation of the noise $\eta(t)$ is given by:

$$v(t) = v_0 + m^{-1} \int_0^t \mathrm{d}t' \left(-\lambda v_0 + \eta(t')\right) e^{-\lambda(t-t')/m}. \tag{2.22}$$

We can now calculate the average and variance of $v(t)$ over all realisations of the noise by applying (2.20):

$$\begin{aligned} \overline{v(t)} &= v_0\, e^{-\lambda t/m}, \\ \overline{\left(v(t) - \overline{v(t)}\right)^2} &= \frac{\Lambda^2}{2m\lambda}\left(1 - e^{-2\lambda t/m}\right). \end{aligned} \tag{2.23}$$

Clearly, after a large amount of time the system loses its memory of the initial conditions (as can be seen from the average tending to zero), and $\overline{v(t)^2}$ tends to a constant value. We can also calculate its position by integrating (2.22), and the average over noise realisations reveals the square-root growth of the displacement:

$$\overline{(x(t) - x_0)^2} = \frac{\Lambda^2}{\lambda^2} t. \tag{2.24}$$

This result is the same as that found shortly before by A. Einstein in his seminal paper on Brownian motion [98].

Of course, we will not always want to solve such simple equations, and will often have to resort to numerical methods. The stochastic Heun algorithm can be used to time-evolve systems described by an equation of motion with the form:

$$\partial_t x(t) = f(x(t), t) + g(x(t), t)\, \eta(t) \tag{2.25}$$

where $f(x(t), t)$ and $g(x(t), t)$ are smooth, deterministic functions of their arguments, and $x(t)$ may be a vector [96, 99]. We discretise time onto a grid with timestep Δt, and $x_n := x(t_n)$ is related to $x_{n+1} := x(t_n + \Delta t)$ by:

$$\begin{aligned} x_{n+1} = x_n &+ \frac{1}{2}\left[f(x_n, t_n) + f(\tilde{x}_{n+1}, t_{n+1})\right] \Delta t \\ &+ \frac{1}{2}\left[g(x_n, t_n) + g(\tilde{x}_{n+1}, t_{n+1})\right] \xi_n, \end{aligned} \tag{2.26}$$

where the intermediate value $\tilde{x}_n$ is given by:

$$\tilde{x}_{n+1} = x_n + f(x_n, t_n)\,\Delta t + g(x_n, t_n)\xi_n. \tag{2.27}$$

The random variables ξ_n represent the integral of the stochastic variable over the timestep, $\xi_n = \int_{t_{n-1}}^{t_n} \mathrm{d}t' \eta(t')$, so these are a sequence of uncorrelated random variables with zero mean (any non-zero average can be moved into the definition of $f(x(t), t)$) and standard deviation $\sqrt{\Delta t}$, which can be seen from the correlation function (2.20).

It is important to note that integrating a stochastic variable is not trivial. If one defines the integral as a discretised sum over the integrand evaluated at each timestep, then when the length of the timestep is taken to zero, the choice of where in the timestep to sample $f(x(t), t)$ and $g(x(t), t)$ affects the result. Two common choices are Itô [100], which samples at the start of the timestep, and Stratonovich [101], which samples in the middle of the timestep. Many results are derived using the Itô formalism, but Itô calculus does not behave in the same way as ordinary calculus (i.e. the chain rule of differentiation is not valid), whereas the Stratonovich choice is consistent with the standard rules of calculus [95]. The results of these two formalisms can be related to each other by a simple transformation of $f(x(t), t)$ and $g(x(t), t)$, and their difference will not be an issue in the work presented in later chapters. As such, we will not discuss the matter further, other than to note that the Heun algorithm presented above corresponds to the Stratonovich interpretation of stochastic calculus [99].

2.2.2 'Real' noise

Of course, in reality there can be no noise that truly has a correlation time of zero, and the structure of the correlation function may be important to the physics of the system. In this situation we may want to generate time-dependent parameters with the desired statistical properties, and to time-evolve the system under their influence. As we have access to actual

realisations of the noise, we do not need specialised stochastic algorithms to numerically integrate the equations of motion, and we can use standard numerical methods.

In order to understand how we might generate noise with an arbitrary two-time correlation function, it is instructive to consider the Fourier transform of the noise $\tilde{\eta}(\omega)$. Firstly, the requirement that the noise is real (which it will be for our purposes) imposes the condition that $\tilde{\eta}(-\omega) = \tilde{\eta}^{\star}(\omega)$, which can be clearly seen from the definition

$$\eta(t) = \frac{1}{\sqrt{2\pi}} \int_{-\infty}^{+\infty} \mathrm{d}\omega \, e^{i\omega t} \, \tilde{\eta}(\omega). \tag{2.28}$$

The form of the two-frequency correlation function of $\tilde{\eta}(\omega)$ is also constrained by the requirement that the two-time correlation function is only a function of the difference between the two times, i.e. $g(t, t') = g(t - t')$. We find that

$$\begin{aligned}
\tilde{g}(\omega, \omega') &= \overline{\tilde{\eta}(\omega)\tilde{\eta}(\omega')} \\
&= \frac{1}{2\pi} \int_{-\infty}^{+\infty} \mathrm{d}t \int_{-\infty}^{+\infty} \mathrm{d}t' e^{-i\omega t - i\omega' t'} \, g(t - t') \\
&= \frac{1}{2\pi} \int_{-\infty}^{+\infty} \mathrm{d}x \int_{-\infty}^{+\infty} \mathrm{d}y \, e^{-i(\omega+\omega')x - i(\omega-\omega')y/2} \, g(y) \\
&= \delta(\omega + \omega') \int_{-\infty}^{+\infty} \mathrm{d}y e^{-i\omega y} g(y) \\
&= \sqrt{2\pi}\delta(\omega + \omega') \, \mathcal{F}[g](\omega),
\end{aligned} \tag{2.29}$$

where the changes of variables are $x = (t + t')/2$ and $y = t - t'$ and $\mathcal{F}[g](\omega)$ is the Fourier transform of $g(t)$ evaluated at ω. Thus we see that noise which is correlated in time only has correlations in frequency between the parts $\omega \to -\omega$ (which we knew had to be the case from the condition that η be real).

Based on this, we can build the desired noise by generating uncorrelated noise in frequency space, filtering it appropriately, and Fourier-transforming it back into time. The following algorithm has been shown to efficiently generate noise with a chosen two-time correlation function $g(t)$ [102]:

- Discretise time onto a grid of length N with a step size Δt, where Δt is much smaller than any timescale in the system. In frequency space this results in a discrete set of frequencies $\omega_\mu = (2\pi\mu)/(N\Delta t)$.

- Generate a string of N complex random numbers $\alpha_\mu = \alpha(\omega_\mu)$, one for each ω_μ, with $\overline{\alpha_\mu} = 0$ and $\overline{\alpha_\mu \alpha_\nu} = \delta_{\mu+\nu,0}$. This can be achieved by generating two strings of uncorrelated real random numbers, a_μ and b_μ. For $\mu \neq 0$ they must be constructed such that $a_\mu = a_{-\mu}$ and $b_\mu = -b_{-\mu}$ with $\overline{a_\mu^2} = \overline{b_\mu^2} = 1/2$, while $\overline{a_0^2} = 1$ and $b_0 = 0$. We can then construct the desired series as $\alpha_\mu = a_\mu + ib_\mu$.

- The noise in frequency space $\tilde{\eta}_\mu = \tilde{\eta}(\omega_\mu)$ is then made by weighting α_μ by the square root of the two-frequency correlation function at that frequency:

$$\tilde{\eta}_\mu = (2\pi)^{-1/4} \sqrt{N\,\Delta t\,\mathcal{F}[g](\omega_\mu)}\alpha_\mu. \tag{2.30}$$

  The discrete two-frequency correlation function is then:

$$\begin{aligned} \tilde{g}(\omega_\mu, \omega_\nu) &= \frac{N\Delta t}{\sqrt{2\pi}} \sqrt{\mathcal{F}[g](\omega_\mu)\,\mathcal{F}[g](\omega_\nu)}\,\overline{\alpha_\mu \alpha_\nu} \\ &= \sqrt{2\pi}\frac{N\Delta t}{2\pi}\,\mathcal{F}[g](\omega_\mu)\delta_{\mu+\nu,0}, \end{aligned} \tag{2.31}$$

  where $(\Delta\omega)^{-1}\delta_{\mu+\nu,0} = (N\Delta t/2\pi)\delta_{\mu+\nu,0}$ is a normalised discrete approximation to a δ-function, so we have come to a discrete approximation of (2.29).

- A fast Fourier transform algorithm can now transform $\tilde{\eta}(\omega_\mu)$ into $\eta(t_n)$.

Noise with a correlation time τ can be approximated by white noise if τ is much smaller than any other timescale in the system by taking the appropriate δ-function limit of the true correlation function as $\tau \to 0$ [95]. This limiting procedure leads to a Stratonovich stochastic differential equation with the same parameters as the original differential equation [95]. As a result, the Stratonovich interpretation is often favoured in physics, as the white noise will usually be an approximation of a smoothly fluctuating variable.

Chapter 3

The disordered XYZ spin chain

In this chapter we study the effect that U(1) symmetry-breaking (i.e. violation of the conservation of the z component of the total magnetisation) has on the MBL transition in one-dimensional spin chains. The results presented in this chapter are part of a more general numerical study [66], which explores energy transport and many-body localisation in the XYZ spin chain. The work on energy transport finds evidence for ballistic transport in the disorder-free model, and diffusive and subdiffusive regimes at weak-to-intermediate disorder strengths. The transport properties of the system in the thermodynamic limit are only visible in very large systems that can only be simulated using matrix-product methods such as time-evolving block decimation (TEBD), which converge poorly when the disorder is strong. The work presented in this chapter therefore uses exact diagonalisation methods on smaller systems to focus on the strong-disorder region of the phase diagram, up to and beyond the MBL transition.

3.1 The XYZ spin chain

The XYZ model is a generalisation of the XXZ model (1.16) with arbitrary couplings between the different components of neighbouring spins. We parametrise the model as:

$$\mathcal{H}_{\mathrm{XYZ}} = \sum_{n=1}^{L} \left[(1+\eta) s_n^x s_{n+1}^x + (1-\eta) s_n^y s_{n+1}^y + \Delta s_n^z s_{n+1}^z + h_n s_n^z \right], \qquad (3.1)$$

where h_n is drawn from a uniform distribution $h_n \in [-W, W]$ as in (1.16), and η is the XY anisotropy parameter which breaks the U(1) symmetry of the model. Rewriting this in terms of spin raising and lowering operators ($s^{\pm} = s^x \pm i s^y$) makes it clear that this new term explicitly breaks the conservation of the z component of the total magnetisation:

$$\mathcal{H}_{\mathrm{XYZ}} = \sum_n \Bigg[\frac{1}{2}\left(s_n^+ s_{n+1}^- + s_n^- s_{n+1}^+\right) + \frac{\eta}{2}\left(s_n^+ s_{n+1}^+ + s_n^- s_{n+1}^-\right) + \Delta s_n^z s_{n+1}^z + h_n s_n^z \Bigg]. \tag{3.2}$$

Similarly, in the fermionic language η is the parameter that violates the conservation of the number of fermions:

$$\mathcal{H}_{\mathrm{XYZ}} = \sum_n \Bigg[\frac{1}{2}\left(c_n^\dagger c_{n+1} + c_{n+1}^\dagger c_n\right) + \frac{\eta}{2}\left(c_n^\dagger c_{n+1}^\dagger + c_{n+1} c_n\right) + \Delta c_n^\dagger c_n c_{n+1}^\dagger c_{n+1} + (h_n - \Delta)\, c_n^\dagger c_n \Bigg], \tag{3.3}$$

where we have once again dropped terms that correspond to constant global energy shifts. Note that breaking the number conservation in this way (as opposed to rotating the on-site fields away from the z-direction, for example) does not destroy the conservation of number parity. Therefore, while the Hilbert space of the XXZ Hamiltonian could be split into independent sectors each corresponding to a different number of up spins, the XYZ model can only be split into two sectors which correspond to an odd or even number of up spins.

We study this model by numerical exact diagonalisation of the Hamiltonian. The full $2^L \times 2^L$ Hamiltonian matrix for a system of length L is constructed using tensor products of L Pauli matrices (e.g. $s_n^\mu = \mathbb{I}_2^{\otimes(n-1)} \otimes s^\mu \otimes \mathbb{I}_2^{\otimes(L-n)}$, where $\mathbb{I}_2$ is the 2×2 identity matrix). Each term in $\mathcal{H}$ is then built by standard multiplication and addition of matrices, and this matrix is then projected into smaller matrices corresponding to a single symmetry sector. The eigenvectors and eigenvalues of the Hamiltonian are found through numerical

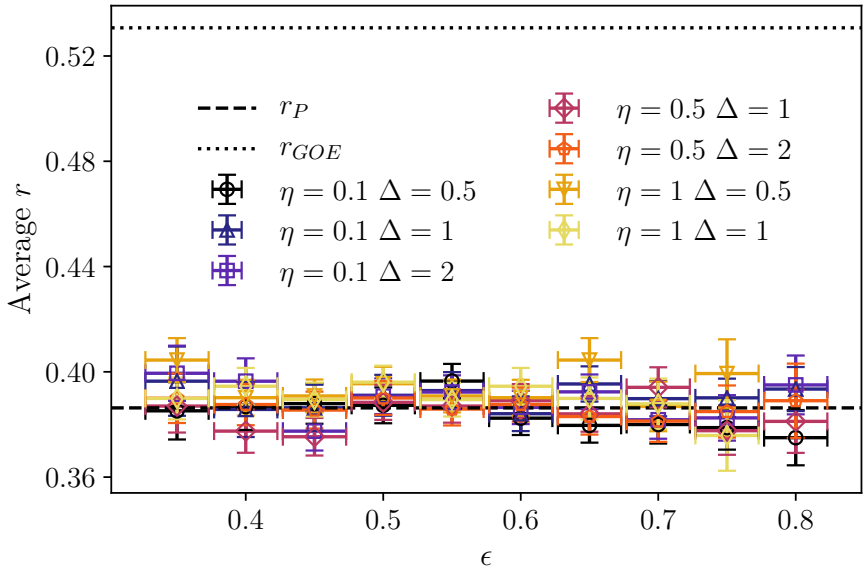

FIGURE 3.1: The gap ratio parameter r of the disorder-free ($W = 0$) XYZ model for a selection of XY anisotropies η and interaction strengths Δ, plotted as a function of energy density ϵ. The values are averaged over a small window in ϵ (indicated by horizontal bars), and twice the standard error is indicated by vertical bars.

diagonalisation in Python using the NumPy and SciPy packages [103].

3.2 The disorder-free XYZ spin chain

In the limit of no disorder, $W = 0$, the XYZ spin chain is known to be formally solvable by Bethe ansatz methods; in other words it is integrable [104, 105]. As discussed in Section 1.4.1, integrability is visible in a lack of level-repulsion in the eigenenergy spectrum, so we would expect to see the level spacings following a Poisson distribution.

Fig. 3.1 shows the average gap ratio parameter r for a selection of combinations of the XY anisotropy η and Ising anisotropy Δ, plotted as a function of the energy density $\epsilon = (E - E_{\min})/(E_{\max} - E_{\min})$ (where $E_{\min}$ and $E_{\max}$ are the lowest and highest eigenenergies of the spectrum, corresponding to $\epsilon = 0$ and 1). The data was taken on a chain of length $L = 16$ with open boundary conditions. In the absence of disorder the system possesses an

additional symmetry under the reflection of the chain about its centre. For a chain with even L there is also a symmetry with respect to the inversion of all spins, because a state with an even number of up spins maps onto another state with an even number of up spins. Therefore, the model represented in Fig. 3.1 with even L can be split into 8 independent sectors.

The averages are taken across r values from all symmetry sectors in a window in ϵ of width ± 0.023 around a target value; the target and window width are indicated by the horizontal position of the point and the horizontal bars respectively. The average and twice the standard error of this value are shown by the vertical position of the point and the vertical bars respectively (where the standard error is defined as $\sigma/\sqrt{M}$ with σ the standard deviation and M the number of values). Clearly these points fall much closer to the Poisson value of $r_P \approx 0.3863$ than to the random-matrix (GOE) value (indicated by the dashed and dotted lines respectively), and the points are more tightly distributed around r_P as L is increased, suggesting that they will fall exactly on this value in the thermodynamic limit. Note that in order to define meaningful averages we only include symmetry sectors which contain at least 200 states in the ϵ window, and then only ϵ windows which contain at least 1000 states from across all eight sectors.

Integrable models also generally exhibit ballistic energy transport [106], which was predicted in [107] and was found in our numerical TEBD study [66], so these results are consistent with our expectations in the $W \to 0$ limit.

3.3 Many-body localisation in the XYZ spin chain

This section presents the data from our numerical study of the disordered XYZ spin chain, and our analysis of these results. We perform exact diagonalisation on the XYZ Hamiltonian with periodic boundary conditions; in the XXZ limit we study the largest sector (with z component of the total magnetisation equal to 0 or $1/2$ for chains with even or odd L respectively; in the

fermionic language this sector corresponds to half-filling), and in the general XYZ case we use the sector with an even number of up spins (the sector with an odd number of up spins displays the same behaviour). In the XXZ limit we are able to quite easily diagonalise systems of up to $L = 17$ spins, and in the XYZ system we diagonalise systems of up to $L = 16$ spins as the sectors are larger and more costly to diagonalise (the matrix dimension is 2^{L-1} in the XYZ model rather than $\binom{L}{L/2}$ which is the case for the XXZ model). The results shown in Sections 3.3.1 to 3.3.3 correspond to 200 eigenstates closest to the middle of the spectrum, $\epsilon = 0.5$, which are the most delocalised states. Results for the entire spectrum are shown in Section 3.3.4 for system sizes of up to $L = 15$ spins. We always use $\Delta = 1.2$ (this value was chosen for the convenience of our TEBD study in order to avoid the unusual transport behaviour found at $\Delta = 1$ [62]), and we investigate XY anisotropies in the range $0 \leq \eta \leq 1$. For $L \leq 15$ (or every L in the XXZ case) we use at least 750 disorder realisations to obtain meaningful averages, while for $L = 16$ we use at least 130 disorder realisations.

The phase diagram of this system is shown in Fig. 3.2, with the position of the MBL transition determined by analysis of the spectral statistics, entanglement properties, and Shannon entropies, as explained below.

3.3.1 Signatures in the eigenenergy spectrum

We begin by examining the behaviour of the r parameter with increasing disorder. For a single disorder realisation we calculate the set of r_n's, defined according to (1.19), for the eigenstates of $\mathcal{H}_{\mathrm{XYZ}}$. The average of these values within a chosen window around a target energy density ϵ gives r for that disorder realisation at that ϵ. This is then averaged over disorder realisations to give $\overline{r}$, which is the quantity of interest. The standard error $\sigma/\sqrt{M}$ (where σ is the standard deviation and M is the number of disorder realisations) is $< 0.25\%$ of the average for all points shown.

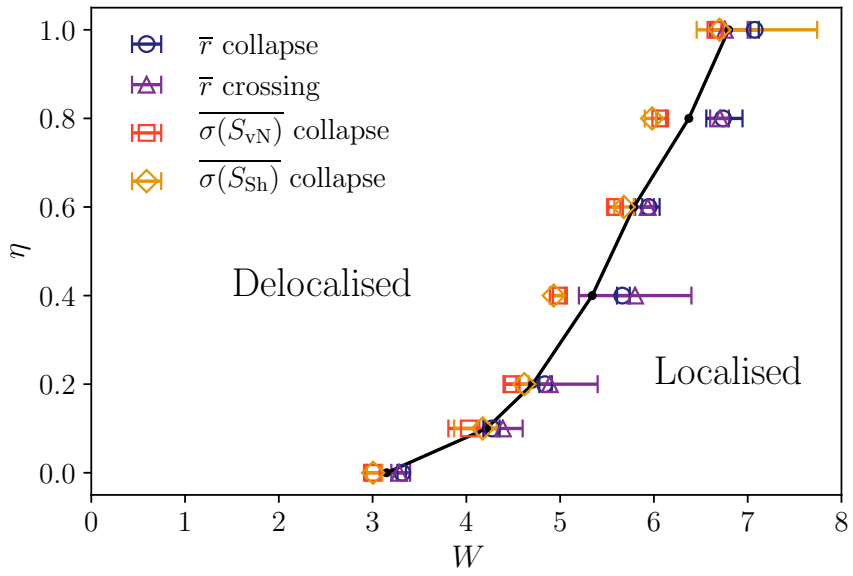

FIGURE 3.2: The phase diagram of the disordered XYZ spin chain. The location of the phase transition was determined from spectral statistics and fluctuations of the half-chain entanglement entropy and Shannon entropy. The black points and line indicate the average value of W_c determined from these measures. The systems studied have an interaction strength $\Delta = 1.2$ and sizes $L \leq 16$ ($L \leq 17$ for $\eta = 0$).

Fig. 3.3 shows $\overline{r}$ for the XYZ chain with $L = 15$ as a function of the disorder strength W for a selection of XY anisotropies η. We see the standard behaviour, with $\overline{r} \approx r_{\mathrm{GOE}}$ for weak disorder followed by a crossover to $\overline{r} \approx r_{\mathrm{P}}$ at stronger disorder, signalling a transition between thermalising and localised phases in the thermodynamic limit. It is immediately clear that increasing the XY anisotropy η shifts the crossover to a significantly larger disorder strength.

To estimate W_c, the critical disorder strength for the MBL transition, we perform a finite-size scaling analysis to extrapolate to the thermodynamic limit. We use the same method for the analysis of the fluctuations of the entanglement entropy in Section 3.3.2 and the fluctuations of the Shannon entropy in Section 3.3.3, so the explanation here will be thorough and not repeated in those subsections. We attempt to fit the data to a universal curve of the form $g[(W - W_c)L^{1/\nu}]$, as has been discussed in previous works [50,

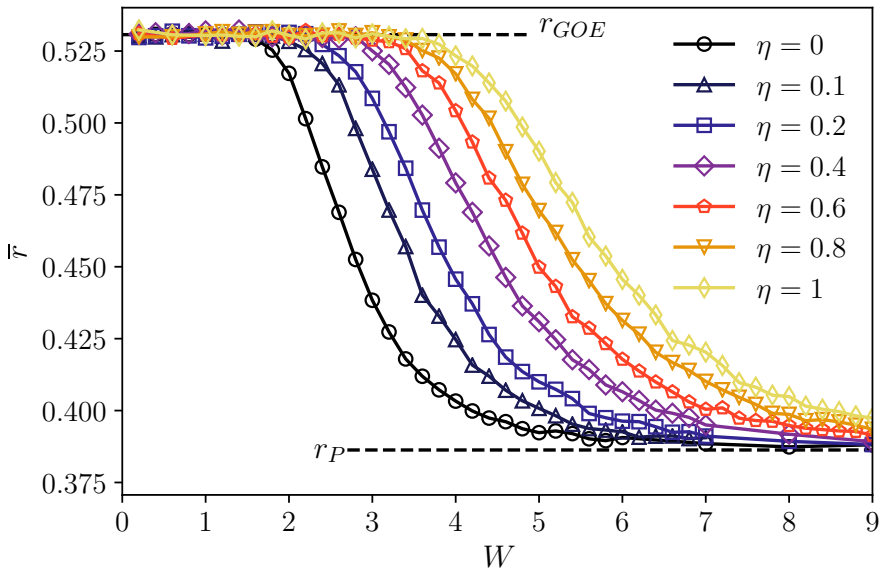

FIGURE 3.3: The disorder-averaged r parameter for the XYZ model with $L = 15$ and $\Delta = 1.2$, plotted as a function of disorder strength W for several values of the XY anisotropy η. The error bars are smaller than the symbol size.

55, 58]. We perform the collapse by interpolating the $r_L(W)$ curves onto a rescaled grid $x := (W - W_c)L^{1/\nu}$ using a third-order polynomial spline, and numerically minimising a cost function F_C over the parameters W_c and ν. The cost function is the integral of the squared difference between a pair of $r_L(x)$ curves over a window of width $2w$ in W centred on W_c, summed over each pair of L's:

$$F_C = \sum_{L,\, L'<L} \int_{-x_0}^{+x_0} \mathrm{d}x \left(r_L(x) - r_{L'}(x)\right)^2, \tag{3.4}$$

where $x_0 = wL_0^{1/\nu}$ where L_0 is the shortest length used. We perform this minimisation procedure for a number of window sizes w to judge the quality of the collapse, subject to the requirement that the window must contain at least 3 data points and must not extend beyond the first/last data point (this only materially affects the $L = 16$ data, which is taken on a smaller grid with larger spacing due to the difficulty of the numerical diagonalisation).

Fig. 3.4 shows $r(W)$ for a range of L for $\eta = 0.4$, and the inset shows the

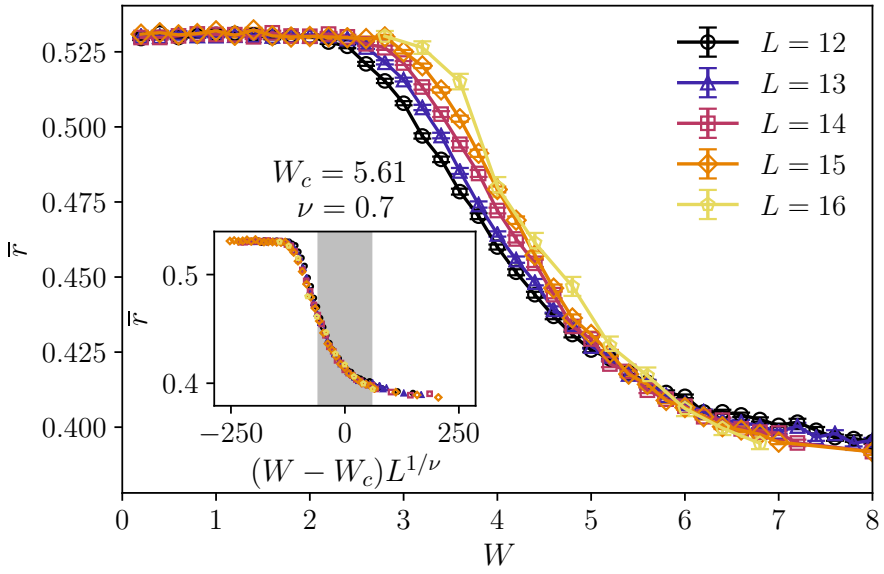

FIGURE 3.4: The finite-size scaling analysis of the r parameter, shown as a function of disorder strength W for several system sizes L, with XY anisotropy $\eta = 0.4$. The inset shows the result of the numerical collapse, performed over a window of half-width $w = 1.7$ (indicated by the shaded region), and the corresponding fitting parameters are indicated in the figure.

result of the scaling collapse performed over a window with $w = 1.7$, which is indicated by the shaded region. Fig. 3.2 shows the values of W_c (blue circles) for the values of η shown in Fig. 3.3, as determined by the finite-size scaling analysis. The points correspond to the averages of the values found by collapses performed over different windows w, and the horizontal bars show the range of values found. The value of W_c is very consistent across window sizes, and its increase with the XY anisotropy η is clear. The exponent ν is shown in Fig. 3.5, where points and vertical bars indicate the average and range respectively of the results from different window sizes. The values of ν for the scaling of the r parameter, shown by blue circles, vary more strongly than W_c with w, and we note that they fall outside of the predicted bound ($\nu \geq 2$ in one dimension) [58], which has been the case in previous studies of this nature [50, 55]. The large error bar on the $\eta = 0.2$ point comes from a single collapse with a very large value of ν, which has not been excluded as the data collapse was not poor.

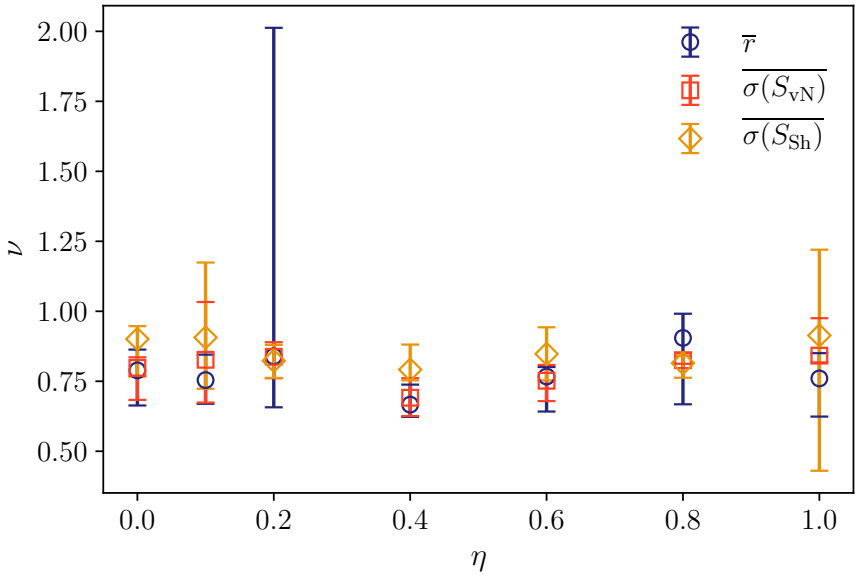

FIGURE 3.5: The values of ν from a finite-size scaling analysis of the spectral statistics and fluctuations of the half-chain entanglement entropy and Shannon entropy in the disordered XYZ chain. The points indicate the average value, and the bars indicate the range of values from all acceptable collapses. The data was taken using an interaction strength $\Delta = 1.2$ and system sizes of $L \leq 16$ ($L \leq 17$ for $\eta = 0$).

This approach may seem somewhat ambitious for such small system sizes, but we can perform a more simple analysis by searching for the disorder strength at which all of the $r_L(W)$ curves cross (which is of course consistent with the location of W_c in the scaling ansatz described above). We locate this point by interpolating the curves for each L onto a fine grid and searching for the minimum of the sum of the squared differences between each curve. We set bounds on this estimation by finding the points at which this cost function takes twice its minimum value. If the cost function is a simple function of W (i.e. it has a single discernible minimum near W_c) then we set the bounds on W_c to be the two real data points on the outside of this bound. Otherwise, we choose the smallest and largest values of W where the cost function crosses twice its minimum as the lower and upper bounds respectively, and estimate W_c as the point halfway between them. The results of this analysis, shown by purple triangles in Fig. 3.2, agree well with the more sophisticated scaling analysis.

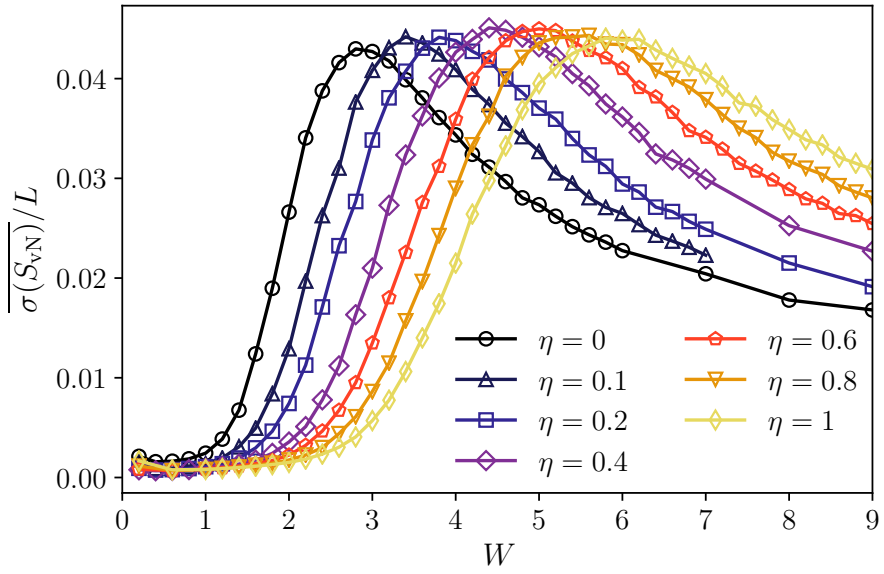

FIGURE 3.6: The disorder-averaged standard deviation of the half-chain entanglement entropy $\overline{\sigma(S_{\mathrm{vN}})}$ for the XYZ model with $L = 15$ and $\Delta = 1.2$, plotted as a function of disorder strength W for several values of the XY anisotropy η. The error bars are smaller than the symbol size.

3.3.2 Signatures in the entanglement

We examine the fluctuations of the half-chain entanglement entropy, which peak at the MBL transition [50]. Using the eigenvectors from the same dataset that was used to analyse the spectral statistics in Section 3.3.1, we calculate the entanglement entropy between two halves of the chain (of sizes $L/2$ and $L/2$ for chains with an even L and $(L+1)/2$ and $(L-1)/2$ for chains with an odd L), and find the standard deviation of these values across the 200 eigenstates in the middle of the spectrum. This is then averaged over disorder realisations to determine $\overline{\sigma(S_{\mathrm{vN}})}$ for each disorder strength W.

Fig. 3.6 shows $\overline{\sigma(S_{\mathrm{vN}})}$ as a function of disorder strength W for a selection of XY anisotropies η, all on systems with $L = 15$. The expected peak is well defined and shows the same shift to larger W as η increases that we observed in the level statistics. The scaling collapse is performed in the same way as is described in Section 3.3.1, but with the additional step of initially normalising the peak-heights to one before collapsing them to the same scaling ansatz

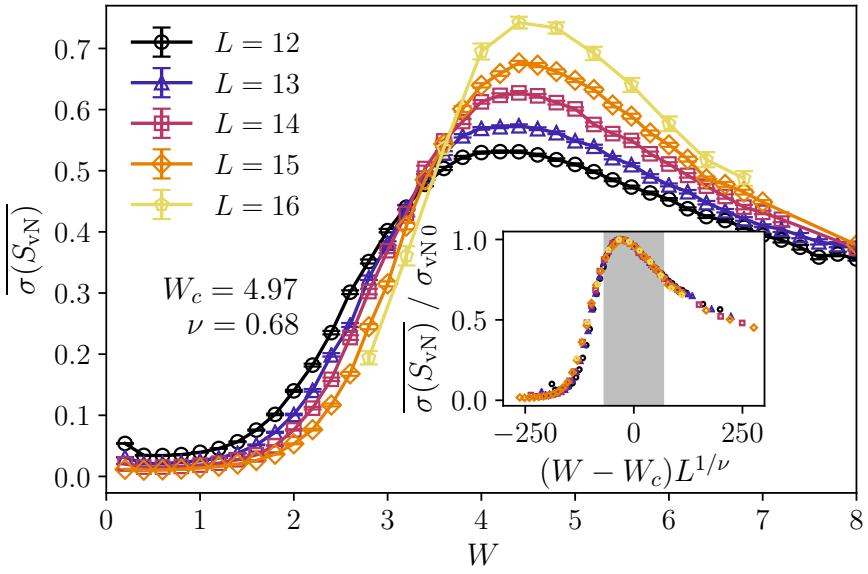

FIGURE 3.7: The finite-size scaling analysis of the standard deviation of the half-chain entanglement entropy $\overline{\sigma(S_{\mathrm{vN}})}$, shown as a function of disorder strength W for several system sizes L, with XY anisotropy $\eta = 0.4$. The inset shows the result of the numerical collapse, performed over a window of half-width $w = 1.7$ (indicated by the shaded region), and the corresponding fitting parameters are indicated in the figure.

$g[(W - W_c)L^{1/\nu}]$. We have not attempted to include the L dependence of the peak height in the scaling ansatz due to the odd-even effects in the half-chain and the limited number of chain lengths ($L \in \{12, 13, 14, 15, 16\}$ for $\eta \neq 0$).

Fig. 3.7 shows $\overline{\sigma(S_{\mathrm{vN}})}$ for a range of L for $\eta = 0.4$, and the inset shows the result of the scaling collapse on the normalised curve, performed over a window with $w = 1.7$ (indicated by the shaded region). The values of W_c found by this analysis are shown by red squares in Fig. 3.2, and the exponents ν are shown by red squares in Fig. 3.5.

3.3.3 Signatures in the Shannon entropy

We perform the same analysis on the standard deviations of the Shannon entropy. Fig. 3.8 shows $\overline{\sigma(S_{\mathrm{Sh}})}$ as a function of disorder strength W for a selection of XY anisotropies η with $L = 15$. Once again the increase in W_c

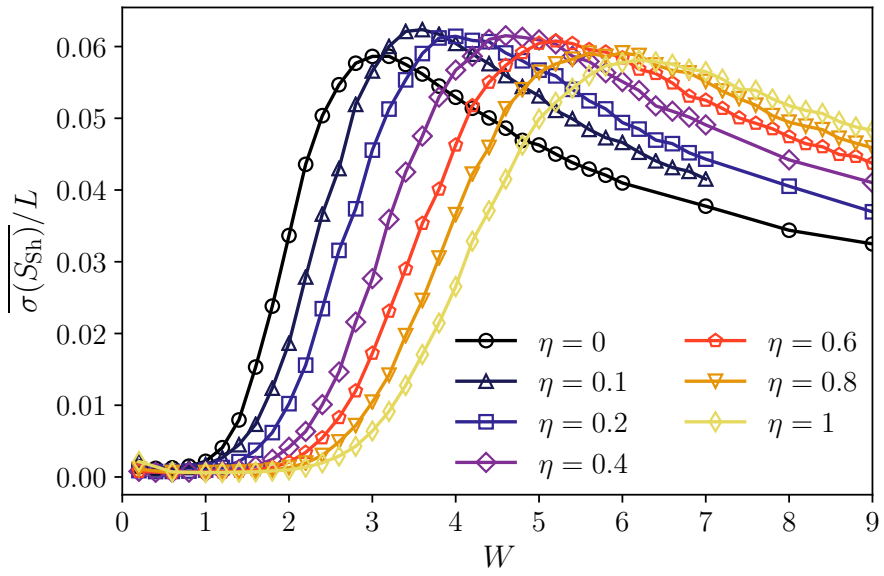

FIGURE 3.8: The disorder-averaged standard deviation of the Shannon entropy $\overline{\sigma(S_{\mathrm{Sh}})}$ for the XYZ model with $L = 15$ and $\Delta = 1.2$, plotted as a function of disorder strength W for several values of the XY anisotropy η. The error bars are smaller than the symbol size.

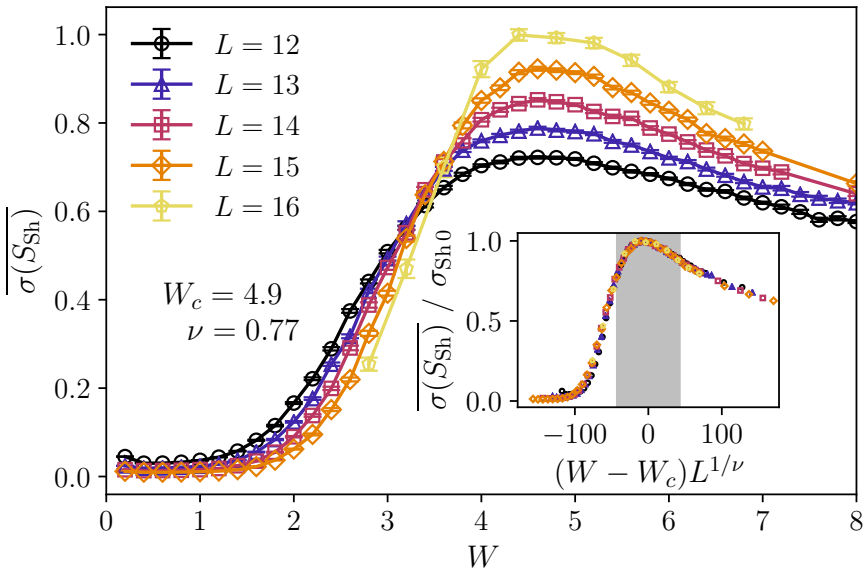

FIGURE 3.9: The finite-size scaling analysis of the standard deviation of the Shannon entropy, shown as a function of disorder strength W for several system sizes L, with XY anisotropy $\eta = 0.4$. The inset shows the result of the numerical collapse, performed over a window of half-width $w = 1.7$ (indicated by the shaded region), and the corresponding fitting parameters are indicated in the figure.

with η is evident.

One example of the numerical collapse of $\overline{\sigma(S_{\mathrm{Sh}})}$ is shown in Fig. 3.9, again using $\eta = 0.4$ and $w = 1.7$. The extracted values of W_c are shown in Fig. 3.2 by gold diamonds, and the exponents ν are shown by gold diamonds in Fig. 3.5. We note that the values of W_c determined by $\overline{\sigma(S_{\mathrm{vN}})}$ and by $\overline{\sigma(S_{\mathrm{Sh}})}$ are in very close agreement, and that they agree well with those determined from the spectral statistics.

3.3.4 The many-body mobility edge

So far in this section we have located the MBL transition by analysing the properties of the eigenstates in the middle of the spectrum. These are the most delocalised states and therefore this result corresponds to the disorder strength at which the entire system becomes localised. However, as discussed in Section 1.3, there is some numerical evidence that the phase diagram of the disordered XXZ model features a many-body mobility edge [55–57]. We now explore this in the XYZ model on systems of up to $L = 15$ spins, using the same analysis as was described in Sections 3.3.1 to 3.3.3. Fig. 3.10 shows the phase diagram of the XYZ model as a function of disorder strength W and energy density ϵ, with data taken at energy densities $\epsilon \in \{0.2, 0.3, 0.4, 0.5, 0.6, 0.7, 0.8\}$. The data was calculated for $\eta = 0.4$ (upper panel) and $\eta = 0.8$ (lower panel) with $\Delta = 1.2$. The analysis was performed on the 200 eigenstates with eigenenergies closest to the target ϵ in each disorder realisation.

These results suggest that the many-body mobility edge survives the introduction of non-number conserving terms in the Hamiltonian. Interestingly, this feature is more pronounced in the spectral statistics than in the entropy measures. The shape of the mobility edge appears to be consistent across the values of η shown in Fig. 3.10 and the $\eta = 0$ case shown in Fig. 1.1. Finite-size effects become severe away from the centre of the spectrum where the density

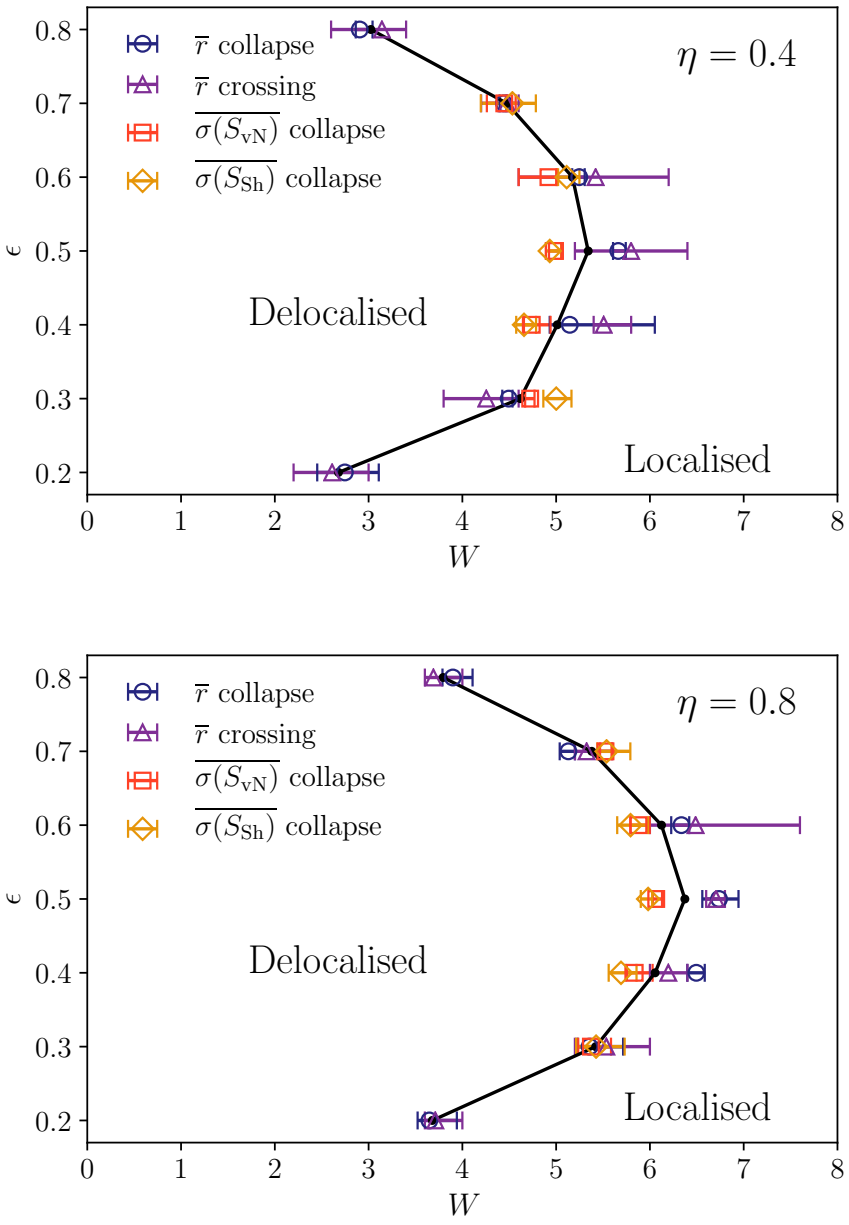

FIGURE 3.10: Energy-resolved phase diagrams of the disordered XYZ chain, shown for XY anisotropies $\eta = 0.4$ (upper panel) and $\eta = 0.8$ (lower panel). The location of the phase transition was determined from spectral statistics and fluctuations of the half-chain entanglement entropy and Shannon entropy. The black points and line indicate the average value of W_c determined from those measures. The systems studied have an interaction strength $\Delta = 1.2$ and sizes $L \leq 15$.

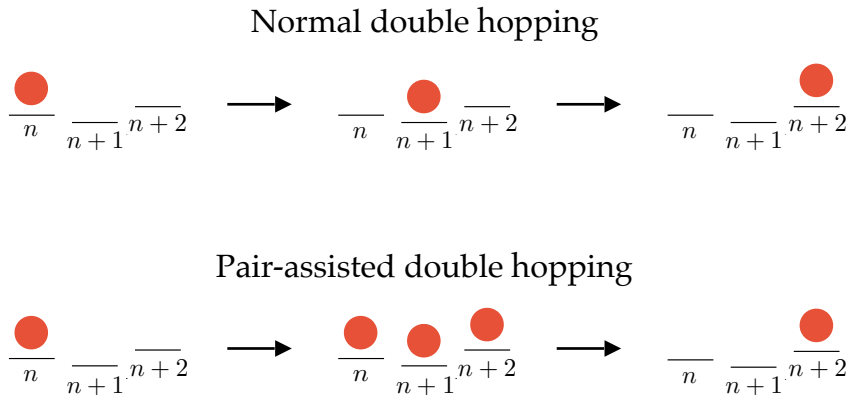

FIGURE 3.11: Schematic of the possible second-order processes that move a fermion by two sites in the XYZ model.

of states is small. It is impossible to reliably collapse the curves of $\sigma(S_{\mathrm{Sh}})$ and $\sigma(S_{\mathrm{Sh}})$ for $\epsilon = 0.2$ and $\epsilon = 0.8$, so these points have been omitted from the phase diagrams. Of course, with the system sizes available to us, we are unable to discern whether this is a real aspect of the phase diagram or a finite-size effect as suggested in [59]. However, if we believe that the mobility edge exists in the $\eta = 0$ limit, then this analysis suggests that it survives when the U(1) symmetry is removed.

3.3.5 The effect of breaking the U(1) symmetry

We have seen throughout this section that increasing the XY anisotropy η pushes the MBL transition to larger disorder strengths. We can gain some intuition for this in the fermionic picture, where $\eta \neq 0$ introduces pair-creation and pair-annihilation terms in $\mathcal{H}_{\mathrm{XYZ}}$. As a result the unitary time evolution can explore states with different numbers of fermions, which would not be possible in the XXZ model, and this offers more routes through which excitations can delocalise. More explicitly, a fermion on site n in the XXZ model can move to site $n+2$ by a second-order process involving two nearest-neighbour hops, as depicted at the top of Fig. 3.11. In the XYZ model this can be achieved with an alternative second-order process, by creating a pair of fermions on sites $n+1$ and $n+2$ and then annihilating the fermions on

sites n and $n+1$, as shown at the bottom of Fig. 3.11.

We can gain some insight if we consider the non-interacting limit of the Hamiltonian (3.3):

$$\mathcal{H}_{\mathrm{XY}} = \sum_n \left[\frac{J}{2} \left(c_n^\dagger c_{n+1} + c_{n+1}^\dagger c_n \right) + \frac{\eta}{2} \left(c_n^\dagger c_{n+1}^\dagger + c_{n+1} c_n \right) + h_n c_n^\dagger c_n \right], \quad (3.5)$$

where J has been introduced in order to keep track of the contribution from the normal hopping term. Deep in the localised phase, we can treat the hopping and pairing terms of the Hamiltonian as a perturbation to the strong diagonal disorder term. In the $\eta = 0$ limit, the amplitude of the second-order process illustrated at the top of Fig. 3.11 is [89]:

$$A_J = \frac{J/2}{(h_{n+1} - h_n)} \frac{J/2}{(h_{n+2} - h_n)} = \frac{J^2}{4(h_{n+1} - h_n)(h_{n+2} - h_n)} \sim \frac{J^2}{W^2}. \quad (3.6)$$

When $\eta \neq 0$ we must include the amplitude from the second-order process illustrated a the bottom of Fig. 3.11:

$$\begin{aligned} A_\eta &= \frac{\eta/2}{([h_n + h_{n+1} + h_{n+2}] - h_n)} \frac{\eta/2}{(h_{n+2} - h_n)} \\ &= \frac{\eta^2}{4(h_{n+1} + h_{n+2})(h_{n+2} - h_n)} \sim \frac{\eta^2}{W^2}, \end{aligned} \quad (3.7)$$

so the full amplitude is $A_J + A_\eta \sim (J^2 + \eta^2)/W^2$. Thus, to this level of approximation, the disordered XY model is effectively the standard tight-binding model with the same disorder strength and a larger effective hopping:

$$J_{\mathrm{eff}}^2 = J^2 + \eta^2. \quad (3.8)$$

If we are willing to apply this conclusion to the interacting model at disorder strengths near the MBL transition, then we might conclude that this explains the shift of W_c to larger values as η is increased.

3.4 Thermalisation in the XYZ spin chain

We further examine the properties of the XYZ model by analysing the extent to which the matrix elements of operators in the eigenbasis of the Hamiltonians obey the ETH ansatz. We consider the bond energy operator for the disorder-free version of the model:

$$\begin{aligned} E^0_{n,n+1} &= (1+\eta)s^x_n s^x_{n+1} + (1-\eta)s^y_n s^y_{n+1} + \Delta s^z_n s^z_{n+1} \\ &= \begin{pmatrix} \Delta/4 & 0 & 0 & \eta/2 \\ 0 & -\Delta/4 & 1/2 & 0 \\ 0 & 1/2 & -\Delta/4 & 0 \\ \eta/2 & 0 & 0 & \Delta/4 \end{pmatrix}, \end{aligned} \tag{3.9}$$

where the matrix representation is written in the Pauli basis. Note that this operator does not depend on the disorder strength, making it simple to analyse. The results for the full bond energy operator:

$$\begin{aligned} E_{n,n+1} =& (1+\eta)s^x_n s^x_{n+1} + (1-\eta)s^y_n s^y_{n+1} + \Delta s^z_n s^z_{n+1} + \frac{h_n}{2}s^z_n + \frac{h_{n+1}}{2}s^z_{n+1} \\ &= \begin{pmatrix} \frac{\Delta+h_n+h_{n+1}}{4} & 0 & 0 & \eta/2 \\ 0 & \frac{-\Delta+h_n-h_{n+1}}{4} & 1/2 & 0 \\ 0 & 1/2 & \frac{-\Delta-h_n+h_{n+1}}{4} & 0 \\ \eta/2 & 0 & 0 & \frac{\Delta-h_n-h_{n+1}}{4} \end{pmatrix} \end{aligned} \tag{3.10}$$

are qualitatively the same, but the matrix elements depend strongly on the disorder strength, making comparisons more difficult than for $E^0_{n,n+1}$.

3.4.1 Diagonal elements

As we discussed in Section 1.2 the diagonal elements of an operator (written in the eigenbasis of the Hamiltonian) determine the long-time average value of the associated observable. In a thermalising system, according to the ETH and Berry's conjecture, we expect them to vary smoothly with energy, and to have Gaussian fluctuations. The diagonal elements of $E^0_{n,n+1}$ will be

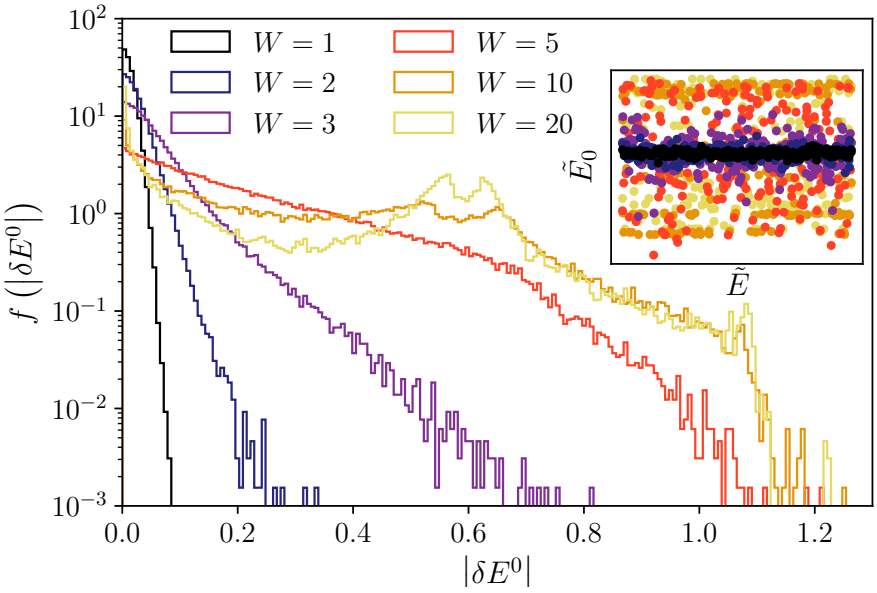

FIGURE 3.12: Histograms of the absolute difference between neighbouring EEVs, $|\delta E^0|$, for a selection of disorder strengths W, with XY anisotropy $\eta = 0.4$, interaction strength $\Delta = 1.2$, and system size $L = 15$. The inset shows the EEVs as a function of eigenenergy for a single disorder realisation, with the colours matching those in the legend of the main figure.

bounded by the values

$$E^{0(\min)}_{n,n+1} = -\frac{\Delta}{4} - \frac{1}{2}, \qquad E^{0(\max)}_{n,n+1} = \frac{\Delta}{4} + \frac{\eta}{2}, \tag{3.11}$$

which are the lowest and highest eigenvalues of (3.9) respectively. Deep in the localised phase we expect that the diagonal elements will tend to values approximately equal to those in (3.9): $\pm\Delta/4$.

We find evidence for the violation of the ETH in the diagonal elements (EEVs) of $E^0_{n,n+1}$ as described in Section 1.4.4, defining $\delta E^0 = \langle E^0_{L,1}\rangle(E_{n+1}) - \langle E^0_{L,1}\rangle(E_n)$ (the periodic boundary conditions mean that the (L,1) pair of sites is not a special choice, and it was simply chosen for computational convenience). Fig. 3.12 shows histograms of $|\delta E^0|$ for a range of disorder strengths in both the ergodic and localised phases. The data correspond to a system with $L = 15$ and $\eta = 0.4$ (these parameters correspond to $W_c \simeq 5.4$ according

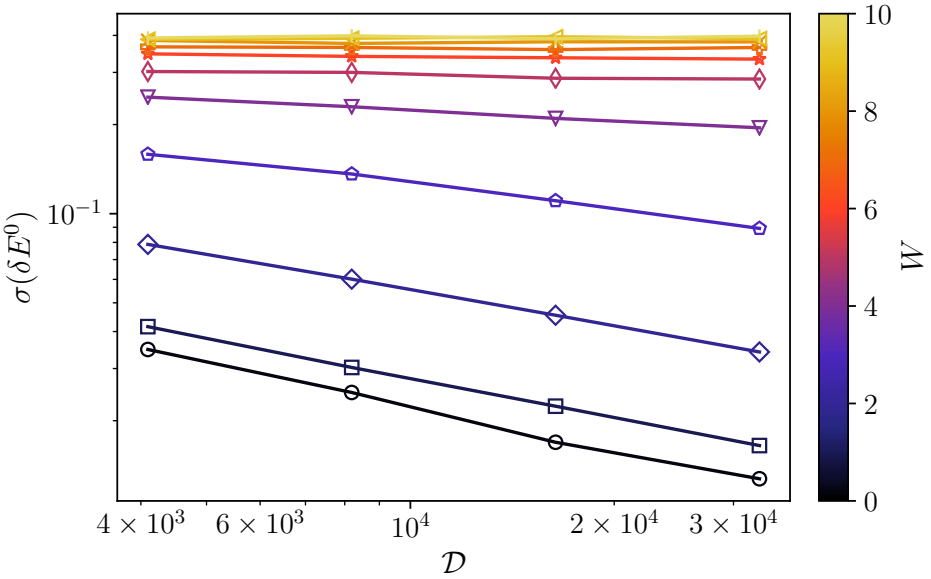

FIGURE 3.13: The standard deviation of δE^0, plotted as a function of state space dimension $\mathcal{D}$ for several disorder strengths W in a system with XY anisotropy $\eta = 0.4$ and interaction strength $\Delta = 1.2$. The colour bar indicates the disorder strength for each curve.

to the previous analysis), using the 200 eigenstates closest to the middle of the band and at least 500 disorder realisations. The inset shows the EEVs plotted against the eigenstate energy for a single disorder realisation, where the energies have been rescaled to lie on top of each other ($\tilde{E} = (E - E_0)/(E_1 - E_0)$ where E_0 and E_1 are the smallest and largest eigenenergies in the sample), and the average of the EEVs in the sample has been subtracted for easier comparison.

At small disorder strengths it is clear from both the histograms and the inset that the EEVs are smooth functions of the eigenenergy. As the disorder strength increases to around W_c, the histograms develop long tails, which extend close to the largest possible value of $|\delta E^0_{\max}| = (\Delta + \eta + 1)/2$ (as determined from (3.11)), which corresponds to the upper limit of the $|\delta E^0|$ axis. For very strong disorder we see the features of the infinite-disorder limit forming: the EEVs cluster around $\pm\Delta/4$, resulting in peaks at 0 and $\Delta/2 = 0.6$ in the histogram of $|\delta E^0|$.

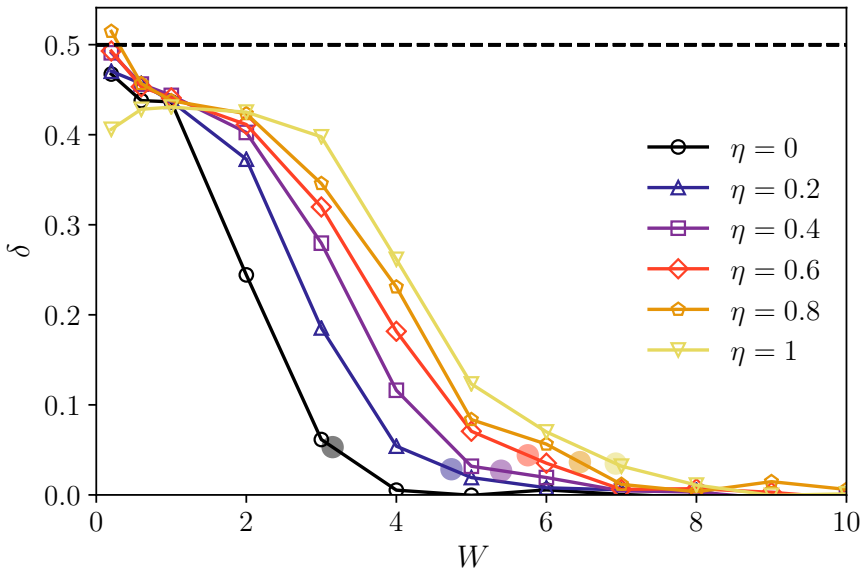

FIGURE 3.14: The EEV scaling exponent δ plotted as a function of disorder strength W for several values of η with $\Delta = 1.2$. The large semi-transparent circles indicate the approximate position of the MBL transition for the XY anisotropy η of the corresponding colour.

The dependence of the fluctuations of the EEVs on system size also shows this behaviour. Fig. 3.13 shows the standard deviation of δE^0 as a function of the size of the state space $\mathcal{D}$ for several disorder strengths with $\eta = 0.4$. There is a clear change from a power-law decay with $\mathcal{D}$ at weak disorder, as is predicted by the ETH (1.14), to a value that is independent of $\mathcal{D}$ at strong disorder. We fit the data using $\sigma(\delta E^0) \sim \mathcal{D}^{-\delta}$ to extract δ as a function of W, using $14 \leq L \leq 17$ for $\eta = 0$ and $12 \leq L \leq 15$ for $\eta \neq 0$. Fig. 3.14 shows the results of the fits for a selection of XY anisotropies, demonstrating that the change to a $\mathcal{D}$-independent value shifts to stronger disorder with increased η, which is consistent with the change in the MBL transition. The approximate position of W_c for each η is shown by the large semi-transparent circle in the corresponding colour, at which point the values of δ have all become similarly small. The expected ETH scaling in the large L limit, $\delta = 0.5$ [63, 86], is shown by the dashed black line, however it is unlikely that we could observe the true value of δ with such modest system sizes.

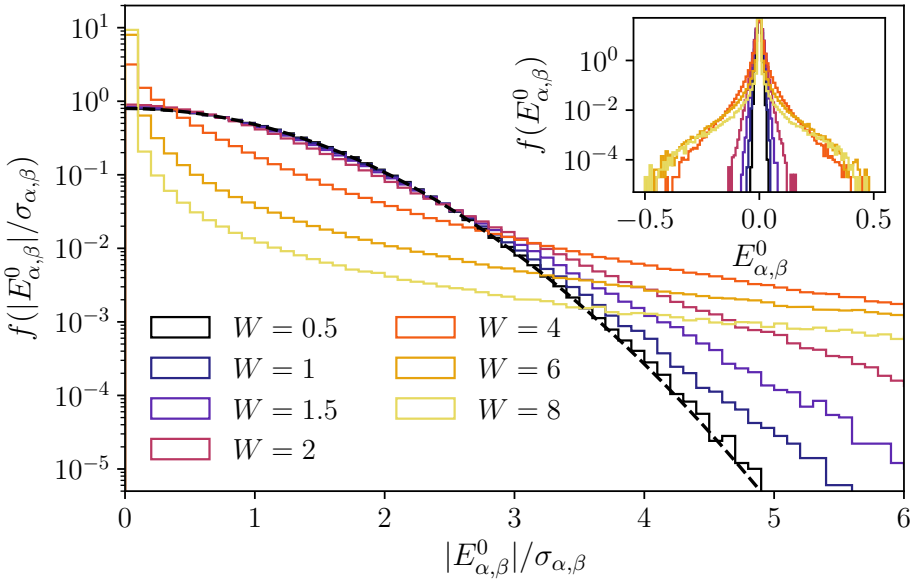

FIGURE 3.15: Histograms of $|E^0_{\alpha,\beta}|/\sigma_{\alpha,\beta}$ for a selection of disorder strengths W, with XY anisotropy $\eta = 0.4$, interaction strength $\Delta = 1.2$, and system size $L = 15$. The dashed black line corresponds to the histogram for a Gaussian distribution. The inset shows the histograms of the unscaled values $E^0_{\alpha,\beta}$ with the same colour scheme.

3.4.2 Off-diagonal elements

The off-diagonal elements of an operator, on the other hand, determine the relaxation of the corresponding observable to its long-time average value. Fig. 3.15 shows histograms of $E^0_{\alpha,\beta} = \langle\alpha|E^0_{L,1}|\beta\rangle$ for a range of disorder strengths, using the 200 eigenstates closest to the centre of the spectrum in a chain with $L = 15$ and $\eta = 0.4$, each including 250 disorder realisations. The main panel shows the distributions of $|E^0_{\alpha,\beta}|$ after rescaling by the standard deviation of the sample, $\sigma_{\alpha,\beta}$, which allows us to compare their shapes. The inset shows the unscaled distributions of $E^0_{\alpha,\beta}$, and the symmetry between positive and negative $E^0_{\alpha,\beta}$ is apparent. The dashed black line in the main figure indicates the appropriately normalised half-Gaussian distribution. There is a clear trend that as the disorder strength increases, the tails of the distribution become larger, and cross over from exponential to power-law decay in the localised phase ($W > W_c \simeq 5.4$). At weak disorder strengths, the distribution of $E^0_{\alpha,\beta}$ is Gaussian, as can be seen from the $W = 0.5$ curve in

Fig. 3.15. However, there is a clear departure from a Gaussian distribution at intermediate disorder strengths in the delocalised phase, where we see that the distributions develop heavy tails. This coincides with the region of sub-diffusive energy transport found in the TEBD study of this model ($W \gtrsim 1.0$ for $\eta = 0.4$) [66]. This suggests that Berry's conjecture is not valid in this region of the phase diagram, and is consistent with the assertion that the violation of Berry's conjecture is associated with anomalous transport [63, 67].

3.5 Summary and outlook

We have presented evidence for a many-body localised phase in the one-dimensional disordered XYZ spin chain, which corresponds to a system of fermions hopping on a lattice with disordered on-site potentials in the absence of fermion number conservation. As such, this takes us beyond systems such as the XXZ spin chain that can be thought of in terms of the dynamics of a fixed number of strongly-interacting particles. The XYZ model does not fall under the scope of the original paper by Basko, Aleiner, and Altshuler [14], which relies on the conservation of particle number, and recent contructions of LIOMs which rely on the same assumptions [43, 44].

The heavy-tailed distributions of off-diagonal matrix elements, and the results of the accompanying TEBD study [66], indicate that there are regions of anomalous energy transport in the ergodic phase of this model. However, we have no true understanding of the mechanism for this behaviour, and this would be an interesting direction for further study.

Chapter 4

Correlated noise in few-level quantum systems

In this chapter we study the effect of correlated, classical noise on the fidelity of a time-dependent state preparation protocol in a few-level quantum system. More specifically, we analyse the probability of performing an adiabatic transformation on the quantum system in the presence of perfectly correlated, time-dependent fluctuations in multiple parameters of the Hamiltonian. We show that the quantum state of the system can become trapped in a small region of the state space, rather than becoming truly randomised, and that this results in a plateau in the state-preparation fidelity as a function of the time for which the system is exposed to the noise. We demonstrate the effect in a simple two-level system where the Bloch sphere picture offers a clear visualisation of the process.

4.1 The model

We consider a two-level quantum system with a time-dependent Hamiltonian, $\mathcal{H}(t)$, which changes from an initial configuration at time $t = 0$ to a final configuration at $t = T$. The instantaneous eigenstates of the system are:

$$\mathcal{H}(t)\left|g(t)\right\rangle = E_g(t)\left|g(t)\right\rangle; \tag{4.1}$$

$$\mathcal{H}(t)\left|e(t)\right\rangle = E_e(t)\left|e(t)\right\rangle, \tag{4.2}$$

where $|g(t)\rangle$ is the ground state and $|e(t)\rangle$ is the excited state, and the eigenstates never become degenerate (i.e. $E_e(t) > E_g(t)$ at all times). We consider a state-preparation protocol in which the system is initialised in the ground state of the initial Hamiltonian $\mathcal{H}(0)$, $|\psi(0)\rangle = |g(0)\rangle$, and the aim is to evolve the system adiabatically and find the system in its ground state at $t = T$, $|g(T)\rangle$. We define the fidelity, $\mathscr{F}(t)$, as the probability of finding the system in the instantaneous ground state of $\mathcal{H}(t)$ at a time t:

$$\mathscr{F}(t) = \left|\langle g(t)|\psi(t)\rangle\right|^2. \tag{4.3}$$

Our measure of adiabaticity is the probability of finding the system in its ground state at the end of the process, $\mathscr{F}(T)$.

As was discussed in Section 2.1.3, if the Hamiltonian changes smoothly with time a higher fidelity can generally be achieved by increasing the duration of the process, so $\mathscr{F}(T) \to 1$ as $T \to \infty$. However, if the Hamiltonian contains a fast, fluctuating noise term, then increasing T will not generally lead to an increased $\mathscr{F}(T)$ as the eigenbasis will still fluctuate rapidly. In fact, one might expect a large T to be detrimental to adiabatic evolution, as the noise will have more time in which to randomise the state of the system (excluding, of course, the possibility that the operators that couple to the noise are diagonal in the eigenbasis of the noise-free system). For an N-level system, the average fidelity of a completely randomised state is $\overline{\mathscr{F}} = 1/N$, where the bar denotes an average over realisations of the noise.

We consider a quantum system which has a Hamiltonian that can be split into a clean part and a noisy part:

$$\mathcal{H}(t) = \mathcal{H}_0(t) + \epsilon\,\eta(t)\,\mathcal{H}_n(t), \tag{4.4}$$

where $\mathcal{H}_0$ and $\mathcal{H}_n$ are operators which change smoothly and deterministically with time, ϵ is a parameter that defines the strength of the noise, and $\eta(t)$ is the noise. We take the noise to be a Gaussian-distributed stochastic variable

with zero mean, $\overline{\eta(t)} = 0$, and a two-time correlator

$$\overline{\eta(t)\eta(t+\tau)} = \delta(\tau). \tag{4.5}$$

We will refer to T as the exposure time, as it is the length of time for which the system is exposed to the noise. The Hamiltonian (4.4) could correspond to a system described by the Hamiltonian $\mathcal{H}_0$ that, for times $t \in [0, T]$, is exposed to a field which couples to the operator $\mathcal{H}_n$ and fluctuates in intensity. This could be, for example, a qubit being transported through a region with two spatially varying magnetic fields; one with a smoothly changing intensity and the other with a fluctuating intensity.

Although the eigenbasis of $\mathcal{H}(t)$ fluctuates quickly and randomly with the noise, the operators $\mathcal{H}_0(t)$ and $\mathcal{H}_n(t)$ evolve smoothly and deterministically. As a result we can define their instantaneous eigenstates and eigenenergies, which also evolve smoothly and deterministically:

$$\mathcal{H}_0(t)\left|\mu_0(t)\right\rangle = E^0_\mu(t)\left|\mu_0(t)\right\rangle; \tag{4.6}$$

$$\mathcal{H}_n(t)\left|\mu_n(t)\right\rangle = E^n_\mu(t)\left|\mu_n(t)\right\rangle, \tag{4.7}$$

where μ may be g or e. We define the initial state and the fidelity in terms of the eigenstates of the noise-free Hamiltonian:

$$\left|\psi(0)\right\rangle = \left|g_0(0)\right\rangle, \tag{4.8}$$

$$\mathscr{F}(t) = \left|\left\langle g_0(t)\middle|\psi(t)\right\rangle\right|^2. \tag{4.9}$$

4.2 The fidelity plateau

When the noise is strong, the Hamiltonian (4.4) will be dominated by the contribution from the noise part, and the noise-free part can be neglected:

$$\mathcal{H}(t) \approx \epsilon\,\eta(t)\,\mathcal{H}_n(t). \tag{4.10}$$

In this limit, the system is best described in the instantaneous eigenbasis of $\mathcal{H}_n(t)$. If T is large enough then the system will adiabatically follow the eigenbasis of $\mathcal{H}_n(t)$. In this limit the relative populations of the states $|g_n(t)\rangle$ and $|e_n(t)\rangle$ become independent of time, and the components of $|\psi(t)\rangle$ only accumulate relative phase.

The time-evolution in this limit is given by

$$\big|\psi(t)\big\rangle = \sum_{\mu=g,e} c_\mu \exp\left(-i\int_0^t \mathrm{d}t'\,\epsilon\,\eta(t')\,E_\mu^n(t')\right)\big|\mu_n(t)\big\rangle, \tag{4.11}$$

where $c_\mu = \langle\mu_n(0)|\psi(0)\rangle = \langle\mu_n(0)|g_0(0)\rangle$, and for the sake of convenience we have chosen a basis in which the geometric phase (2.11) vanishes (this can be achieved by defining the eigenstates with an appropriately chosen time-dependent global phase; this phase is deterministic and therefore does not affect the following arguments).

Calculating the fidelity of this state, and performing the average over noise realisations, gives

$$\mathscr{F}_a(t) = \mathscr{F}_0(t) + \big(\mathscr{F}_1(t) - \mathscr{F}_0(t)\big)e^{-\epsilon^2\left\langle(E_g^n - E_e^n)^2\right\rangle_t t/2}, \tag{4.12}$$

where $\langle x\rangle_t = t^{-1}\int_0^t \mathrm{d}t' x(t')$ is an average over times up to t and $\mathscr{F}_1(0) = 1$. This quantity decays from one to an average value:

$$\begin{aligned}\mathscr{F}_0(t) \;=\; & \big|\left\langle g_n(0)\middle|g_0(0)\right\rangle\left\langle g_0(t)\middle|g_n(t)\right\rangle\big|^2 \\ & + \big|\left\langle e_n(0)\middle|g_0(0)\right\rangle\left\langle g_0(t)\middle|e_n(t)\right\rangle\big|^2\end{aligned} \tag{4.13}$$

as the relative phase between the components of the wavefunction becomes fully randomised by the noise (i.e. uniformly distributed between 0 and 2π). The average value $\mathscr{F}_0(t)$ depends on the instantaneous properties of $\mathcal{H}_0(t)$ and $\mathcal{H}_n(t)$, but not on T. The quantity $\mathscr{F}_1(t)$ sets the initial value $\mathscr{F}_a(0) = 1$,

and has the form:

$$\mathscr{F}_1(t) = \Big|\big\langle g_0(t)\big|\Big(\sum_{\mu} c_\mu \big|\mu_n(t)\big\rangle\Big)\Big|^2. \tag{4.14}$$

The evolution described by (4.11) implies that the fidelity must stay between the values:

$$2\mathscr{F}_0(t) - \mathscr{F}_1(t) \leq \mathscr{F}(t) \leq \mathscr{F}_1(t). \tag{4.15}$$

Therefore, despite the fact that the eigenbasis of $\mathcal{H}(t)$ fluctuates rapidly, strong noise may not fully randomise the state of the system. Instead it distributes the state over the small fraction of the state space where the populations of $|\mu_n(t)\rangle$ are constant. This results in a plateau at a value of $\mathscr{F}_0(T)$ when the disorder-averaged state-preparation fidelity is plotted as a function of exposure time T.

The Bloch sphere picture allows us to visualise this effect by comparing the evolution on the Bloch spheres defined by the instantaneous eigenstates of $\mathcal{H}_n(t)$ and $\mathcal{H}_0(t)$. The initial state corresponds to the 'north' pole on the Bloch sphere defined by $\mathcal{H}_0(0)$, as it is the ground state of this Hamiltonian. On the surface of the $\mathcal{H}_n(0)$ Bloch sphere it corresponds to a point at an angle θ_0 to the $|g_n(0)\rangle$ pole. The evolution described in (4.11) corresponds to a random walk where the system stays at the same angle θ_0 to the instantaneous $|g_n(t)\rangle$ pole. If T is sufficiently large, the ensemble of final states will be distributed on a ring at a constant angle θ_0 from the $|g_n(T)\rangle$ pole, as shown on the left of Fig. 4.1. The eigenstates of $\mathcal{H}_0(T)$ and $\mathcal{H}_n(T)$ are related by a unitary transformation, so their Bloch spheres are related by a simple rotation. This rotation preserves the form of the ring of final states, but changes the angular position of its centre and spreads the ensemble of states over a range of heights, as shown on the right of Fig. 4.1. The bounds defined in (4.15) are equal to the fidelities corresponding to the points at the top and bottom of the ring on the $\mathcal{H}_0(T)$ Bloch sphere.

The fidelity is equal to half of the z coordinate of the state on the $\mathcal{H}_0$ Bloch

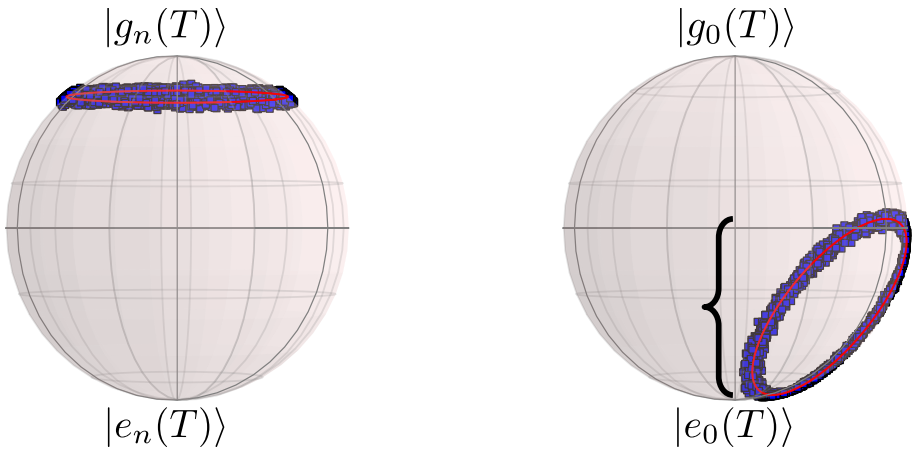

FIGURE 4.1: The distribution of final states on the Bloch sphere in the strong-noise limit. The sphere on the left represents the state of the system in the $\mathcal{H}_n(T)$ eigenbasis; the sphere on the right in the $\mathcal{H}_0(T)$ eigenbasis. On the right the distribution of final-state fidelities (i.e. the range of z coordinates) is indicated by a left-brace.

sphere as measured from the south pole. When the phase is fully randomised the average value of the fidelity, given by $\mathscr{F}_0(t)$, corresponds to the z coordinate of the centre of the ring. The distribution of fidelities resulting from this ring is:

$$f(x) = \frac{1}{\pi\tilde{\mathscr{F}}}\left[1 - \left(\frac{x - \mathscr{F}_0}{\tilde{\mathscr{F}}}\right)^2\right]^{-1/2} \tag{4.16}$$

with $\tilde{\mathscr{F}}(t) = 2\,|\langle g_n(0)|g_0(0)\rangle\,\langle g_0(0)|e_n(0)\rangle\,\langle e_n(t)|g_0(t)\rangle\,\langle g_0(t)|g_n(t)\rangle|$. If the factor in the modulus sign above is purely real, then $\tilde{\mathscr{F}}(t) = |\mathscr{F}_1(t) - \mathscr{F}_0(t)|$.

4.3 Requirements for the fidelity plateau

In the previous section we discussed the properties of the fidelity plateau in the presence of strong, correlated noise. However, we have so far neglected to comment on the conditions required to see this behaviour (i.e. the criteria required to access the strong-noise limit). The strength of the noise can be most easily understood by considering the system in terms of the instantaneous eigenstates of $\mathcal{H}_n(t)$:

$$|\psi(t)\rangle = \sum_{\mu=g,e} c_\mu(t)\,|\mu_n(t)\rangle. \tag{4.17}$$

The equations of motion for the coefficients $c_g(t)$ and $c_e(t)$ are given by (2.6):

$$i\begin{pmatrix}\dot{c}_g\\ \dot{c}_e\end{pmatrix} = \left[\begin{pmatrix}\langle g_n|\mathcal{H}_0|g_n\rangle & \langle g_n|\mathcal{H}_0|e_n\rangle\\ \langle e_n|\mathcal{H}_0|g_n\rangle & \langle e_n|\mathcal{H}_0|e_n\rangle\end{pmatrix} - i\begin{pmatrix}\langle g_n|\dot{g}_n\rangle & \langle g_n|\dot{e}_n\rangle\\ \langle e_n|\dot{g}_n\rangle & \langle e_n|\dot{e}_n\rangle\end{pmatrix} + \epsilon\,\eta\begin{pmatrix}E_g^n & 0\\ 0 & E_e^n\end{pmatrix}\right]\begin{pmatrix}c_g\\ c_e\end{pmatrix}, \tag{4.18}$$

where all of the time labels have been suppressed for brevity.

The plateau relies on three conditions:

1. Transitions due to $[\mathcal{H}_0, \mathcal{H}_n] \neq 0$ must be negligible. This requires that the first term in the square brackets of (4.18) is small compared to the third.

2. Non-adiabatic transitions between the instantaneous eigenstates of $\mathcal{H}_n$ must also be negligible. This requires that the second term in the square brackets of (4.18) is small compared to the third.

3. The noise must be strong enough to completely randomise the relative phase between the components of the initial state in a time T.

We will now examine these requirements on a more quantitative level.

4.3.1 Negligible transitions due to $[\mathcal{H}_0, \mathcal{H}_n] \neq 0$

We can determine whether this first condition is satisfied by rescaling the time variable: $t = sT$ with $s \in [0, 1]$. For the clean part of (4.4) this is a trivial transformation, as it simply results in a rescaling of the matrix elements by a factor of T. However, the noisy part must be treated with care. If we examine the result of rescaling time in the correlation function of the noise, we find:

$$\overline{\eta(t)\eta(t')} = \delta(t - t') = \delta\left(T[s - s']\right) = T^{-1}\,\delta(s - s'), \tag{4.19}$$

so the appropriate rescaling of the noise is:

$$\eta(t) \to T^{-1/2}\,\eta(s). \tag{4.20}$$

The full Schrödinger equation is therefore rescaled as:

$$i\partial_s|\psi(s)\rangle = \left[T\mathcal{H}_0(s) + \epsilon\sqrt{T}\,\eta(s)\,\mathcal{H}_n(s)\right]|\psi(s)\rangle. \tag{4.21}$$

The different scaling behaviours of the two terms make it clear that the 'strength' of the noise depends on how long the system is exposed to it. The deterministic part has a comparable strength to the noise when the two terms on the right-hand side of (4.21) have a similar magnitude:

$$T\Delta E_0 \sim \epsilon\sqrt{T}\,\Delta E_n, \tag{4.22}$$

where ΔE_0 is the typical size of $E_e^0(t) - E_g^0(t)$. Similarly, ΔE_n is the typical size of $E_e^n(t) - E_g^n(t)$. This allows us to define a 'quantum' time t_q, before which the transitions due to $\mathcal{H}_0$ may be neglected:

$$t_q \sim \left(\epsilon\frac{\Delta E_n}{\Delta E_0}\right)^2. \tag{4.23}$$

4.3.2 Negligible non-adiabatic transitions

The second condition can be analysed by the same rescaling of time by T. The second term in the square brackets of (4.18) gains the same T^{-1} factor as the time derivative on the left-hand side, which cannot cancel the $\sqrt{T}$ factors in the noise term. The non-adiabatic effects of the process can therefore no longer be neglected when the non-adiabatic term is comparable with the noise term:

$$\epsilon\sqrt{T}\,\Delta E_n \sim\ D_n\,(\Delta E_n)^{-1}, \tag{4.24}$$

where D_n is the typical magnitude of $\langle g_n(s)|\partial_s\mathcal{H}_n(s)|e_n(s)\rangle$. This is consistent with the intuitive idea that non-adiabatic effects become weaker for processes performed over longer times. We can now define an 'adiabatic' time t_a, after which non-adiabatic transitions become negligible:

$$t_a \sim \left(\frac{D_n}{\epsilon\,(\Delta E_n)^2}\right)^2. \tag{4.25}$$

4.3.3 Completely dephased components of the wavefunction

If the previous two conditions are satisfied, then only the third term in the square brackets of (4.18) needs to be retained. In this case, the evolution in (4.11) describes the system well, and the disorder-averaged fidelity is given by $\mathscr{F}_a(t)$. The plateau occurs when the exponential factor in (4.12) is negligible:

$$\exp\left(-\frac{1}{2}\epsilon^2 \left\langle (E_g^n - E_e^n)^2 \right\rangle_t t\right) \ll 1, \tag{4.26}$$

or equivalently:

$$\epsilon^2 \left\langle (E_g^n - E_e^n)^2 \right\rangle_t t \gg 1. \tag{4.27}$$

Therefore the phase is randomised provided that the exposure time exceeds the 'dephasing' time t_ϕ:

$$t_\phi \sim \left(\frac{1}{\epsilon\, \Delta E_n}\right)^2. \tag{4.28}$$

Combining these conditions we find that in order to observe the plateau we require:

$$t_\phi,\, t_a \ll T \ll t_q. \tag{4.29}$$

Fig. 4.2 shows a cartoon schematic of the plateau in the disorder-averaged fidelity as a function of exposure time T. The first region (when read in order of increasing T) corresponds to processes that are performed too quickly, $T < t_\phi, t_a$, and the plateau is destroyed by non-adiabatic transitions and/or obscured by insufficient dephasing of the wavefunction components. The plateau at $\mathscr{F}_0(T)$ exists in the second region, where the conditions in (4.29) are satisfied. The third region corresponds to processes that are performed too slowly, $T > t_q$; the plateau has been destroyed by transitions generated by $\mathcal{H}_0$, and $\overline{\mathscr{F}(T)}$ decays to $1/2$ as the state becomes fully randomised. The value at $T = 0$ is given by an instantaneous projection of the initial state on the target state: $\overline{\mathscr{F}(T=0)} = |\langle g_0(T)|g_0(0)\rangle|^2$.

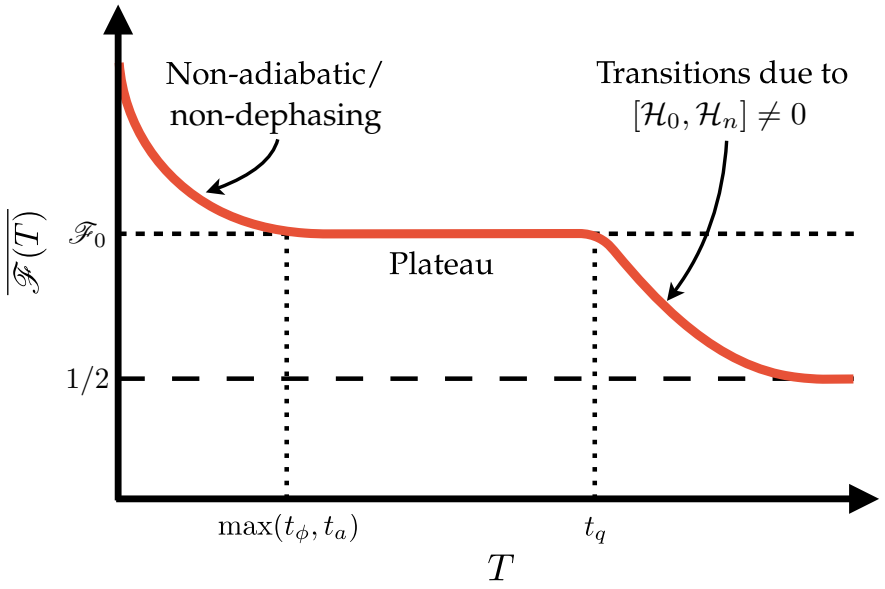

FIGURE 4.2: A schematic of the plateau in the disorder-averaged state-preparation fidelity $\overline{\mathscr{F}(T)}$ when plotted as a function of exposure time T. For short exposure times, $T < t_\phi, t_a$, the plateau cannot form due to non-adiabatic transitions and/or insufficient time to fully dephase the components of the wavefunction. For large exposure times, $T > t_q$, transitions due to $\mathcal{H}_0$ destroy the plateau, and the disorder-averaged fidelity decays to $1/2$. The plateau at $\mathscr{F}_0$ is visible at intermediate times.

4.4 Numerical demonstration

We now compare the results in the previous sections to an explicit model. We consider a simple example of (4.4), in which the Bloch spheres corresponding to $\mathcal{H}_0(t)$ and $\mathcal{H}_n(t)$ rotate at constant rates, and the energy gaps between their eigenstates are constant in time:

$$\begin{aligned} \mathcal{H}(t) &= E_0 \left[\cos\left(\vartheta_0(t)\right)\sigma^z + \sin\left(\vartheta_0(t)\right)\sigma^x\right] \\ &\quad + \epsilon\,\eta(t)\,E_n\left[\cos\left(\vartheta_n(t)\right)\sigma^z + \sin\left(\vartheta_n(t)\right)\sigma^x\right] \end{aligned} \tag{4.30}$$

where the angles $\vartheta_\alpha(t)$ change linearly with time:

$$\vartheta_\alpha(t) = \vartheta_\alpha(0) + \left(\vartheta_\alpha(T) - \vartheta_\alpha(0)\right)\frac{t}{T}. \tag{4.31}$$

The eigenstates of $\mathcal{H}_\alpha(t)$ are:

$$\big|g_\alpha(t)\big\rangle = \sin\frac{\vartheta_\alpha(t)}{2}\big|\uparrow\big\rangle - \cos\frac{\vartheta_\alpha(t)}{2}\big|\downarrow\big\rangle; \tag{4.32}$$

$$\big|e_\alpha(t)\big\rangle = \cos\frac{\vartheta_\alpha(t)}{2}\big|\uparrow\big\rangle + \sin\frac{\vartheta_\alpha(t)}{2}\big|\downarrow\big\rangle, \tag{4.33}$$

and the corresponding eigenvalues are $\pm E_\alpha$. Choosing a Hamiltonian with no σ^y components does not materially change the physics, but it does make the mathematical expressions less cumbersome (for example, the simple eigenvectors shown above will give no geometric phase contribution (2.11)). The equations of motion for $c_g(t)$ and $c_e(t)$ then become:

$$\begin{aligned} i\begin{pmatrix}\dot{c}_g\\ \dot{c}_e\end{pmatrix} &= \Bigg[E_0\begin{pmatrix}-\cos\left(\vartheta_n-\vartheta_0\right) & \sin\left(\vartheta_n-\vartheta_0\right)\\ \sin\left(\vartheta_n-\vartheta_0\right) & \cos\left(\vartheta_n-\vartheta_0\right)\end{pmatrix} \\ &\qquad - i\,\frac{\Delta\vartheta_n}{2T}\begin{pmatrix}0 & -1\\ 1 & 0\end{pmatrix} + \epsilon\,\eta\,E_n\begin{pmatrix}-1 & 0\\ 0 & 1\end{pmatrix}\Bigg]\begin{pmatrix}c_g\\ c_e\end{pmatrix}, \end{aligned} \tag{4.34}$$

where $\Delta\vartheta_n = \vartheta_n(T) - \vartheta_n(0)$, and the terms have been separated in the same way as in (4.18).

The height of the fidelity plateau can also be written simply in terms of the angles $\vartheta_\alpha(t)$:

$$\begin{aligned} \mathscr{F}_0(t) &= \cos^2\left(\frac{\vartheta_n(0)-\vartheta_0(0)}{2}\right)\cos^2\left(\frac{\vartheta_n(t)-\vartheta_0(t)}{2}\right) \\ &\qquad + \sin^2\left(\frac{\vartheta_n(0)-\vartheta_0(0)}{2}\right)\sin^2\left(\frac{\vartheta_n(t)-\vartheta_0(t)}{2}\right), \end{aligned} \tag{4.35}$$

and the fidelity of any individual noise realisation (should the system satisfy the conditions outlined in Section 4.3) must stay within the bounds:

$$\begin{aligned} \mathscr{F}_{\text{lims}}(t) &= \left(\cos\left(\frac{\vartheta_n(0)-\vartheta_0(0)}{2}\right)\cos\left(\frac{\vartheta_n(t)-\vartheta_0(t)}{2}\right)\right. \\ &\qquad \left. \pm\,\sin\left(\frac{\vartheta_n(0)-\vartheta_0(0)}{2}\right)\sin\left(\frac{\vartheta_n(t)-\vartheta_0(t)}{2}\right)\right)^2. \end{aligned} \tag{4.36}$$

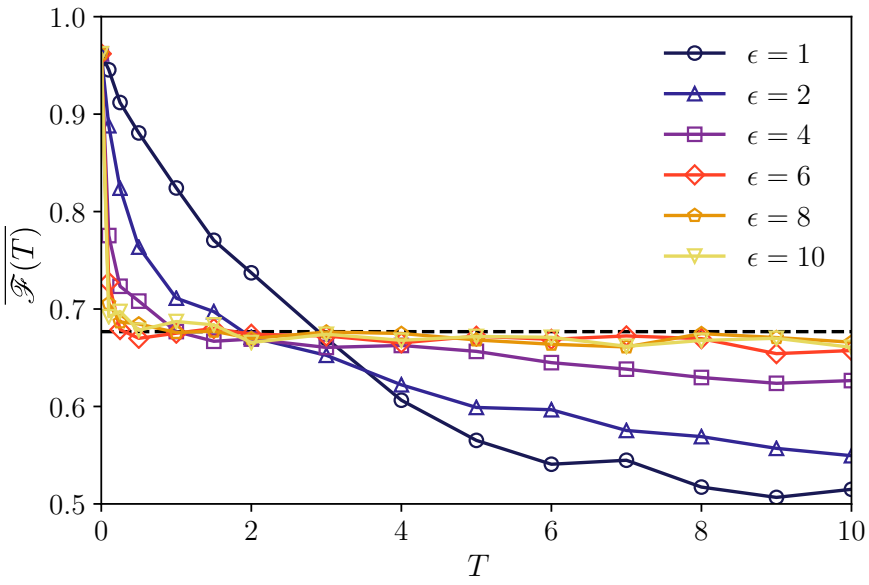

FIGURE 4.3: The disorder-averaged state-preparation fidelity, $\overline{\mathscr{F}(T)}$, plotted as a function of the exposure time T for several noise strengths ϵ. The plateau value $\mathscr{F}_0(T)$ is indicated by the horizontal dashed black line. All points are averaged over M realisations of the noise such that $\sigma/\sqrt{M} < 0.01$, where σ is the standard deviation.

We analyse the model by numerically time-evolving the state using the Heun algorithm for stochastic differential equations discussed in Section 2.2.1. The graphs shown here correspond to the parameters: $E_0 = 1$, $E_n = 1$, $\vartheta_0(0) = \pi/4$, $\vartheta_0(T) = \pi/8$, $\vartheta_n(0) = \pi/8$, and $\vartheta_n(T) = \pi/2$. Note that for this choice of parameters $\vartheta_0(T/4) = \vartheta_n(T/4)$, which results in the limits in (4.36) becoming equal to each other (and equal to the plateau value $\mathscr{F}_0(T/4)$) at $t = T/4$. The plateau occurs at a value of $\mathscr{F}_0(T) \approx 0.677$.

Fig. 4.3 shows the disorder-averaged fidelity as a function of the exposure time, for various noise strengths. It decays from $\mathscr{F}(0) = |\langle g_0(T)|g_0(0)\rangle|^2$ (the result of an instantaneous projection, as described in Section 2.1.2) to the value $\mathscr{F}_0(T)$, indicated by the dashed black line. When the noise is strong, the fidelity stays at the value of $\mathscr{F}_0(T)$, forming a long plateau; for weak noise, it almost immediately resumes decaying towards $1/2$, the value naïvely

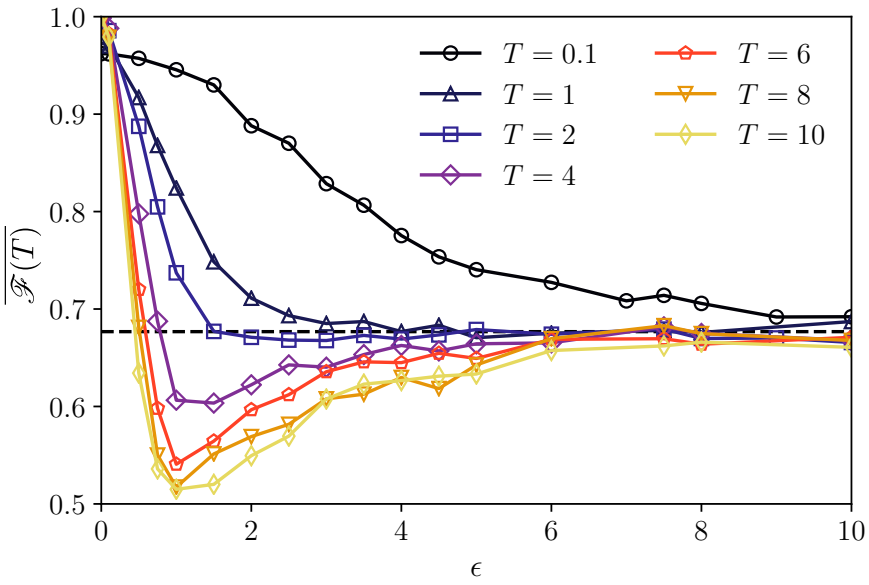

FIGURE 4.4: The disorder-averaged state-preparation fidelity, $\overline{\mathscr{F}(T)}$, plotted as a function of noise strength ϵ for several exposure times T. The plateau value $\mathscr{F}_0(T)$ is indicated by the horizontal dashed black line. All points are averaged over M realisations of the noise such that $\sigma/\sqrt{M} < 0.01$, where σ is the standard deviation.

expected for a two-state system. At intermediate noise strengths, such as $\epsilon = 4$ in the figure, the decay in the fidelity pauses around the plateau value before it resumes its decay towards $1/2$. This is due to transitions caused by the non-commutativity of $\mathcal{H}_0(t)$ and $\mathcal{H}_n(t)$, which become significant for $T \gtrsim t_q$.

Fig. 4.4 shows the disorder-averaged fidelity as a function of noise strength, for various exposure times. For each T the average fidelity tends to the plateau value (the dashed line) as the noise becomes strong. As the noise strength ϵ is reduced, the curves diverge from $\mathscr{F}_0(T)$, and this effect is seen most strongly for large T, where $\overline{\mathscr{F}(T)}$ becomes increasingly close to $1/2$. This can be understood by the intuitive fact that the noise, which is not strong enough to cause adiabatic following in the $\mathcal{H}_n$ basis, has more time in which to randomise the state of the system.

Now that we have seen that the plateau exists, we can ask whether our

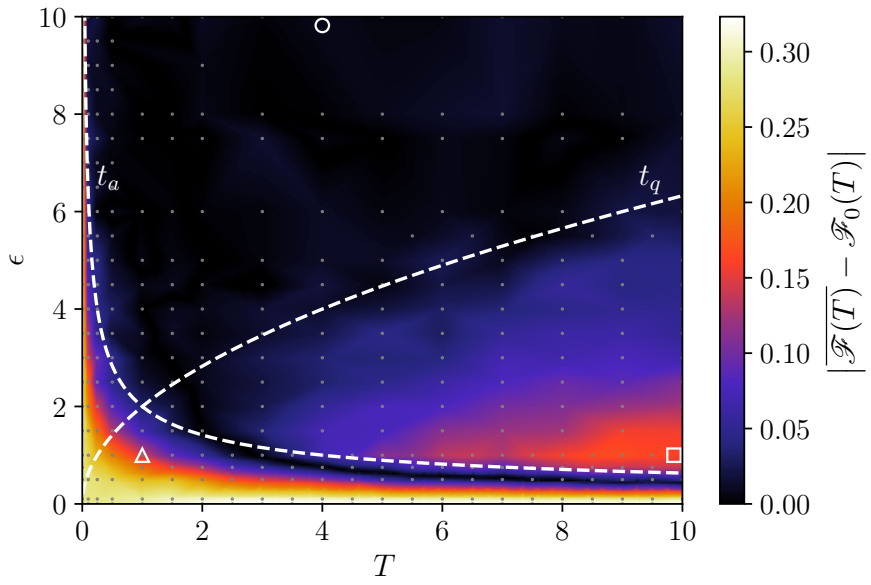

FIGURE 4.5: The absolute deviation of the disorder-averaged fidelity from the plateau value, $|\overline{\mathscr{F}(T)} - \mathscr{F}_0(T)|$, as a function of noise strength ϵ and exposure time T. The white dashed lines show t_a and t_q. All points (indicated by the grey markers) are averaged over M realisations of the noise such that $\sigma/\sqrt{M} < 0.015$, where σ is the standard deviation.

predictions of its behaviour are correct. Fig. 4.5 shows the absolute value of the deviation of the disorder-averaged fidelity from the plateau value, $|\overline{\mathscr{F}(T)} - \mathscr{F}_0(T)|$, as a function of the noise strength ϵ and exposure time T. The grey markers indicate the location of the data points, and the colour scale corresponds to an interpolation between these points. We see that for large ϵ and not too small or large T, the plateau appears as a large dark region in the upper portion of the graph. The dashed white lines indicate the 'adiabatic' time, $t_a = 4/\epsilon^2$, and the 'quantum' time, $t_q = \epsilon^2/4$, where the constants have been chosen by eye. These curves capture the edges of the plateau well, so we can conclude that we have correctly understood the behaviour of the plateau. We have found that $t_\phi \ll t_a$, so this has been omitted from the graph. Note that the dark region just below the t_a curve when $T > t_q$, where $\overline{\mathscr{F}(T)} \approx \mathscr{F}_0(T)$, is not part of the plateau. This is simply a result of the fact that for these parameters $\mathscr{F}_0(T) > 1/2$, so $\overline{\mathscr{F}(T)}$ must pass through $\mathscr{F}_0(T)$ in order to decay to $1/2$.

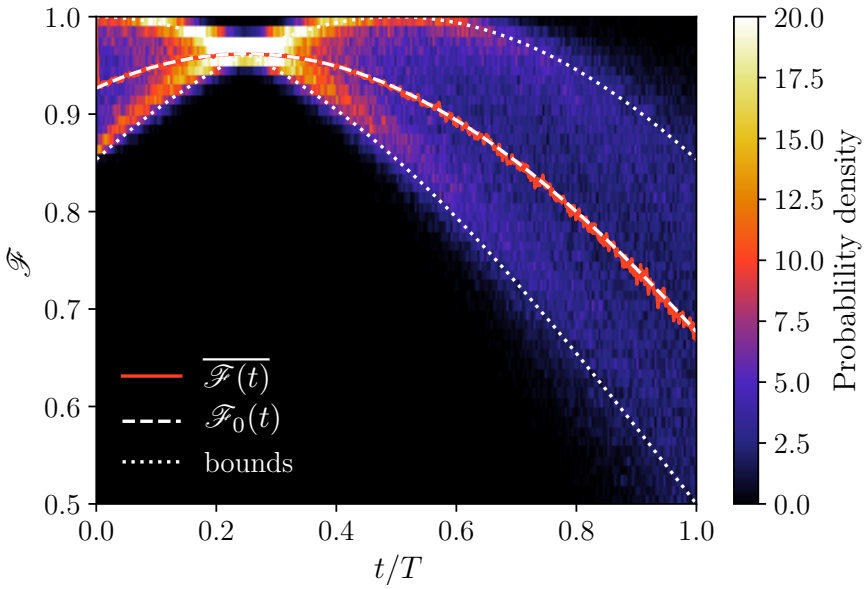

FIGURE 4.6: Histograms of fidelity as a function of time (vertical slices) for parameters in the plateau, $T = 4$ and $\epsilon = 10$ (the white circle in Fig. 4.5). The white dashed and dotted lines show $\mathscr{F}_0(t)$ and the bounds respectively, and the red line shows the average fidelity of the numerical data $\overline{\mathscr{F}(t)}$.

A last check that we can make is that the wavefunction itself is behaving correctly, and that the plateau corresponds to the fidelity staying within the bounds described in (4.15). Fig. 4.6 shows a time-resolved histogram of the fidelity $\mathscr{F}(t)$ for $T = 4$ and $\epsilon = 10$, the point indicated by the white circle in Fig. 4.5, which is safely within the plateau. The fidelity stays well within the expected bounds (indicated by the dotted white lines), even when the bounds close to a point at $t = T/4$. The average value of the numerical data, $\overline{\mathscr{F}(t)}$ (the solid red line), is also in good agreement with the prediction of $\mathscr{F}_0(t)$ (indicated by the dashed white line).

Fig. 4.7 shows the time-resolved histograms for two sets of parameters that do not fall within the plateau. It is clear that the distributions have significant weight outside of the bounds predicted for the strong noise limit, and that the numerical average is far from $\mathscr{F}_0(t)$. The top panel shows data for $T = 1$ and $\epsilon = 1$ (corresponding to the white triangle in Fig. 4.5), which is too fast to be in the plateau (i.e. $T < t_a$). The bottom panel shows data for $T = 10$ and

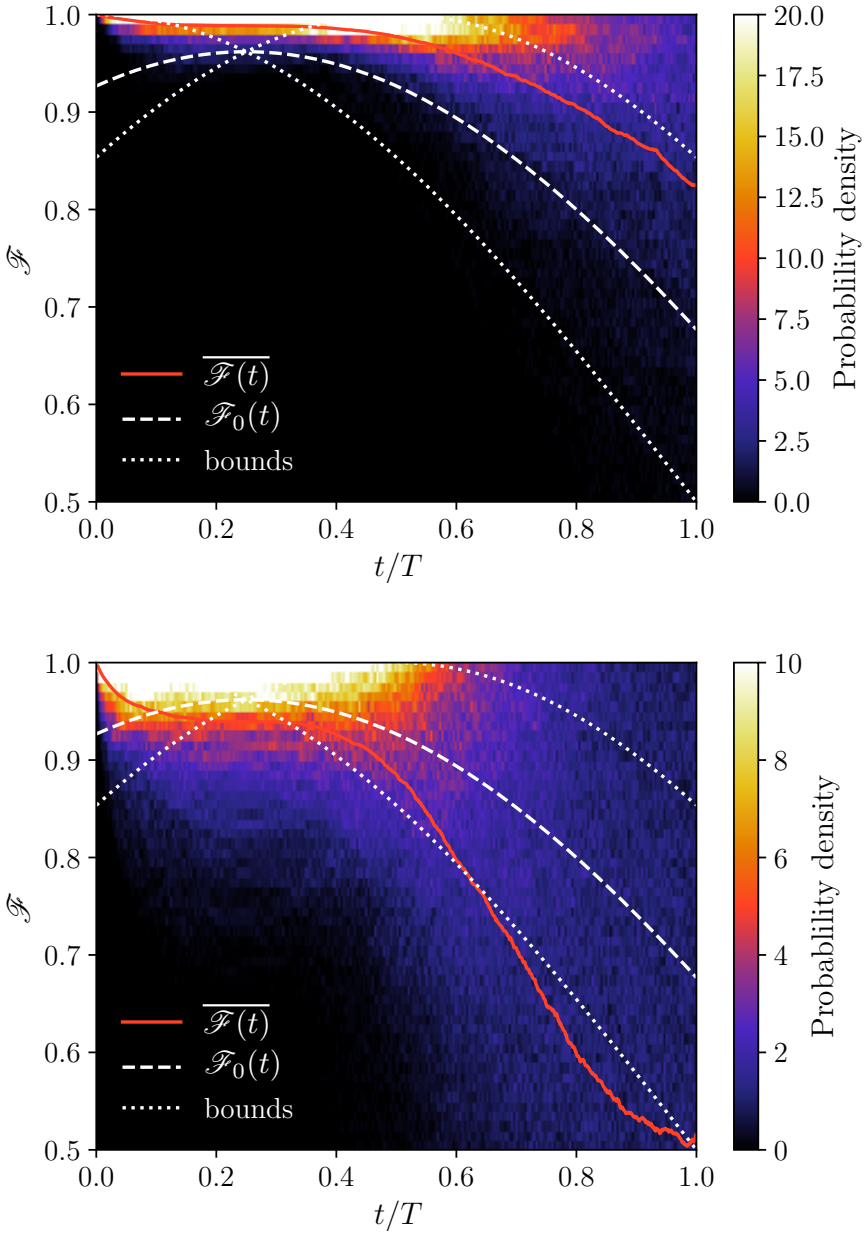

FIGURE 4.7: Histograms of fidelity as a function of time (vertical slices) for parameters outwith the plateau. The white dashed and dotted lines show $\mathscr{F}_0(t)$ and the bounds respectively, and the red line shows the average fidelity of the numerical data $\overline{\mathscr{F}(t)}$. Top: $T = 1$ and $\epsilon = 1$ (the white triangle in Fig. 4.5) is too fast to observe the plateau. Bottom: $T = 10$ and $\epsilon = 1$ (the white square in Fig. 4.5) is too slow to observe the plateau.

$\epsilon = 1$ (corresponding to the white square in Fig. 4.5), which is too slow for the plateau, allowing $\mathcal{H}_0$ to significantly change the populations in the $\mathcal{H}_n$ basis. This can be seen in the broad distribution of $\mathscr{F}$ as t becomes large, indicating that the noise can distribute the state quite evenly across the entire state space. This contrasts with the upper panel in which the distribution remains narrow, showing that the noise has not had sufficient time to randomise the state.

4.5 Imperfectly correlated noise

We now turn our attention to the case of imperfect correlations between the noise variables. This could, for example, be in the form of several independent noise variables in $\mathcal{H}_n(t)$, which appear as prefactors multiplying non-commuting operators. This means that we can no longer define a deterministic and smoothly varying eigenbasis of $\mathcal{H}_n(t)$ and we wish to understand how this changes the results of the previous sections.

To see these effects most clearly, we consider a static model with no $\mathcal{H}_0$ component, which means that $t_a \to 0$ and $t_q \to \infty$. We choose a Hamiltonian of the form:

$$\mathcal{H}(t;\alpha) = E_x\sigma^x\,\eta_x(t;\alpha) + E_z\sigma^z\,\eta_z(t;\alpha) \tag{4.37}$$

where the two noise parameters are Gaussian-distributed stochastic variables. The noise variables have averages of zero and the two-time correlators:

$$\begin{aligned}\overline{\eta_x(t;\alpha)\,\eta_x(t';\alpha)} = \overline{\eta_z(t;\alpha)\,\eta_z(t';\alpha)} = \delta(t-t');\\ \overline{\eta_x(t;\alpha)\,\eta_z(t';\alpha)} = \alpha\,\delta(t-t'),\end{aligned} \tag{4.38}$$

so $\alpha \in [0,1]$ quantifies the amount of correlation between the two variables ($\alpha = 0$ corresponds to completely uncorrelated variables, and $\alpha = 1$ corresponds to perfectly correlated variables). The $\alpha = 1$ limit is simple, as $\eta_x(t;1) = \eta_z(t;1)$, and (4.11) is an exact solution of the Schrödinger equation.

When $\alpha < 1$, it is instructive to define two new noise variables:

$$\begin{aligned}\chi_1(t) &= \frac{1}{\sqrt{2+2\alpha}}\left(\eta_x(t)+\eta_z(t)\right);\\ \chi_2(t) &= \frac{1}{\sqrt{2-2\alpha}}\left(\eta_x(t)-\eta_z(t)\right),\end{aligned} \tag{4.39}$$

which are statistically independent and have the two-time correlators:

$$\overline{\chi_a(t)\chi_b(t')} = \delta_{a,b}\delta(t-t'). \tag{4.40}$$

Writing the Hamiltonian (4.37) in terms of these independent noise variables we find:

$$\begin{aligned}\mathcal{H}(t;\alpha) = &\sqrt{\frac{1+\alpha}{2}}\left(E_x\sigma^x + E_z\sigma^z\right)\chi_1(t)\\ &+\sqrt{\frac{1-\alpha}{2}}\left(E_x\sigma^x - E_z\sigma^z\right)\chi_2(t).\end{aligned} \tag{4.41}$$

When written in this form, it is clear that a small value of $1-\alpha$ results in only a small perturbation away from the perfectly correlated Hamiltonian $\mathcal{H}(t;1)$.

We will work in the basis of $\mathcal{H}(t;1)$, initialising the system in its ground state, $|g_{\alpha=1}\rangle$, and studying the effect that reducing α has on the populations of the states in this basis. In the limit of perfectly correlated noise, $\alpha = 1$, these populations are independent of time. We analyse the population imbalance:

$$\mathcal{I}(t) = \left|\langle g_{\alpha=1}|\psi(t)\rangle\right|^2 - \left|\langle e_{\alpha=1}|\psi(t)\rangle\right|^2, \tag{4.42}$$

which is related to the fidelity by $\mathcal{I}(t) = 2\mathscr{F}(t) - 1$, but decays to zero when the state is fully randomised. For our initial state, $|\psi(0)\rangle = |g_{\alpha=1}\rangle$, the initial value of the imbalance is $\mathcal{I}(0) = 1$.

Fig. 4.8 shows the decay of the disorder-averaged imbalance $\overline{\mathcal{I}(t)}$ with time for several values of α, in a system where $E_x = E_z = 1/\sqrt{2}$. We see the expected behaviour that $\mathcal{I}(t) = 1$ for $\alpha = 1$, and an exponential decay for $\alpha < 1$ that becomes faster with decreasing α. Clearly, the system is sensitive

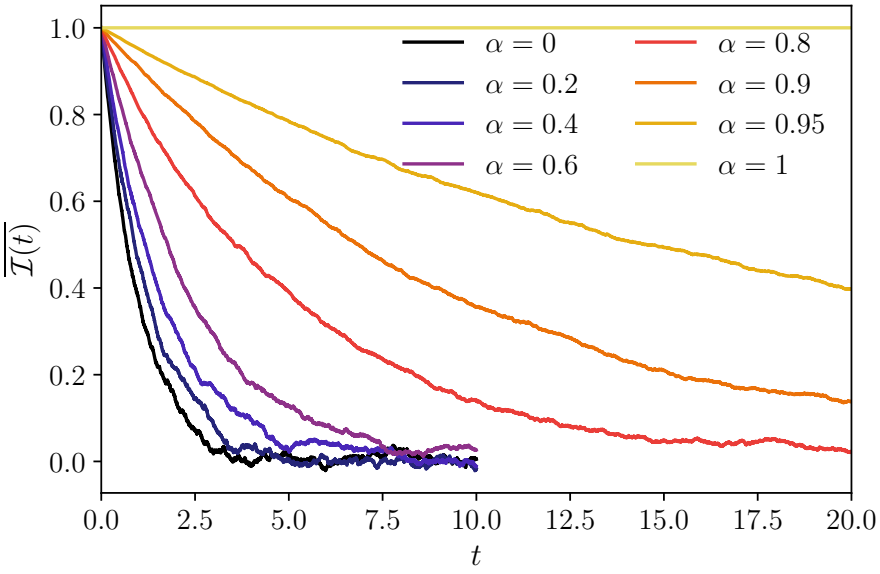

FIGURE 4.8: The disorder-averaged imbalance $\overline{\mathcal{I}(t)}$ plotted as a function of time for several values of the correlation parameter α.

to non-perfect correlations between the noise variables, and for values of $T \approx 5$, where we saw the plateau in Sec. 4.4, we would require $\alpha \gtrsim 0.95$ in order to still observe the plateau.

4.6 Summary and outlook

We have demonstrated that correlated noise in a state-preparation protocol can lead to a plateau in the fidelity at a non-trivial value. This is a form of localisation in state space at intermediate times, which is caused by the separation of timescales between the clean and noisy parts of the Hamiltonian. Future work could explore whether this phenomenon can be exploited in a state-preparation protocol to achieve a high fidelity process. Additionally, it would be interesting to see whether a non-trivial generalisation of this phenomenon could be observed in a system with a higher-dimensional state space and multiple uncorrelated noise terms.

Chapter 5

Time-dependent disorder in Anderson-localised systems

In this chapter we analyse the behaviour of a non-interacting, Anderson-localised system that is subjected to an additional time-dependent disorder potential. As discussed in Section 1.1, in the absence of the time-dependent terms every eigenstate is localised and excitations do not move through the system. However, as discussed in Section 2.1.2, the time-dependence will have a delocalising effect as it drives transitions between the instantaneous eigenstates of $\mathcal{H}(t)$. We show that the time-dependent noise causes excitations to spread diffusively, and analyse the effect that the spatial and temporal correlations of the noise have on this behaviour. We then show some preliminary results based on the idea of using this as a toy model to describe the ergodic phase of an interacting, many-body-localisable system. By exposing the system to noise with diffusively spreading correlations, we might aim to mimic interactions with other particles that are diffusing through the system.

5.1 The model

We consider a one-dimensional non-interacting Anderson model, as described in Section (1.1), with time-dependent disorder:

$$\mathcal{H}(t) = J \sum_{\langle i,j \rangle} \left(|i\rangle\langle j| + |j\rangle\langle i| \right) + \sum_j \left[\epsilon_j + \eta_j(t) \right] |j\rangle\langle j|, \tag{5.1}$$

where $\langle i, j \rangle$ denotes pairs of nearest-neighbour sites, ϵ_j is the static part of the disorder on site j, and $\eta_j(t)$ is the time-dependent part of the disorder. The static part of the disorder is uncorrelated between sites, and each ϵ_j is drawn from a Gaussian distribution with mean zero and standard deviation W. The time-dependent parts, $\eta_j(t)$, are also Gaussian-distributed with mean zero and standard deviation Λ, but with arbitrary spatial and temporal correlations:

$$g_j(t) = \overline{\eta_i(t_0)\eta_{i+j}(t_0 + t)} \tag{5.2}$$

where the bar denotes an average over disorder realisations. Importantly the statistical properties of the noise are invariant under translations in both space and time, i.e. the correlation function as written above is independent of i and t_0. The time-independent part of this model provides a simple system with localised eigenstates and, because this is a single-particle problem, we are able to easily simulate large systems with several hundred sites.

We measure the delocalisation by initialising the system with a particle localised on a single site in the middle of the lattice at $t = 0$, and numerically determining the spreading of the wavefunction under the unitary evolution described by the Schrödinger equation (2.1). We quantify the width of the wavefunction with the second moment of the probability distribution:

$$\sigma(t) = \sqrt{\langle x^2 \rangle_t - \langle x \rangle_t^2}, \tag{5.3}$$

where $x = \sum_j j \, |j\rangle\langle j|$ and $\langle A \rangle_t = \langle \psi(t)|A|\psi(t)\rangle$. Clearly our initial condition has $\sigma(0) = 0$.

We evaluate the time-evolution of $|\psi(t)\rangle$ numerically, using standard fourth-order Runge-Kutta integration [108], and setting $J = 1$.

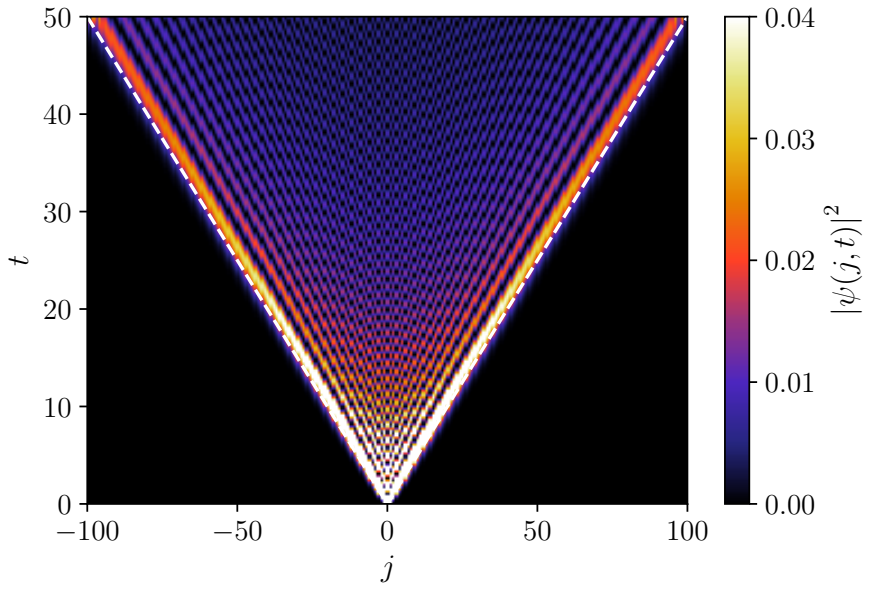

FIGURE 5.1: The probability density as a function of position and time in the disorder-free model: $W = 0, \Lambda = 0$. A particle is initially located on the central site and the white dashed lines indicate $j = \pm 2Jt$.

5.2 Some simple limits

Before considering the full problem, we can first consider some limits in which we know the behaviour of the system.

The disorder-free model ($W = 0, \Lambda = 0$)

In the absence of disorder, as discussed in Section 1.1.1, the eigenstates of the system are plane waves, which propagate ballistically (i.e. at a constant speed that is set by the gradient of the dispersion relation at their energy). This results in a wavepacket with a width that grows linearly in time, $\sigma(t) \sim t$, as the components of the initial state dephase according to (2.4). This behaviour is shown in Fig. 5.1. Each eigenstate $|k\rangle$ will propagate at a speed of $v_k = -2J \sin k$, so the fastest modes will travel with velocities of $\pm 2J$, and the resulting expanding wavefront will be at $x = \pm 2Jt$. The dashed white lines in Fig. 5.1 indicate this front.

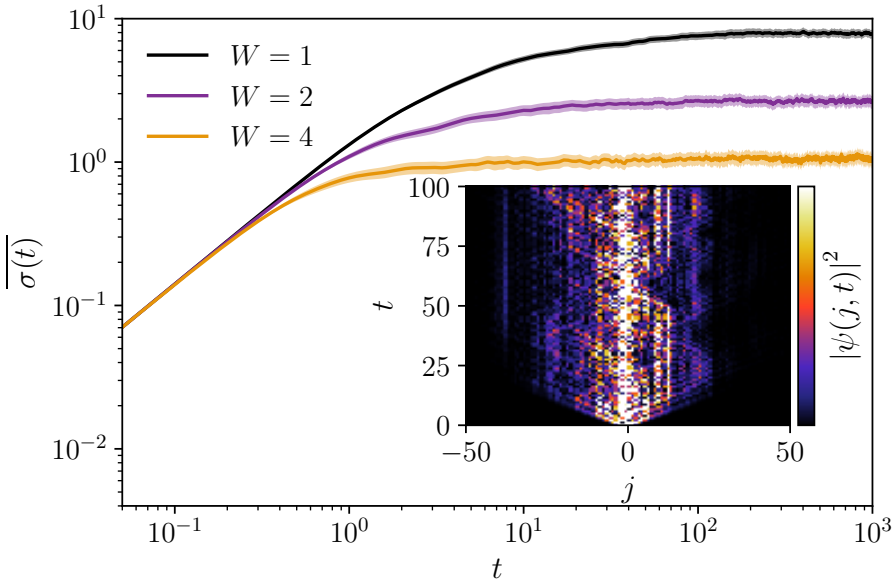

FIGURE 5.2: The growth of the width of the wavepacket for several disorder strengths W in the static disordered model ($\Lambda = 0$). The inset shows the probability density as a function of position and time for a single disorder realisation with $W = 1$. Averages are performed over 100 realisations of the disorder potential, and the shaded regions indicate the standard error in $\overline{\sigma(t)}$.

The static disordered model ($\Lambda = 0$)

This is the standard Anderson insulator, which has eigenstates that decay exponentially over a localisation length ξ from their centre. As a result, the initial state is formed of a superposition of eigenstates that are centred within $\sim \xi$ of the central site, and a negligible contribution from more distant states. The particle therefore does not spread continuously as in the disorder-free system, but is limited to a region on the order of the localisation length ξ. Fig. 5.2 shows the disorder-averaged wavepacket width for several disorder strengths; the particle in a system with a larger W expands to fill a smaller region of the lattice. The inset shows the probability density for a single realisation of the disorder with $W = 1$. There is an initial fast expansion as the components of the wavefunction dephase, before the average density settles at a constant width.

Temporally correlated noise

The effects of noise with temporal correlations but no spatial correlations have been explored in some previous works. Time-dependent noise applied to a system with no static disorder ($W = 0$ and $\Lambda \neq 0$ in our language) has been shown to inhibit the ballistic expansion seen in the disorder-free model, and the wavepacket spreads diffusively (i.e. $\overline{\sigma(t)} \sim \sqrt{t}$) [109, 110]. It was shown that the classical diffusion constant of the model could be well approximated analytically and depends on the correlation time and magnitude of the noise [110]. More recently, the model with static background disorder ($W \neq 0$) has been studied, with a noise correlator of $g_j(t) = \delta_{j,0}\Lambda^2 \exp(-t/\tau)$ [111]. It was observed that at large times the wavepacket spreads diffusively, in contrast to the static case without the noise. Interestingly, the width of the wavepacket was found to spread subdiffusively (i.e. $\overline{\sigma(t)} \sim t^\beta$ with $\beta < 0.5$) at intermediate times as the correlation time τ becomes large.

5.3 Gaussian noise

We now consider the problem with noise that has Gaussian correlations in both space and time:

$$g_j(t) = \Lambda^2 \exp\left(-\frac{j^2}{\chi^2}\right) \exp\left(-\frac{t^2}{\tau^2}\right), \tag{5.4}$$

where τ and χ are the correlation time and length of the noise respectively. We generate the noise as described in Section 2.2, using the correlation function in reciprocal space and time:

$$g(\omega, k) = \Lambda^2 \, \frac{\tau\chi}{2} \, \exp\left(-\frac{\tau^2\omega^2}{4}\right) \exp\left(-\frac{\chi^2 k^2}{4}\right). \tag{5.5}$$

We must rely on numerical calculations for this problem, as the method used previously to approximate the system with $\chi = 0$ using a classical rate equation [110, 111] will not work for $\chi \neq 0$. This is because there are correlations between the dynamical phase accumulated by particles on nearby sites in

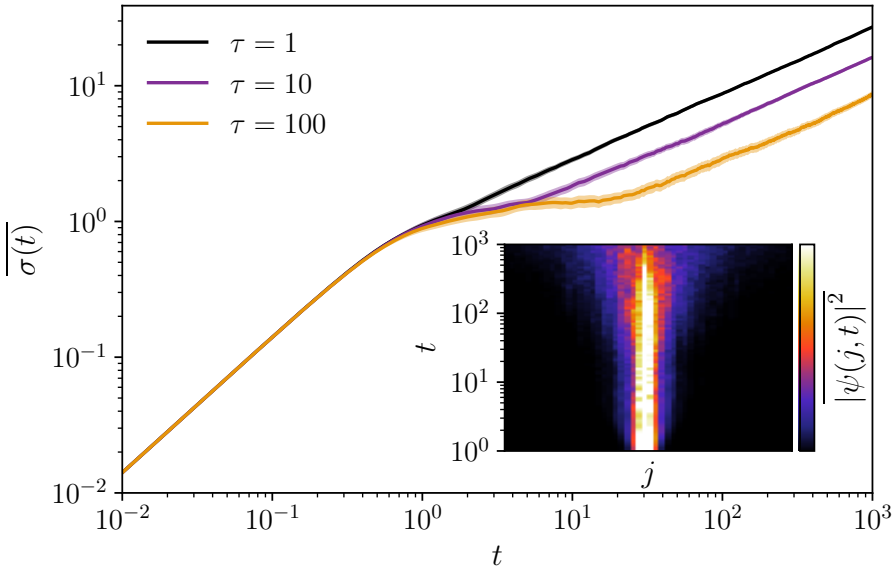

FIGURE 5.3: The width of the wavepacket $\overline{\sigma(t)}$ under Gaussian noise with several correlation times τ and no spatial correlations. The noise strength is $\Lambda = 2$ and the disorder strength is $W = 2$. The inset shows the disorder-averaged density as a function of position and time for $\tau = 100$. The results are averaged over 100 noise and disorder realisations, and the shaded regions indicate the standard error in $\overline{\sigma(t)}$.

the zeroth order ($J = 0$) solution, so cross-terms do not average to zero in the expansion to the next order in J. We perform the numerics on a lattice with $L = 401$, which keeps the particle away from the boundaries for the maximum time of our simulations, $T = 1000$.

Fig. 5.3 shows the growth of the wavepacket width $\overline{\sigma(t)}$ in a system with $W = 2$ due to Gaussian noise with strength $\Lambda = 2$ for several correlation times τ but no spatial correlation $\chi = 0$. The lines and shaded regions in each colour indicate the average and standard error respectively, taken over 100 realisations of the disorder and noise. As the correlation time is increased we observe a growing intermediate region in $\sigma(t)$ where the particle spreads subdiffusively before crossing over into diffusive growth. This is consistent with the results on noise with exponential correlations in time [111]. The region of slow transport can be seen in the inset of the figure, which shows the disorder-averaged density $\overline{|\psi(j,t)|^2}$ for $\tau = 100$. Clearly the width of the

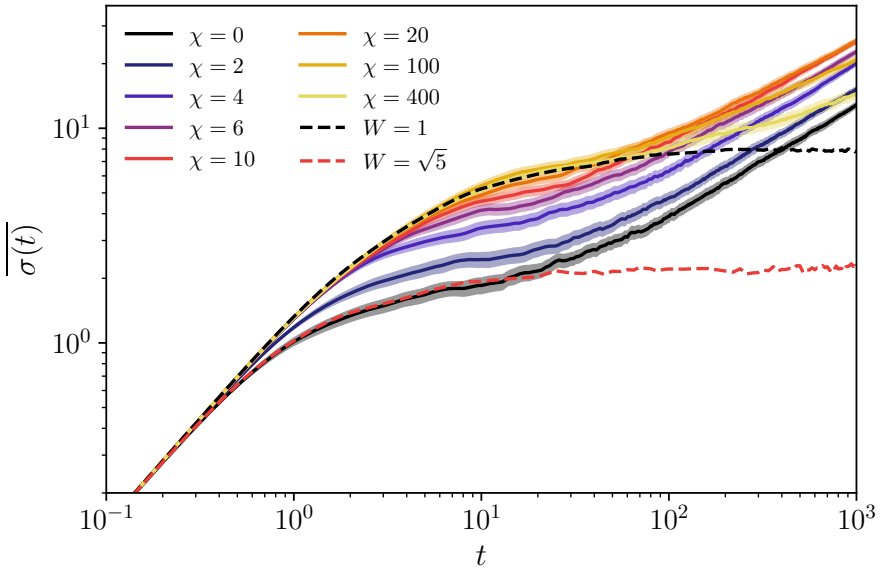

FIGURE 5.4: The width of the wavepacket $\overline{\sigma(t)}$ under Gaussian noise with several correlation lengths χ and correlation time $\tau = 100$. The noise strength is $\Lambda = 2$ and the disorder strength is $W = 1$. The dashed lines correspond to systems with $\Lambda = 0$ and a disorder strength chosen to match the $\chi \to 0$ ($W \to \sqrt{W^2 + \Lambda^2}$) and $\chi \to \infty$ ($W \to W$) limits. The results are averaged over 100 noise and disorder realisations, and the shaded regions indicate the standard error in $\overline{\sigma(t)}$.

density grows much more slowly over the period $t \approx 1 - 10$ compared to at $t > 10$.

Fig. 5.4 shows the growth of the wavepacket width $\sigma(t)$ in a system with $W = 1$ due to Gaussian noise with strength $\Lambda = 2$ for several correlation lengths χ. The correlation time $\tau = 100$ is large so that the subdiffusive region is noticeable and the correlation lengths range from shorter to longer than the localisation length in this model, which we have numerically determined to be $\xi(W = 1) \approx 9$. Increasing the correlation length extends the initial fast expansion of the wavepacket, which can be understood as a result of decreased fluctuations between the onsite energies of neighbouring sites. When $\chi \neq 0$, the noise is effectively constant over a region of length $l < \chi$, which results in an effectively weaker disorder compared to the $\chi = 0$ system and therefore a larger localisation length for the particle to expand into.

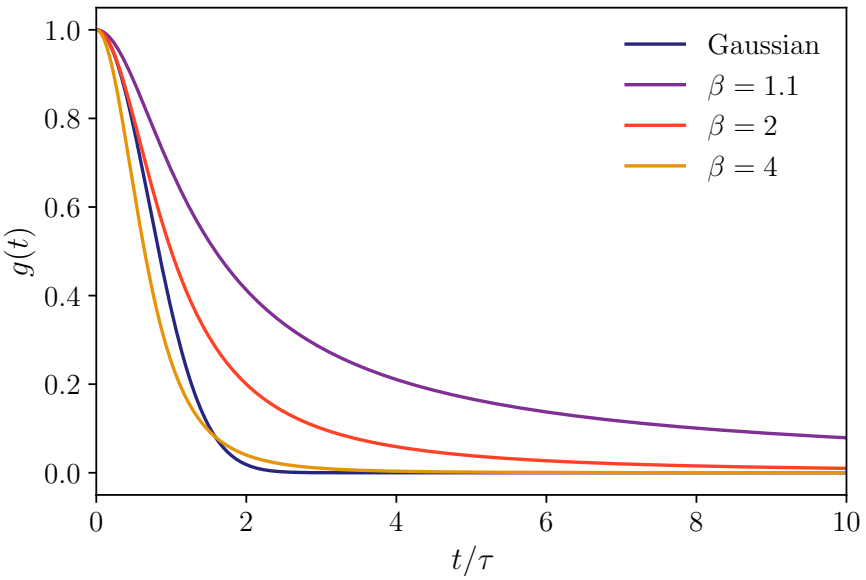

FIGURE 5.5: A comparison of the Gaussian two-time correlation function with a selection of power-law correlation functions.

More quantitatively, when $\chi = 0$ the onsite field at any instant is an independent Gaussian-distributed variable with a standard deviation of $\sqrt{W^2 + \Lambda^2}$, whereas for $\chi \neq 0$ the onsite field over a distance $l \ll \chi$ has a standard deviation of W and an average value given by the instantaneous value of the noise in that region. At larger times we see that the transport becomes slower when χ is increased beyond ξ, which is a result of the same effect. At short distances the noise behaves as an almost uniform time-dependent energy offset, which does not cause transitions. The delocalising effect of the noise must therefore occur due to longer-ranged hopping processes, which happen more slowly, resulting in reduced transport. The dashed lines in Fig. 5.4 show the wavepacket width $\sigma(t)$ for static systems with $W = 1$ and $W = \sqrt{5}$, which behave similarly to the $\chi = 400$ and $\chi = 0$ curves respectively for short times, before the noise has caused significant non-adiabatic transitions.

5.4 Power-law noise

We now turn our attention to noise with correlations that last much longer in time, specifically those that decay with a power-law:

$$g(t) = \Lambda^2 \left[1 + \left(\frac{t}{\tau}\right)^2\right]^{-\beta/2}, \tag{5.6}$$

where the exponent β controls how slowly the correlations decay. Fig. 5.5 shows a comparison of these correlation functions with the Gaussian form used in the previous section, showing that the correlations are more persistent in this case. In frequency space this becomes:

$$g(\omega) = \frac{\Lambda^2\, 2^{1-\beta/2}\, \tau}{\Gamma(\beta/2)} \left|\omega\tau\right|^{\frac{\beta-1}{2}} K_{\left|\frac{\beta-1}{2}\right|}\left(|\omega\tau|\right), \tag{5.7}$$

where $\Gamma(x)$ is the gamma function and $K_\alpha(x)$ is the α^{th} order modified Bessel function of the second kind [5]. For $\beta > 1$ this expression remains finite as $\omega \to 0$, so we can generate this noise exactly.

Fig. 5.6 shows $\overline{\sigma(t)}$ for systems exposed to power-law correlated noise with several exponents β and decay times τ, including the corresponding curve for Gaussian-correlated noise. All of the systems are exposed to noise with no spatial correlations. We see that power-law correlations with $\beta = 2$ result in very similar behaviour to the case of Gaussian noise, although the correlation function decays much more slowly. However, for $\beta = 1.1$, which has a very slow decay of correlations in the noise, we find that the slow transport caused by noise with $\tau = 100$ is even more pronounced than it is in the system with Gaussian noise. This is a result of the noise fluctuating more slowly when the correlation function is large for a long time, making the non-adiabatic transitions weaker. It appears that in all of these cases the transport still changes from subdiffusive to diffusive in the long-time limit.

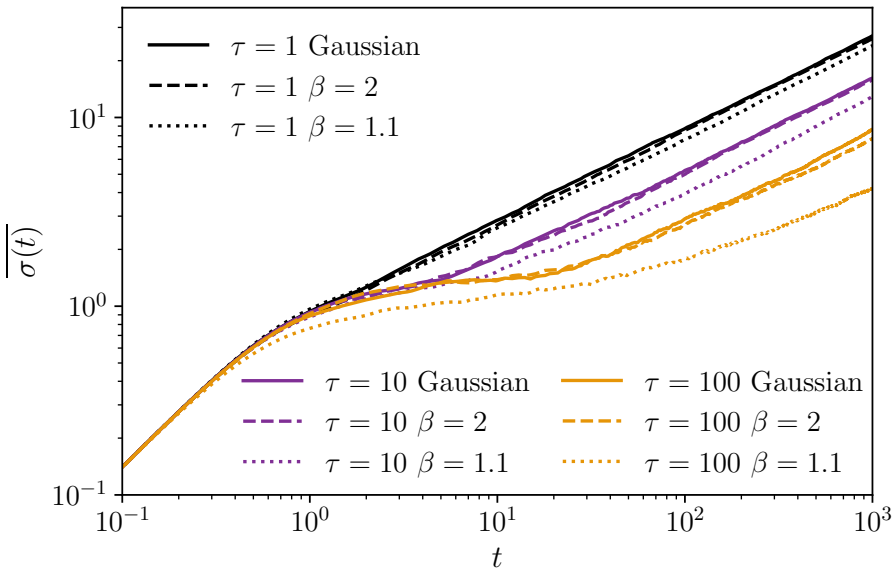

FIGURE 5.6: The width of the wavepacket $\overline{\sigma(t)}$ under power-law noise with several correlation times τ and exponents β. The solid lines correspond to systems experiencing Gaussian noise with the same correlation times as the curves of the same colour. The noise strength is $\Lambda = 2$, the disorder strength is $W = 2$, and the results are averaged over 100 noise and disorder realisations.

5.5 Diffusive noise

A potential extension of this work would be to attempt to mimic the behaviour of a system of interacting particles in a disordered lattice. In this picture the noise takes on the role of interactions with mobile excitations that are moving in the system. We would therefore be looking to explore the ergodic phase preceding the MBL transition, in which the hypothetical particles are mobile. An alternative system could be the case of spinful fermions in a spin-independent disorder potential. In this case, the particle density becomes localised while the magnetisation does not (even for very strong disorder) [112], and the noise could represent the interaction between the localised and delocalised parts of the system. We can expose the particle to noise that spreads diffusively with a diffusion constant D, and then extract the particle's diffusion constant D_p from the time-evolved wavefunction using the relation $\sigma(t) = \sqrt{2D_p t}$. If we can find a solution where $D = D_p$

then we have found a self-consistent solution where the particles diffuse in the same way as the noise. A more interesting result would be a failure to converge to a solution with $D = D_p$, which could suggest that the transport may not be diffusive, but something more unusual.

If we wish to mimic diffusing particles with the noise, we require a correlation function that resembles the Green's function of a diffusing particle:

$$g(\omega, k) = \frac{1}{i\omega + Dk^2}. \tag{5.8}$$

By Fourier-transforming this into real space and time we find:

$$g(t, x) = \frac{1}{2\pi} \int_{-\infty}^{+\infty} \mathrm{d}\omega \int_{-\infty}^{+\infty} \mathrm{d}k \, e^{ikx + i\omega t} \, \frac{1}{i\omega + Dk^2} \tag{5.9}$$

$$= \frac{1}{2\pi} \int_{-\infty}^{+\infty} \mathrm{d}\omega \, e^{i\omega t} \frac{\pi}{\sqrt{i\omega D}} \exp\left(-x\sqrt{\frac{i\omega}{D}}\right) \tag{5.10}$$

$$= \Theta(t)\sqrt{\frac{\pi}{Dt}} \exp\left(-\frac{x^2}{4Dt}\right), \tag{5.11}$$

where $\Theta(t)$ is the Heaviside step function. An obvious difficulty in turning this into a correlation function is that $g(t, 0)$ diverges as $t \to 0$, and we cannot explicitly generate this noise in the same way that we generated the Gaussian noise.

We can avoid this by slightly altering the correlation function, with a simple choice (i.e. a choice that can be Fourier-transformed analytically) being:

$$\tilde{g}(t, x) = \sqrt{\frac{2\pi}{x_0^2 + 2D|t|}} \exp\left(-\frac{x^2}{2(x_0^2 + 2D|t|)} - \lambda|t|\right), \tag{5.12}$$

which is well-behaved for negative t and is normalised such that $\tilde{g}(0, 0) = \sqrt{2\pi}/x_0$. This results in a reciprocal space correlation function:

$$\tilde{g}(\omega, k) = 2\, e^{-k^2 x_0^2/2} \, \frac{\lambda + Dk^2}{(\lambda + Dk^2)^2 + \omega^2}, \tag{5.13}$$

where the small cutoff x_0 removes the divergence in $g(t, x)$ at small t and

x, and the small cutoff λ removes the divergence in $g(\omega, k)$ at small ω and k. While we can generate realisations of this noise, we require a fine grid in frequency space to accurately reproduce the desired correlation function when λ is small, which is computationally expensive for the grid sizes and maximum times that we require (i.e systems with $\sim 10^2$ sites to times $\sim 10^3$).

5.6 Summary and outlook

In this chapter we have explored the response of a particle in an Anderson-localised system to a time-dependent disorder potential with a variety of spatiotemporal correlations. We have observed that at long times the particle spreads diffusively, while for intermediate times there is a period of subdiffusive transport. This intermediate region is present in disorder with Gaussian and power-law correlations in time, and grows when the correlation time of the noise is large. We also found that noise with long-range spatial correlations slows the spreading of the particle at late times.

Examining the response of the system to noise with diffusive spatiotemporal correlations would be an interesting extension, and could offer a contrasting viewpoint in the study of transport in the approach to many-body localisation. One could also explore the effect of spatially-correlated time-dependent disorder on a small number of interacting particles, which could be simulated on reasonably large system sizes (e.g. a system of 3 fermions on a 50-site lattice has a state space of comparable size to the zero-magnetisation sector of the 16-site XXZ model), and this may give some insight into the behaviour of strongly interacting systems.

Summary

In this thesis we have analysed the properties of three disordered quantum systems. To conclude, I will briefly summarise the findings described in the previous chapters, and make some closing remarks.

The first system that we considered was the XYZ spin chain in a disordered magnetic field, a generalisation of the XXZ model with the inclusion of terms that break the conservation of the z component of the total magnetisation. We find that, similarly to the U(1) symmetric XXZ model, the system undergoes a transition to a many-body localised phase in the presence of strong disorder. We have shown that the critical disorder strength for this transition increases significantly as the strength of the U(1) symmetry-breaking terms is increased, which we attribute to a larger number of available channels for delocalisation. The diagonal matrix elements of the bond-energy operator are consistent with this picture, while a change in the shape of the distributions of off-diagonal matrix elements deep in the ergodic phase suggests the existence of a transition between diffusive and subdiffusive energy transport. These findings are consistent with results on energy transport in large boundary-driven systems simulated with matrix-product methods. While the observation of MBL in a new model is interesting, it is perhaps the signs of anomalous transport that are most compelling. Unambiguously observing these effects in the dynamics of the system is difficult with exact numerical methods, which are limited to very small system sizes, and the statistical behaviour of matrix elements is a somewhat indirect measure. While a number of numerical studies suggest that the effect is real, a true microscopic understanding of this phenomenon is still lacking, and this is an important topic for future research.

We then studied a two-level quantum system described by a time-dependent Hamiltonian with a deterministic part and a randomly fluctuating noise part. We have shown that if the noise in multiple parameters of the Hamiltonian is perfectly correlated, then the noise does not fully randomise the state at intermediate times. This localisation in state space can then result in a plateau in the disorder-averaged state-preparation fidelity of an adiabatic transformation of the deterministic part of the Hamiltonian. A possible extension of this would be to explore the possibility of observing this effect in a more complicated system (i.e. a system with more than two levels) in the presence of multiple noise terms.

The third system was a single Anderson-localised fermion hopping on a one-dimensional lattice with an additional time-dependent disorder potential on each site, which we analysed for time-dependent disorder with a variety of spatiotemporal correlation functions. Our results indicate that time-dependent disorder with a large correlation time leads to a period of subdiffusive transport which grows with the correlation time, and that long-range spatial correlations inhibit transport at late times. We have also suggested a possible direction for further work on this system, by considering noise with diffusive spatiotemporal correlations, with an aim of mimicking interactions between the particle and other excitations diffusing through the system.

While disordered quantum systems have been explored for decades, studies of these systems are currently particularly pertinent due to the ongoing progress in experiments with cold gases. Advances in this field mean that we are approaching a situation in which the system can be manipulated so accurately that all unintentional disorder is absent, and intentional disorder can be introduced in a controlled way. This control, coupled with the large natural timescales in these systems, also make them ideal for probing non-equilibrium physics in both closed and open quantum systems. In this way, experiments are converging on the simple toy models favoured by theorists

to describe the basic fundamental aspects of nature, offering new avenues to understanding systems which are beyond the scope of current theoretical methods (such as, for example, MBL in higher-dimensional systems). This potential change in the dynamic between experiment and theory, with experiments filling gaps in our understanding of simple theoretical models, is without doubt an exciting prospect for all of physics.

Bibliography

[1] P. W. Anderson, "Absence of diffusion in certain random lattices", Phys. Rev. **109**, 1492 (1958).

[2] B. Kramer and A. MacKinnon, "Localization: Theory and experiment", Rep. Prog. Phys. **56**, 1469 (1993).

[3] P. Phillips, "Anderson localization and the exceptions", Annu. Rev. Phys. Chem. **44**, 115 (1993).

[4] A. Scardicchio and T. Thiery, "Perturbation theory approaches to Anderson and many-body localization: some lecture notes", arXiv: 1710.01234 (2017).

[5] M. Abramowitz and I. Stegun, *Handbook of Mathematical Functions* (Dover, New York, 1965).

[6] S. John and M. J. Stephen, "Wave propagation and localization in a long-range correlated random potential", Phys. Rev. B **28**, 6358 (1983).

[7] K. Ishii, "Localization of eigenstates and transport phenomena in the one-dimensional disordered system", Progress of Theoretical Physics Supplement **53**, 77 (1973).

[8] E. Abrahams, P. Anderson, D. Licciardello, and T. Ramakrishnan, "Scaling theory of localization: Absence of quantum diffusion in two dimensions", Phys. Rev. Lett. **42**, 673 (1979).

[9] P. Markoš, "Numerical analysis of the Anderson localization", Acta Physica Slovaca **56**, 561 (2006).

[10] L. Fleishman and P. W. Anderson, "Interactions and the Anderson transition", Phys. Rev. B **21**, 2366 (1980).

[11] T. Shahbazyan and M. Raikh, "Surface plasmon in a two-dimensional Anderson insulator with interactions", Phys. Rev. B **53**, 7299 (1996).

[12] Z. Wang, M. P. A. Fisher, S. M. Girvin, and J. T. Chalker, "Short-range interactions and scaling near integer quantum Hall transitions", Phys. Rev. B **61**, 8326 (2000).

[13] T. Nattermann, T. Giamarchi, and P. Le Doussal, "Variable-range hopping and quantum creep in one dimension", Phys. Rev. Lett. **91**, 056603 (2003).

[14] D. M. Basko, I. L. Aleiner, and B. L. Altshuler, "Metal–insulator transition in a weakly interacting many-electron system with localized single-particle states", Ann. Phys. **321**, 1126 (2006).

[15] A. De Luca, B. L. Altshuler, V. E. Kravtsov, and A. Scardicchio, "Anderson localization on the Bethe lattice: nonergodicity of extended states", Phys. Rev. Lett. **113**, 046806 (2014).

[16] B. L. Altshuler, E. Cuevas, L. B. Ioffe, and V. E. Kravtsov, "Nonergodic phases in strongly disordered random regular graphs", Phys. Rev. Lett. **117**, 156601 (2016).

[17] D. J. Luitz and Y. Bar Lev, "The ergodic side of the many-body localization transition", Annalen der Physik **529**, 1600350 (2017).

[18] R. Nandkishore and D. A. Huse, "Many-body localization and thermalization in quantum statistical mechanics", Annu. Rev. Condens. Matter Phys. **6**, 15 (2015).

[19] V. Khemani, S. P. Lim, D. N. Sheng, and D. A. Huse, "Critical properties of the many-body localization transition", Phys. Rev. X **7**, 021013 (2017).

[20] D. S. Wiersma, P. Bartolini, A. Lagendijk, and R. Righini, "Localization of light in a disordered medium", Nature **390**, 671 (1997).

[21] S. John, "Localization of light", Phys. Today **44**, 32 (1991).

[22] S. E. Skipetrov and I. M. Sokolov, "Absence of Anderson localization of light in a random ensemble of point scatterers", Phys. Rev. Lett. **112**, 023905 (2014).

[23] I. Bloch, J. Dalibard, and W. Zwerger, "Many-body physics with ultracold gases", Rev. Mod. Phys. **80**, 885 (2008).

[24] I. Bloch, J. Dalibard, and S. Nascimbène, "Quantum simulations with ultracold quantum gases", Nature Physics **8**, 267 (2012).

[25] L. Tarruell, D. Greif, T. Uehlinger, G. Jotzu, and T. Esslinger, "Creating, moving and merging Dirac points with a Fermi gas in a tunable honeycomb lattice", Nature **483**, 302 (2012).

[26] K. I. Petsas, A. B. Coates, and G. Grynberg, "Crystallography of optical lattices", Phys. Rev. A **50**, 5173 (1994).

[27] S. Aubry and G. André, "Analyticity breaking and Anderson localization in incommensurate lattices", Ann. Isr. Phys. Soc. **3**, 133 (1980).

[28] G. Roati, C. D'Errico, L. Fallani, M. Fattori, C. Fort, M. Zaccanti, G. Modugno, M. Modugno, and M. Inguscio, "Anderson localization of a non-interacting Bose–Einstein condensate", Nature **453**, 895 (2008).

[29] J. Billy, V. Josse, Z. Zuo, A. Bernard, B. Hambrecht, P. Lugan, D. Clément, L. Sanchez-Palencia, P. Bouyer, and A. Aspect, "Direct observation of Anderson localization of matter waves in a controlled disorder", Nature **453**, 891 (2008).

[30] M. Schreiber, S. S. Hodgman, P. Bordia, H. P. Lüschen, M. H. Fischer, R. Vosk, E. Altman, U. Schneider, and I. Bloch, "Observation of many-body localization of interacting fermions in a quasi-random optical lattice", Science **349**, 842 (2015).

[31] J. Y. Choi, S. Hild, J. Zeiher, P. Schauß, A. Rubio-Abadal, T. Yefsah, V. Khemani, D. A. Huse, I. Bloch, and C. Gross, "Exploring the many-body localization transition in two dimensions", Science **352**, 1547 (2016).

[32] S. S. Kondov, W. R. McGehee, W. Xu, and B. DeMarco, "Disorder-induced localization in a strongly correlated atomic Hubbard gas", Phys. Rev. Lett. **114**, 083002 (2015).

[33] M. Srednicki, "Thermal fluctuations in quantized chaotic systems", Journal of Physics A: Mathematical and General **29**, L75 (1996).

[34] M. V. Berry, "Regular and irregular semiclassical wavefunctions", J. Phys. A **10**, 2083 (1977).

[35] J. M. Deutsch, "Quantum statistical mechanics in a closed system", Phys. Rev. A **43**, 2046 (1991).

[36] M. Srednicki, "Chaos and quantum thermalization", Phys. Rev. E **50**, 888 (1994).

[37] L. D'Alessio, Y. Kafri, A. Polkovnikov, and M. Rigol, "From quantum chaos and eigenstate thermalization to statistical mechanics and thermodynamics", Adv. Phys. **65**, 239 (2016).

[38] J.-S. Caux and J. Mossel, "Remarks on the notion of quantum integrability", J. Stat. Mech. Theory Exp. **2011**, P02023 (2011).

[39] E. Ilievski, J. De Nardis, B. Wouters, J.-S. Caux, F. H. L. Essler, and T. Prosen, "Complete generalized Gibbs ensembles in an interacting theory", Phys. Rev. Lett. **115**, 157201 (2015).

[40] J. Z. Imbrie, V. Ros, and A. Scardicchio, "Local integrals of motion in many-body localized systems", Annalen der Physik **529**, 1600278 (2017).

[41] J. Z. Imbrie, "Diagonalization and many-body localization for a disordered quantum spin chain", Phys. Rev. Lett. **117**, 027201 (2016).

[42] T. E. O'Brien, D. A. Abanin, G. Vidal, "Explicit construction of local conserved operators in disordered many-body systems", Phys. Rev. B **94**, 144208 (2016).

[43] L. Rademaker and M. Ortuño, "Explicit local integrals of motion for the many-body localized state", Phys. Rev. Lett. **116**, 010404 (2016).

[44] V. Ros, M. Müller, and A. Scardicchio, "Integrals of motion in the many-body localized phase", Nuclear Physics B **891**, [Corrigendum. *Nuclear Physics B*, 900:446 - 448, 2015], 420 (2015).

[45] J. Z. Imbrie, "On many-body localization for quantum spin chains", J. Stat. Phys. **163**, 998 (2016).

[46] M. Rigol, V. Dunjko, and M. Olshanii, "Thermalization and its mechanism for generic isolated quantum systems", Nature **452**, 854 (2008).

[47] M. Rigol and M. Srednicki, "Alternatives to eigenstate thermalization", Phys. Rev. Lett. **108**, 110601 (2012).

[48] H. Kim, T. N. Ikeda, and D. A. Huse, "Testing whether all eigenstates obey the eigenstate thermalization hypothesis", Phys. Rev. E **90**, 052105 (2014).

[49] C. R. Laumann, A. Pal, and A. Scardicchio, "Many-body mobility edge in a mean-field quantum spin glass", Phys. Rev. Lett. **113**, 200405 (2014).

[50] J. A. Kjall, J. H. Bardarson, and F. Pollmann, "Many-body localization in a disordered quantum Ising chain", Phys. Rev. Lett. **113**, 107204 (2014).

[51] S. Stagraczyński, L. Chotorlishvili, M. Schüler, M. Mierzejewski, and J. Berakdar, "Many-body localization phase in a spin-driven chiral multiferroic chain", Phys. Rev. B **96**, 054440 (2017).

[52] M. Serbyn, Z. Papić, and D. A. Abanin, "Thouless energy and multifractality across the many-body localization transition", Phys. Rev. B **96**, 104201 (2017).

[53] D. J. Luitz, F. Huveneers, and W. De Roeck, "How a small quantum bath can thermalize long localized chains", Phys. Rev. Lett. **119**, 150602 (2017).

[54] P. Jordan and E. Wigner, "Über das Paulische Äquivalenzverbot", Z. Phys. **47**, 631 (1928).

[55] D. J. Luitz, N. Laflorencie, and F. Alet, "Many-body localization edge in the random-field Heisenberg chain", Phys. Rev. B **91**, 081103 (2015).

[56] M. Serbyn, Z. Papić, and D. A. Abanin, "Criterion for many-body localization-delocalization phase transition", Phys. Rev. X **5**, 041047 (2015).

[57] I. Mondragon-Shem, A. Pal, T. L. Hughes, and C. R. Laumann, "Many-body mobility edge due to symmetry-constrained dynamics and strong interactions", Phys. Rev. B **92**, 064203 (2015).

[58] A. Chandran, C. R. Laumann, and V. Oganesyan, "Finite size scaling bounds on many-body localized phase transitions", arXiv: 1509.04285 (2015).

[59] W. De Roeck, F. Huveneers, M. Müller, and M. Schiulaz, "Absence of many-body mobility edges", Phys. Rev. B **93**, 014203 (2016).

[60] Y. Bar Lev, G. Cohen, and D. R. Reichman, "Absence of diffusion in an interacting system of spinless fermions on a one-dimensional disordered lattice", Phys. Rev. Lett. **114**, 100601 (2015).

[61] K. Agarwal, S. Gopalakrishnan, M. Knap, M. Müller, and E. Demler, "Anomalous diffusion and Griffiths effects near the many-body localization transition", Phys. Rev. Lett. **114**, 160401 (2015).

[62] M. Žnidarič, A. Scardicchio, and V. K. Varma, "Diffusive and subdiffusive spin transport in the ergodic phase of a many-body localizable system", Phys. Rev. Lett. **117**, 040601 (2016).

[63] D. J. Luitz and Y. Bar Lev, "Anomalous thermalization in ergodic systems", Phys. Rev. Lett. **117**, 170404 (2016).

[64] V. K. Varma, A. Lerose, F. Pietracaprina, J. Goold, and A. Scardicchio, "Energy diffusion in the ergodic phase of a many body localizable spin chain", J. Stat. Mech. Theory Exp. **2017**, 053101 (2017).

[65] J. J. Mendoza-Arenas, M. Žnidarič, V. K. Varma, J. Goold, S. R. Clark, and A. Scardicchio, "Asymmetry in energy versus spin transport in certain interacting disordered systems", Phys. Rev. B **99**, 094435 (2019).

[66] M. Schulz, S. R. Taylor, C. A. Hooley, and A. Scardicchio, "Energy transport in a disordered spin chain with broken U(1) symmetry: Diffusion, subdiffusion, and many-body localization", Phys. Rev. B **98**, 180201 (2018).

[67] S. Roy, Y. Bar Lev, and D. J. Luitz, "Anomalous thermalization and transport in disordered interacting Floquet systems", Phys. Rev. B **98**, 060201 (2018).

[68] L. D'Alessio and A. Polkovnikov, "Many-body energy localization transition in periodically driven systems", Ann. Phys. (N. Y.) **333**, 19 (2013).

[69] P. Ponte, A. Chandran, Z. Papić, and D. A. Abanin, "Periodically driven ergodic and many-body localized quantum systems", Ann. Phys. (N. Y.) **353**, 196 (2015).

[70] P. Ponte, Z. Papić, F. Huveneers, and D. A. Abanin, "Many-body localization in periodically driven systems", Phys. Rev. Lett. **114**, 140401 (2015).

[71] A. Lazarides, A. Das, and R. Moessner, "Fate of many-body localization under periodic driving", Phys. Rev. Lett. **115**, 030402 (2015).

[72] D. A. Abanin, W. D. Roeck, and F. Huveneers, "Theory of many-body localization in periodically driven systems", Ann. Phys. (N. Y.) **372**, 1 (2016).

[73] V. Oganesyan and D. A. Huse, "Localization of interacting fermions at high temperature", Phys. Rev. B **75**, 155111 (2007).

[74] A. Pal and D. A. Huse, "Many-body localization phase transition", Phys. Rev. B **82**, 174411 (2010).

[75] M. Serbyn and J. E. Moore, "Spectral statistics across the many-body localization transition", Phys. Rev. B **93**, 041424 (2016).

[76] Y. Avishai, J. Richert, and R. Berkovits, "Level statistics in a Heisenberg chain with random magnetic field", Phys. Rev. B **66**, 052416 (2002).

[77] J. M. Gómez, R. A. Molina, A. Relaño, and J. Retamosa, "Misleading signatures of quantum chaos", Phys. Rev. E **66**, 036209 (2002).

[78] T. Guhr, A. Mueller-Groeling, and H. A. Weidenmueller, "Random matrix theories in quantum physics: common concepts", Phys. Rep. **299**, 189 (1998).

[79] Y. Y. Atas, E. Bogomolny, O. Giraud, and G. Roux, "Distribution of the ratio of consecutive level spacings in random matrix ensembles", Phys. Rev. Lett. **110**, 084101 (2013).

[80] M. Žnidarič, T. Prosen, and P. Prelovšek, "Many-body localization in the Heisenberg XXZ magnet in a random field", Phys. Rev. B **77**, 064426 (2008).

[81] J. H. Bardarson, F. Pollmann, and J. E. Moore, "Unbounded growth of entanglement in models of many-body localization", Phys. Rev. Lett. **109**, 017202 (2012).

[82] M. Serbyn, Z Papić, and D. A. Abanin, "Universal slow growth of entanglement in interacting strongly disordered systems", Phys. Rev. Lett. **110**, 260601 (2013).

[83] E. J. Torres-Herrera and L. F. Santos, "Extended nonergodic states in disordered many-body quantum systems", Ann. Phys. (Berl.) **529**, 1600284 (2017).

[84] A. De Luca and A. Scardicchio, "Ergodicity breaking in a model showing many-body localization", Europhys. Lett. **101**, 37003 (2013).

[85] C. L. Baldwin, C. R. Laumann, A. Pal, and A. Scardicchio, "The many-body localized phase of the quantum random energy model", Phys. Rev. B **93**, 024202 (2016).

[86] W. Beugeling, R. Moessner, and M. Haque, "Finite-size scaling of eigenstate thermalization", Phys. Rev. E **89**, 042112 (2014).

[87] A. Mitra, "Quantum quench dynamics", Annu. Rev. Condens. Matter Phys. **9**, 245 (2018).

[88] M. Born and V. Fock, "Beweis des Adiabatensatzes", Z. Phys. **51**, 165 (1928).

[89] A. Messiah, *Quantum Mechanics* (Dover Publications, 1999).

[90] J. Roland and N. J. Cerf, "Quantum search by local adiabatic evolution", Phys. Rev. A **65**, 042308 (2002).

[91] L. D. Landau, "Zur Theorie der Energieubertragung. II", Phys. Z. Sowjetunion **2**, 46 (1932).

[92] C. Zener, "Non-adiabatic crossing of energy levels", Proc. R. Soc. A **137**, 696 (1932).

[93] E. Majorana, "Atomi orientati in campo magnetico variabile", Nuovo Cimento **9**, 43–50 (1932).

[94] E. C. G. Stueckelberg, "Theorie der unelastischen Stösse zwischen Atomen", Helv. Phys. Acta **5**, 369 (1932).

[95] C. Gardiner, *Handbook of stochastic methods for physics, chemistry, and the natural sciences* (Springer, 2004).

[96] T. C. Gard, *Introduction to Stochastic Differential Equations* (M. Dekker, 1988).

[97] P. Langevin, "Sur la théorie du mouvement brownien", Comptes Rendus Acad. Sci. **146**, 530 (1908).

[98] A. Einstein, "Über die von der molekularkinetischen Theorie der Wärme geforderte Bewegung von in ruhenden Flüssigkeiten suspendierten Teilchen", Ann. Phys. (Berl.) **322**, 549 (1905).

[99] D. Garcia-Alvarez, "A comparison of a few numerical schemes for the integration of stochastic differential equations in the Stratonovich interpretation", arXiv: 1102.4401 (2011).

[100] K. Itô, "Stochastic integral", Proc. Imp. Acad. **20**, 519 (1944).

[101] R. Stratonovich, "A new representation for stochastic integrals and equations", SIAM J. Control **4**, 362 (1966).

[102] A. H. Romero and J. M. Sancho, "Generation of short and long range temporal correlated noises", Journal of Computational Physics **156**, 1 (1999).

[103] The code can be found at `https://github.com/scott-taylor-condmat/ED_For_XYZ`.

[104] R. Baxter, *Exactly Solved Models in Statistical Mechanics* (London: Academic, 1982).

[105] T. Inami and H. Konno, "Integrable XYZ spin chain with boundaries", J. Phys. A **27**, L913 (1994).

[106] J. J. Mendoza-Arenas, S. R. Clark, and D. Jaksch, "Coexistence of energy diffusion and local thermalization in nonequilibrium XXZ spin chains with integrability breaking", Phys. Rev. E **91**, 042129 (2015).

[107] X. Zotos, F. Naef, and P. Prelovšek, "Transport and conservation laws", Phys. Rev. B **55**, 11029 (1997).

[108] W. H. Press, S. A. Teukolsky, W. T. Vetterling, and B. P. Flannery, *Numerical Recipes in C (2nd Ed.): The Art of Scientific Computing* (Cambridge University Press, 1992).

[109] Y. Yin, D. E. Katsanos, and S. N. Evangelou, "Quantum walks on a random environment", Phys. Rev. A **77**, 022302 (2008).

[110] A. Amir, Y. Lahini, and H. B. Perets, "Classical diffusion of a quantum particle in a noisy environment", Phys. Rev. E **79**, 050105 (2009).

[111] S. Gopalakrishnan, K. R. Islam, and M. Knap, "Noise-induced subdiffusion in strongly localized quantum systems", Phys. Rev. Lett. **119**, 046601 (2017).

[112] P. Prelovšek, O. S. Barišić, and M. Žnidarič, "Absence of full many-body localization in the disordered Hubbard chain", Phys. Rev. B **94**, 241104 (2016).